Technical Report Documentation Page

1. Report No. FHWA/TX-07/0-5202-2	2. Government Accession No.	3. Recipient's Catalog No.
4. Title and Subtitle Field Suction and Effect of Cracking in Highly Plastic Clay		5. Report Date September 2006 6. Performing Organization Code
7. Author(s) Jeffrey A. Kuhn and Dr. Jorge G. Zornberg		8. Performing Organization Report No. 0-5202-2
9. Performing Organization Name and Address Center for Transportation Research The University of Texas at Austin 3208 Red River, Suite 200 Austin, TX 78705-2650		10. Work Unit No. (TRAIS) 11. Contract or Grant No. 0-5202
12. Sponsoring Agency Name and Address Texas Department of Transportation Research and Technology Implementation Office P.O. Box 5080 Austin, TX 78763-5080		13. Type of Report and Period Covered Technical Report, Fall 2004 to Fall 2006 14. Sponsoring Agency Code

15. Supplementary Notes
Project performed in cooperation with the Texas Department of Transportation and the Federal Highway Administration.

16. Abstract

A study was conducted to determine field suction values as well as the effect of cracking on the hydraulic properties of compacted highly plastic clays. This investigation consisted of an experimental program involving a series of instrumented soil column tests on highly plastic clay prepared under controlled compaction conditions and subjected to evaporation, infiltration, and a second evaporation stage. During both evaporation and infiltration stages, water content and suction profiles were measured. Analysis was conducted using the results of the experimental program to determine the effect of cracking on the hydraulic properties of the soil. This analysis indicates that cracking has a significant effect on the soil-water retention curve and the hydraulic conductivity of the compacted highly plastic clay under unsaturated conditions. The results of this analysis allow determination of field suction values and depth of moisture fluctuation. This study is complimented with slope stability analyses, evaluation of the recurrence rate of failures, and an overview of site visits conducted in this study.

17. Key Words Clay, Cracking, Hydraulic, Soil Water Retention Curve, Instant Profiling method, Hydraulic Conductivity Function, Slopes		18. Distribution Statement No restrictions. This document is available to the public through the National Technical Information Service, Springfield, Virginia 22161; www.ntis.gov.	
19. Security Classif. (of report) Unclassified	20. Security Classif. (of this page) Unclassified	21. No. of pages 176	22. Price

Form DOT F 1700.7 (8-72) Reproduction of completed page authorized

Field Suction and Effect of Cracking in Highly Plastic Clay

Jeffrey A. Kuhn
Dr. Jorge G. Zornberg

CTR Technical Report:	0-5202-2
Report Date:	September 2006
Project:	0-5202
Project Title:	Determination of Field Suction Values in High PI Clays for Various Surface Conditions and Drain Installations
Sponsoring Agency:	Texas Department of Transportation
Performing Agency:	Center for Transportation Research at The University of Texas at Austin

Project performed in cooperation with the Texas Department of Transportation and the Federal Highway Administration.

Center for Transportation Research
The University of Texas at Austin
3208 Red River
Austin, TX 78705

www.utexas.edu/research/ctr

Disclaimers

Author's Disclaimer: The contents of this report reflect the views of the authors, who are responsible for the facts and the accuracy of the data presented herein. The contents do not necessarily reflect the official view or policies of the Federal Highway Administration or the Texas Department of Transportation (TxDOT). This report does not constitute a standard, specification, or regulation.

Patent Disclaimer: There was no invention or discovery conceived or first actually reduced to practice in the course of or under this contract, including any art, method, process, machine manufacture, design or composition of matter, or any new useful improvement thereof, or any variety of plant, which is or may be patentable under the patent laws of the United States of America or any foreign country.

Engineering Disclaimer

NOT INTENDED FOR CONSTRUCTION, BIDDING, OR PERMIT PURPOSES.

Research Supervisor: Dr. Jorge G. Zornberg

Acknowledgments

The authors express appreciation to the TxDOT Project Director and members of the Project Monitoring Committee.

Table of Contents

List of Figures

List of Tables

Chapter 1. Field Suction and Effect of Cracking in Highly Plastic Clay

1.1 Motivation

Compacted highly plastic clays are the material of choice in engineering applications such as hydraulic barriers, but they are also used in projects such as earthen structures, where granular materials are generally preferred. The use of highly plastic clays for backfill materials is most common in regions, such as central Texas, where conventional backfill materials (e.g.,, granular soils and clays of low plasticity) are not readily available or are too expensive to transport to a construction site.

The Texas Department of Transportation (TxDOT) has often used highly plastic clay as backfill material for highway embankments. TxDOT has experienced a number of slope failures involving these highly plastic clay backfills. Water infiltration has been reported by TxDOT personnel as the cause of these surficial instabilities. Cracking of compacted highly plastic clay situated near the soil-atmosphere interface is though to play a significant role in this infiltration process. Compacted highly plastic clays are susceptible to cracking because of the significant volume changes that these soils undergo during cycles of wetting and drying. Because the effect of cracking on the water infiltration processes is not well understood, gaining insight into this problem is central to understanding the stability of geotechnical structures constructed with highly plastic clays. Another aspect to investigate is the need to account for long term diffusive processes, which according to Aubeny and Lytton (2003) lead to a continuous decrease in suction with time. The validity of such diffusive processes may be evaluated by comparing the initial suction of backfill under typical placement conditions with the expected long-term suction defined using average relative humidity conditions for central Texas.

The effect of cracking on the hydraulic properties of unsaturated highly plastic clays is yet to be quantified. Much of the research on the hydraulic properties of unsaturated highly plastic clays has focused on problems related to waste containment projects, where careful measures are taken to prevent cracking. As a result, most studies on this topic have focused on intact (i.e., un-cracked) specimens. Past research has also been limited by the specimen size required to accommodate representative cracking patterns and the long testing times required for the characterization of the hydraulic properties of unsaturated clays. Considering the lack of information from the literature, an important objective of the experimental component of this study is to characterize the effects of cracking on the hydraulic properties of unsaturated highly plastic clays.

1.2 Scope of this Report

The research component presented in this report involves a series of evaporation and infiltration experiments aimed at determining the effect of cracking on the hydraulic properties of unsaturated highly plastic clays. This research component involved the preparation of laboratory specimens and equipment, the collection of data, the analysis of data, and an evaluation of the implications of experimental results on the long-term stability of highly plastic clay slopes. Changes in water content, suction, and weight in the specimen were monitored during controlled infiltration and evaporation stages. Specifically, these experiments involved a

series of four soil columns. The first two soil columns were used to investigate the effect of boundary conditions on cracking. The third and fourth soil columns were constructed with lateral restraints, which proved useful in the first two soil columns. The analysis of the results collected from the third and fourth soil columns is the primary focus of the experimental study presented in this report.

The following aspects are addressed in the main body of this report to accomplish the objective of this experimental research component: (i) discussion of earlier research concerning the effects of cracking on the hydraulic properties of unsaturated highly plastic clays, (ii) description of instrumentation, testing methods and materials used in this research component, (iii) analysis of the experimental results collected from the soil columns, including assessment of the significance of findings on the stability of highly plastic clay slopes, and (iv) conclusions and recommendations.

The main body of this report presents the experimental study in six chapters. Following the introduction presented in Chapter 1, Chapter 2 provides the background on past research on the effects of cracking on the hydraulic properties of highly plastic clays. This background includes an overview of cracking in highly plastic clays, water retention characteristics of highly plastic clays, and the rates of evaporation and infiltration in highly plastic clays.

An overview of the materials and methods used in the experimental program is presented in Chapter 3. This includes a description of the soil column experiments and of the instrumentation used in this research component. The instrumentation of the soil columns is a particularly challenging aspect of this research component that merits detailed discussion.

The experimental results obtained from the testing program are presented in Chapter 4. The initial suction obtained in highly plastic clays under typical soil placement conditions is investigated. The volumetric water content, suction, and water balance data obtained from each of the soil column experiments is then presented.

Chapter 5 presents an analysis of data obtained during the experimental testing program. The analytical techniques that were used in this research component to interpret the testing program data are introduced. Specifically, data from the soil column tests are used to determine the soil water retention curves (SWRC) and the hydraulic conductivity functions (K-function) of unsaturated soils for intact and cracked clays. This is followed by a discussion of the impact of these findings on our understanding of the mechanisms governing the stability of highly plastic clay slopes. Finally, suggestions for further research involving the interpretation and application of the hydraulic properties of unsaturated highly plastic clays are presented.

The findings of this research are summarized in Chapter 6. Specifically, conclusions are drawn concerning the effect of cracking on the water retention characteristics and on the rates of evaporation and infiltration in highly plastic clays.

In addition to the experimental study, this report presents a series of evaluations based on the results obtained from laboratory testing. Specifically, this report also includes the evaluation of the depth of moisture fluctuation (Appendix A), basis for the slope stability analysis relevant to this project (Appendix B), and an evaluation of the recurrence rate of failures (Appendix C). Finally, Appendix D provides an overview of site visits conducted as part of this project to evaluate the stability of TxDOT projects involving highly plastic clays. The complimentary document, TxDOT Report 0-5202-3 (Wright and Aguettant 2006) provides the shear strength characterization.

Chapter 2. Background on Cracking and Instrumentation

Background gathered from past studies regarding the following topics are presented in this section: (i) variables controlling cracking including sources of cracks as well as techniques used to mitigate the severity of cracking, (ii) the state of knowledge concerning the effects of cracking on the water retention curve (iii) the state of knowledge concerning the effects of cracking on rates of evaporation and infiltration, and (iv) background on the physical principles underlying the operation of the instrumentation used during this research program as well as experience on the use of such instrumentation in highly plastic clays.

2.1 Cracking of Highly Plastic Clays

Cracking results when shrinkage strains occur during drying of highly plastic clay. Soil placement conditions (i.e., gravimetric water content, volumetric water content, dry unit weight, and degree of saturation) and the environmental conditions have been found to influence cracking highly plastic clays. Investigations concerning the effects of soil placement conditions and environmental conditions are summarized in the following sections.

2.1.1 Soil Placement Conditions

Aspects that have been found to influence the shrinkage of soils include the clay content of the soil, the clay mineralogy, the placement water content, and the compactive effort. Kleppe and Olson (1985) investigated the effect of clay content on shrinkage strains. They performed a series of shrinkage tests on mixtures of clay and sand, varying the clay content. The severity of cracking was found to increase with increasing clay content. The clay mineralogy of the compacted highly plastic clay was also found to affect the shrinkage strains. Smectites have the highest shrinkage susceptibility as they undergo significant volume changes with changes in water content. The clay mineralogy is typically reflected in the plasticity index of the soil, with PI > 40 generally implying high Smectite content. High PI clays are expected to have the most significant shrinkage strains.

The effect of placement water content on shrinkage was investigated by Daniel and Wu (1993). Shrinkage was found to increase with increasing placement water content. Albrecht and Benson (2001) confirmed Daniel and Wu (1993) results by showing that shrinkage strains were a function of the ratio of water volume to total volume in the compacted specimen (i.e., the volumetric water content). If a soil specimen is compacted dry of optimum water content to the same dry unit weight as a soil specimen compacted wet of optimum, the drier specimen undergoes smaller shrinkage strains. Albrecht and Benson (2001) also investigated the effect of compaction effort on the amount of shrinkage strain and found that soils compacted at higher compactive efforts generally result in lower shrinkage strains.

The previous studies focused on the assessment of cracking in compacted clay landfill liners and not on the hydraulic properties of cracked soils. Nonetheless, knowledge of the effect of soil placement conditions on cracking is important for limiting the amount of cracking that occurs in the field. According to Albrecht and Benson (2001), cracking in compacted clays can be minimized by using a soil with low clay content compacted near its optimum water content with high compactive effort.

2.1.2 Environmental Conditions

The shrinkage strains that occur during drying are affected by the environment under which the soil is dried. The influence of environmental conditions such as the potential for precipitation, evaporation and plant transpiration on the development of shrinkage strains has been investigated. The effects of specimen saturation on cracking are reported in this section to indicate possible effects of infiltration on cracking in the field. Additionally, the effects of relative humidity and evaporation rate on cracking are reported to indicate the effects of evaporation on cracking in the field.

Shrinkage strains that occur during drying have been found to increase if samples are soaked in water immediately after compaction (Kleppe and Olson 1985; Albrecht and Benson 2001). Additionally, Albrecht and Benson (2001) found that when soil specimens are compacted both wet and dry of optimum and then saturated before drying, the same shrinkage strains are observed for the two specimens. This finding further support that shrinkage strains are a function of volumetric water content (Albrecht and Benson 2001).

Kayyal (1995) investigated the effect of ambient relative humidity on the development of cracks in highly plastic clay. Specimens were compacted, submerged in water, dried in an oven at 60º C, and submerged in water a second time. Then specimens were then dried at three different relative humilities. The rate of evaporation was found to be inversely proportional to the relative humidity.

The drying process has been reported to involve three stages. The first stage involves a constant rate of water evaporation from the surface of the soil. Kayyal (1995) found that the majority of cracking in highly plastic clays occurred during the constant rate stage as the result of soil shrinkage. The second stage of the drying process is characterized by a decreasing rate of evaporation. The menisci of the air water interface decreases in curvature and finally fails to allow air to enter the specimen. Kayyal (1995) observed the formation of micro-cracks during the falling rate stage, and noted that these cracks most likely result from suction gradients that impart stress within the soil specimen. The third stage of evaporation occurs when the rate of evaporation decreases to the point at which evaporation occurs principally by diffusion. Accordingly, low initial volumetric water content and a high relative humidity during drying can help in mitigating the amount of cracking.

The effect of the evaporation rate on cracking was evaluated theoretically by Abu-Hejleh and Znidarčić (1995). Abu-Hejleh and Znidarčić (1995) developed a desiccation theory to model the propagation of cracks in mine dredgings. The authors conducted experimental analysis to determine the characteristics of clay during drying and used their model to predict settlement, pore pressure distributions, void ratio distribution, depth of cracking, and cracking volume with time under different evaporation conditions. Abu-Hejleh and Znidarčić (1995) predicted larger cracking depths and cracking volumes than under slower evaporation rates using their model. Several other theories concerning the mechanical aspects of cracking have also been proposed (Konrad and Ayad 1997; Alonso and Gens 1999; and Augier et al. 2002).

2.2 Water Retention Characteristics of Highly Plastic Clays

The shape of the soil-water retention curve (i.e., the relationship between the volumetric water content and soil suction) has been reported to be affected by the soil index of plasticity, compaction gravimetric water content, and compactive effort among other variables. The significance of these variables on the SWRC, if any, has been a controversial issue in the literature.

Tinjum et al. (1997) found that SWRC for highly plastic clays typically plots above clays of low plasticity. Miller et al. (2002) confirmed this trend. The shape of the SWRC for highly plastic clay is often characterized as "shallow" because significant changes in suction correspond to small changes in volumetric water content.

The effect of placement water content on the shape of the SWRC was investigated by Tinjum et al. (1997) using results from pressure plate extractor tests. In this research component, specimens were compacted at optimum water content and water contents approximately ± 5% of optimum. Higher air entry pressures were measured for clays compacted wet of optimum. The SWRC was also found to have a more significant gradient ($d\theta/d\psi$) when soil is compacted wet of optimum, while lower gradient for soils with a higher plasticity index was observed. Over the range in water content tested, the effect of water content on the shape of the SWRC was found to outweigh the effect of compactive effort. Tinjum et al. (1997) attributed this effect to the soil clod theory (Olson 1962; Benson and Daniel 1990).

Zornberg et al. (2003) evaluated the effect of compaction effort and placement water content on the SWRCs of low plasticity clays. The SWRCs were obtained using hanging column tests for lower suctions, pressure plate extractor tests for midrange suctions, and thermocouple psychrometer tests for higher suctions. Unlike the results reported by Tinjum et al. (1997), Zornberg et al. (2003) found essentially no effect of placement water content and compactive effort on the SWRC.

Miller et al. (2002) also investigated the effect of water content on the shape of the SWRC. A pressure membrane apparatus was used to measure the SWRC of compacted clays. Soils were compacted at gravimetric water contents ± 2% of optimum. The placement water content was found to have little impact on the SWRC within the relatively narrow range of water contents tested. The compaction effort was, however, found to have a significant effect on the shape of the SWRC. Soils placed with higher compactive efforts were observed to have higher suctions for the same volumetric water content than soils prepared with lower compactive effort. SWRCs were also measured for soil samples collected in the field. No significant difference was observed between the measured SWRCs of field and laboratory specimens.

2.3 Evaporation and Infiltration Rates

2.3.1 The Hydraulic Conductivity of Saturated Highly Plastic Clays that have Undergone Cracking

The hydraulic conductivity of saturated highly plastic clays that have undergone cracking has been investigated in studies related to waste containment. Cracking of compacted clay liners occurs as water evaporates from the soil during construction of the liner and throughout its service life. Past studies have indicated that confinement has a significant effect on the hydraulic conductivity of saturated cracked clays. Boyton and Daniel (1980) investigated cracking in compacted clays and found that the hydraulic conductivity of saturated specimens that have undergone cracking decreases with increasing effective stress. The measured hydraulic conductivity was, however, observed to remain approximately constant at an effective stress greater than 56 kPa. The decrease in hydraulic conductivity with increasing effective stress was attributed to the closing of cracks within the specimens. Sims et al. (1996) performed similar tests and confirmed this trend in hydraulic conductivity (up until effective stresses of 120 kPa).

A similar investigation by Albrecht and Benson (2001) showed that healing of cracks is unlikely despite prolonged periods of hydration unless confinement is applied. To achieve a

hydraulic conductivity less than 1×10^{-7} cm/s, an effective stress greater than 60 kPa was required, which is consistent with results reported by Boyton and Daniel (1980).

2.4 Effect of Soil Placement Conditions on K-function

Meerdink et al. (1996) measured the hydraulic conductivity function (K-function) of unsaturated soils for two compacted clays in the field and laboratory. Suction and volumetric water content were measured along a vertical soil profile. Suction was measured using thermocouple psychrometers and tensiometers. Volumetric water content was measured using time domain reflectometry. Meerdink et al. (1996) used the instant profiling method to determine the K-function. The instant profiling method is described in Section 5.3.2. In the laboratory, a fan was used to blow air across the top of specimens and used to obtain the K-function during drying. Then, a controlled flow rate of water was applied to the top of the column and used to obtain the K- function during wetting. The placement water content was found to have little effect on the K-function above 200 kPa of suction for samples compacted wet and dry of optimum. The compactive effort was found to strongly affect the K-function for suctions greater than 200 kPa. Specifically, the hydraulic conductivity obtained in specimens compacted under modified Proctor compaction effort resulted was an order of magnitude lower hydraulic conductivity than that of specimens compacted using standard Proctor compaction effort. Meerdink et al. also measured the hydraulic conductivity of saturated laboratory specimens compacted dry and wet of optimum water content. The hydraulic conductivity measured for specimens compacted dry of optimum water content was two orders of magnitude greater than the hydraulic conductivity of specimens compacted wet of optimum.

2.4.1 Effect of Cracking on the K-function

Meerdink et al. (1996) found that the K-function of compacted clay is unaffected by water content at suctions greater than 200 kPa. Based on this observation, Meerdink et al. (1996) proposed that the increase in the hydraulic conductivity of saturated clay associated with compacting dry of optimum may not be a problem in arid regions where the soil typically remains dry throughout the year. Meerdink et al. (1995) suggested compacting clays dry of optimum to minimize the shrinkage strains and resulting cracking associated with compaction at higher volumetric water contents while maintaining the same K-function at suctions greater than 200 kPa.

In review of Meerdink et al.'s (1997) results, Day (1997) indicated that compacting clays dry of optimum results in significant soil swelling during periods of high precipitation. Drying was observed to result in reduction of soil volume, but this reduction in volume did not return the soil to its original density. Day (1997) indicated that compaction of soil to high density was not practical when repairing compacted clay liners, as swelling occurs at the low confining stresses typical for liners and ultimately leads to a reduced density. Meerdink et al. (1997) responded by pointing out that experimental results observed by Albrecht (1996) supported compacting dry of optimum because of the associated reduction in shrinkage strains. Additionally, Meerdink et al. (1997) indicated that "intuition and data in the literature" supported the idea that cracking has little effect on the K-function. Meerdink et al. (1997) suggested that cracking may possibly decrease the K-function due to the reduction in void ratio occurring with cracking.

Aubeny and Lytton (2003) took a different approach to evaluate the flow of water in unsaturated compacted highly plastic clays slopes. The laboratory component of Aubeny and Lytton's study consisted of measuring the time-dependent changes in suction within a Shelby

tube of sampled highly plastic clay. One face of the tube was open to the atmosphere to allow evaporation. A "diffusion coefficient" was then back-calculated using measurements from the experiment. Aubeny and Lytton (2003) conducted a flow analysis using the estimated diffusion coefficient. The diffusion process was assumed to take place from a boundary located at the furthest depth of cracking. Aubeny and Lytton (2003) reported eight feet as a typical cracking depth. The suction at the bottom of the cracks was reported to range from 10 to 100 kPa, and the initial suction after compaction operations was assumed to range from 300 to 1000 kPa. Water movement was evaluated between the boundary at the furthest depth of cracking and the underlying soil. These conditions led to loss in suction at depth (i.e., increasing water content), and slope failure was considered to occur because of the decrease in suction to a point at which the stability of the slope is compromised.

2.5 Background on Instrumentation Used in this Research Component

2.5.1 Time Domain Reflectometry Probes

Time domain reflectometry (TDR) probes were used in this research component to measure the volumetric water content and define the vertical volumetric water content profiles in the soil column experiments. TDR technology involves measurement of the dielectric constant of soil. The dielectric constant is a material property that reflects the material's ability to attenuate an external electrical field. The bulk dielectric constant of the soil depends on the dielectric constant values of each of the soil constituents: soil particles, water, and air. The dielectric constant of water is an order of magnitude greater than that of soil particles, because water is a strong electric dipole with the ability to freely rotate as a fluid. Consequently, the bulk dielectric constant of soil is strongly affected by its volumetric water content. The measured dielectric constant of soil can be calibrated to define the soil volumetric water content.

Commonly used TDR probes consist of a set of parallel metal rods of various lengths, diameters, and spacings. The probes used in this research component have three rods that are 80 mm in length, 3.2 mm in diameter, and a spacing of 25 mm between the outer rods (Figure 2.1). The central rod acts as the transmission line in a coaxial cable, and the two outer rods act as shields. These probes are used in combination with a cable tester. The cable tester applies voltage pulses to the probe with a rise-time of nanoseconds and measures the time of the reflected wave form with a resolution of nanoseconds.

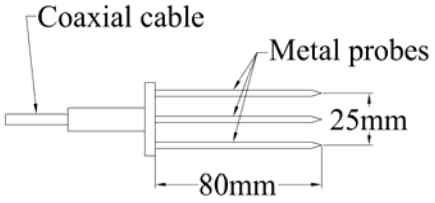

Figure 2.1: TDR probe schematic (Model 6111 Mini Buriable Waveguide, Soilmoisture Equipment Corporation)

TDR probe measurements are obtained by transmitting an electrical pulse through a coaxial cable attached to the TDR probe. Upon reaching the TDR probe, two reflections can be observed. The first reflection occurs when the pulse transitions from the coaxial cable to the metal rods, and the second occurs when the signal reaches the end of the metal rod. The time difference between the arrivals of the two reflections at the cable tester can be used to define the dielectric constant of the surrounding medium.

The relationship between the dielectric constant and the time difference between reflections can be derived as follows: The velocity (v) of the electromagnetic wave traveling through the probe equals the length of travel (twice the length of the TDR probe, $2L$) divided by the time between the two signals (Siddiqui et al. 2000):

$$v = \frac{2L}{t} \qquad \text{Equation 2.01}$$

The wave velocity equals the speed of light in a vacuum, c, divided by the square root of the apparent dielectric constant of the insulating material, Ka (Siddiqui et al. 2000):

$$v = \frac{c}{\sqrt{Ka}} \qquad \text{Equation 2.02}$$

By combining Equation 2.01 and Equation 2.02, the apparent dielectric constant of the soil can be determined from the time of travel:

$$K_a = \left(\frac{ct}{2L}\right)^2 \qquad \text{Equation 2.03}$$

Because the speed of light in a vacuum and the length of a particular probe are constant values, the time of travel or the inferred dielectric constant can be correlated with the soil volumetric water content.

The TDR probe allows measurement of the dielectric constant of the soil between the outer rods and within a field that extends around the rod (Cabral et al. 1999). For the TDR probes used in this research component, the zone of measurement involves a width of 25 mm within the plane of the rods. As a result, TDR probes provide an average reading of volumetric water content within a small volume of soil.

To measure the soil dielectric constant, a graph of voltage versus time can be used to define the time between reflections. The time between reflections may be defined manually or using the cable tester's built-in software. The software package for the cable tester used in this research component has a built-in software package called TRASE (Soil Moisture Equipment Corp., Santa Barbra Ca.). When the cable tester is set to autolog, the unit constructs tangent lines for the incoming and reflected pulses and calculates the travel time. In highly plastic clays, highly organic soils, clays with high electrical conductance, soils with saline pore water, and soils compacted at very high or very low densities, the two reflections may not be sufficiently clear. This is caused by excessive dissipation of the pulse as it travels through the soil. In this case, the TRASE software does not return a value of volumetric water content and the results must be analyzed graphically. Graphical interpretation requires significant data storage and does not allow the user to monitor water content continually with time. Graphical interpretation does, however, allow for consistent measurements to be taken in soils that are typically considered problematic for TDR measurements.

The problem with performing TDR measurements in highly plastic clay is the poor signal reflections which result from high energy dissipation. This high degree of energy dissipation is a result of the high electrical conductivity of the soil which results in attenuation of the signal in the soil. As a result, a diminished signal is returned to the cable tester. Empirical relationships between volumetric water content and TDR probe measurements have been developed, but these relationships have been reported to yield inaccurate results for highly plastic clays (Roth et al. 1990). This problem can be minimized by coating the probes with an insulation material of low electrical conductivity, such as latex paint. The use of coating was investigated in this research component but was not implemented due to uncertainty as to the wear of the coating with time. Instead, a soil-specific calibration was performed using uncoated probes in the Eagle Ford clay and is presented in Section 3.3. A full discussion concerning the use of coated TDR probes in Eagle Ford clay can be found in Kuhn (2005).

2.5.2 Heat Dissipation Unit Probes

Heat dissipation unit (HDU) probes were used in this research component to measure vertical suction profiles during the soil column experiments. Unlike other suction measurement techniques (e.g., tensiometers, thermocouple psychrometers), HDU probes require only minimal maintenance and can accurately measure suction values ranging from 10 to 1,000 kPa. Accordingly, HDU probes cover most of the suction range covered by tensiometers and most of that covered by thermocouple psychrometers (Scanlon 2002). HDU probes are also more durable than thermocouple psychrometers and can be placed in the soil before compaction. Also, high water contents do not damage HDUs; as in the case with thermocouple psychrometers.

HDU probes infer soil suction by measuring the change in temperature of a ceramic stone in response to a timed heat pulse. The observed temperature increase is a function of the thermal conductivity of the ceramic, which is in turn a function of the volumetric water content of the ceramic. Because the suction within the soil is in equilibrium with the suction in the ceramic, the temperature response of the ceramic can be reliably correlated to the soil suction. Typical relationships between thermal conductivity and suction are shown in Figures 2.2(a), while typical soil water retention curves of the HDU probes are shown in and 2.2(b) (Scanlon et al. 2002). In summary, the relationship between temperature rise and matric potential can be stated as a function of the ceramic thermal conductivity, the ceramic water content, the ceramic matric potential and the soil matric potential. Although suction is measured indirectly when using HDU probes, the sensors are calibrated by applying a known suction, and measuring a temperature rise.

The HDU probes used in this research component consist of a heating element and thermocouple junction contained inside of a needle, which is pushed inside of a porous ceramic stone (Figure 2.3). Although the components of the HDU probes are identical, small manufacturing differences require performing probe-specific calibrations. The air entry pressure of the porous ceramic is approximately 10 kPa. Accordingly, when an HDU probe is placed into a soil mass with a suction exceeding 10 kPa, the pressure inside the ceramic body comes to equilibrium with the pressure in the surrounding soil matrix. The sensitivity of the HDU probe to changes in suction is a function of its pore size distribution. The volumetric water content of the HDU probe varies significantly for suctions ranging from 10 to 500 kPa. The thermal conductivity of the sensor also varies significantly between 10 and 500 kPa (Figure 2.2(a)). This results in the greatest sensitivity within this range of suction. At matric potentials ranging from 500 to 1,000,000 kPa, the volumetric water content of the ceramic approaches its residual water

content and results in less sensitive measurements. However, readings taken when the ceramic is near its residual water content have been reported by some researchers (Reedy 2004; Flint et al. 2002).

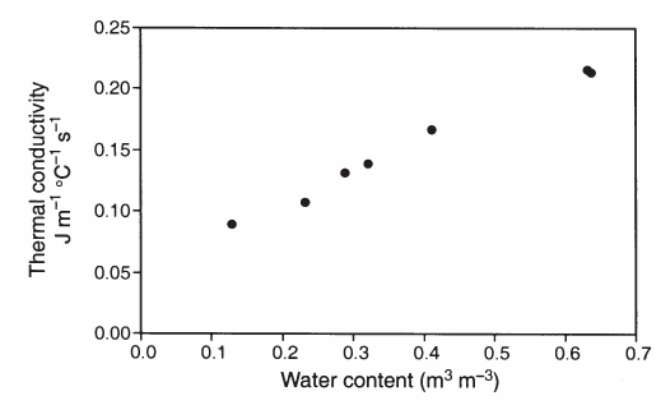

(a)

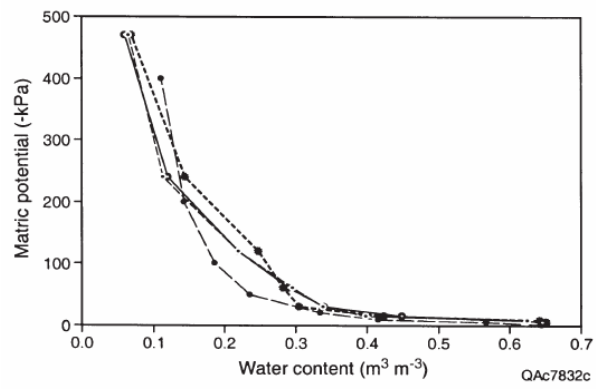

(b)

Figure 2.2: HDU responses: (a) Thermal conductivity of HDU over range in water contents (Scanlon et al. 2002); (b) Typical water retention curves for HDUs (Scanlon et al. 2002)

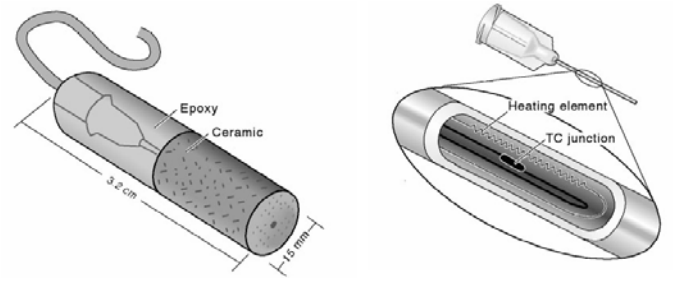

Figure 2.3: HDU body and heating assembly
(Model 229-L Campbell Scientific, Logan Utah)

Chapter 3. Materials and Methods Used in the Experimental Program

3.1 Characterization of Eagle Ford Clay

The highly plastic clay used for the experimental testing program conducted in this research component was obtained from an outcrop of Eagle Ford Shale in Round Rock, Texas. The clay was excavated with a backhoe from a depth of approximately 10 ft on the Southeast embankment of the intersection of Hester's Crossing and Interstate 35. The clay was transported to the laboratory at The University of Texas in plastic 55-gallon drums.

The clay was dried by placing it on metal trays in a temperature controlled room at a temperature of 49°C for a minimum of 48 hours. The dry soil was then broken down with a hammer and passed through a soil crushing machine (Chipmunk Jaw Crusher model VD 67, Bico Inc., Burbank, CA). The soil was then sieved and particles passing the # 10 sieve were set aside for testing. Particles not passing the #10 sieve were reprocessed using the soil crushing machine until the material passed the # 10 sieve.

Standard geotechnical index properties were obtained. These included specific gravity, Atterberg limits, particle size distribution, and compaction curves based on standard Proctor and modified Proctor compaction. All of these index properties were determined in general accordance with American Society of Testing and Materials (ASTM) Standards. Measured properties of Eagle Ford clay and the associated ASTM standards are summarized in Table 3.1.

Table 3.1 Properties of Eagle Ford clay

Test	Index Parameter	Value	ASTM Standard
Specific Gravity	Specific Gravity, G_s	2.74	D 845-02
Atterberg Limits	Liquid Limit, LL	88	D 4318
	Plastic Limit, PL	39	D 4318
	Shrinkage Limit, SL	18	D 4943
Particle Size Analysis	% Passing 0.075 mm (# 200 Sieve)	97	D 422-63
	% Passing 0.002 mm	76	D 422-63
Standard Proctor Compaction	Optimum water content, %	24	D 1557
	Maximum dry unit weight, $\gamma_{d\,max}$ (kN/m^3)	15.2	D 1557
Modified Proctor Compaction	Optimum water content, ω_{opt} (%)	14	D 698
	Maximum dry unit weight, $\gamma_{d\,max}$ (kN/m^3)	17.8	D 698
Hydraulic Conductivity of Saturated Soil	Hydraulic conductivity of Saturated Soil, K_{sat} (cm/s) (ω = 24%; γ_d= 15.2 kN/m3)	2×10^{-10}	D 5084

3.1.1 Specific Gravity

Two specific gravity measurements of the processed soil were performed. The specific gravity values obtained were 2.731 and 2.742. The average of these two measurements is reported in Table 3.1.

3.1.2 Atterberg Limits

The Atterberg limits were determined for the fraction of the processed soil passing the #40 sieve. A plasticity index of 49 was measured (Table 3.1). The Eagle Ford clay classifies as highly plastic clay (CH) according to the Unified Soil Classification System. A shrinkage limit of 18 was measured for The Eagle Ford clay.

3.1.3 Particle Size Distribution

A sieve analysis was not conducted on the Eagle Ford clay since 100% of the soil particles passed the #10 sieve after processing. A hydrometer test was conducted on the processed material to determine the particle size distribution. The resulting particle size distribution for Eagle Ford clay is shown in Figure 3.1. The particle size distribution curve indicates that less than 4% of the Eagle Ford clay consists of sand size particles (particle size coarser than 0.075 mm). The grain size distribution curve also indicates that approximately 76% of the Eagle Ford clay consists of clay size particles (particle size smaller than 0.002 mm).

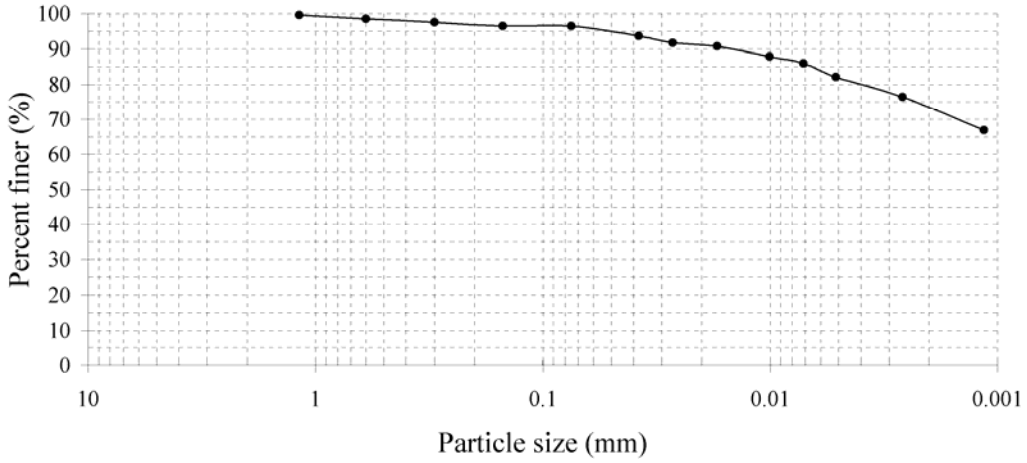

Figure 3.1: Particle size distribution curve for Eagle Ford clay

3.1.4 Compaction Characteristics

Standard and modified Proctor compaction tests were conducted on the processed soil (ASTM D 1557 and D 698). The compaction curves are shown in Figure 3.2. The optimum water content is approximately 14% for modified Proctor compaction and 24% for standard Proctor compaction. The maximum dry unit weight is 113.5 pcf (17.8 kN/m^3) for modified Proctor compaction and 97 pcf (15.2 kN/m^3) for standard Proctor compaction (Table 3.1).

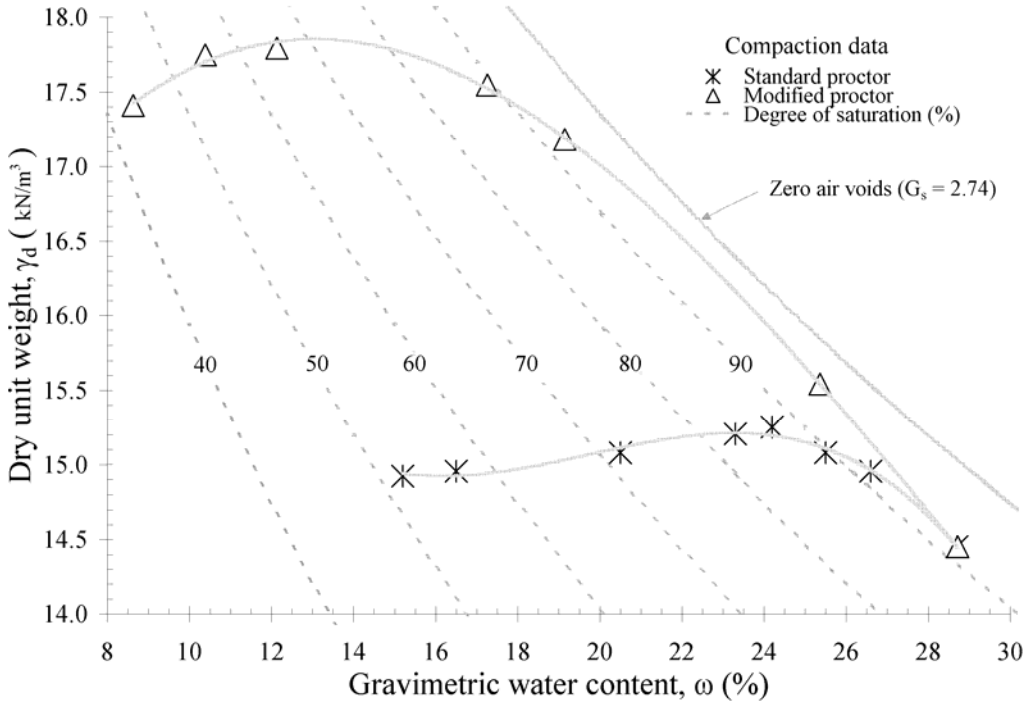

Figure 3.2: Compaction curves for Eagle Ford clay

3.1.5 Hydraulic Conductivity of Saturated Eagle Ford Clay

The hydraulic conductivity was measured for a saturated specimen compacted at optimum water content. The hydraulic conductivity was measured as 2 x 10^{-10} cm/s.

3.2 Setup of the Experimental Testing Program

A series of evaporation and infiltration experiments was conducted to characterize the effects of cracking on the hydraulic properties of unsaturated highly plastic clays. Additional experiments were conducted to evaluate the soil placement conditions (i.e., soil conditions immediately after compaction operations). Details of each experiment are included in this section. A summary of the experimental testing program is shown in Table 3.2. Specifically, the main characteristics of the tests conducted to evaluate soil placement conditions and of the soil column tests conducted to characterize the effects of cracking on the hydraulic properties of unsaturated highly plastic clay are presented. The table includes the boundary conditions, soil placement conditions, the sequence of testing, and the variables measured for each experiment. The boundary conditions, evaluation of soil placement conditions, construction of soil columns, and the material and methods for constructing soil columns are discussed in the subsequent sections.

Table 3.2 Summary of experimental testing program

	Objective	Evaluation of soil placement conditions						Characterization of the effects of cracking on the hydraulic properties of unsaturated highly plastic clay			
	Experiment	Atmospheric boundary condition			Suction under soil placement conditions			Soil Column 1	Soil Column 2	Soil Column 3	Soil Column 4
		Controlled Suction			HDC measurement			laterally-unrestrained	rigid laterally-restrained	rigid laterally-restrained	rigid laterally-restrained
Boundary Condition	Top	Controlled temp and humidity 25°C 32, 68, 83, & 97% RH			N/A			Controlled temp and humidity 25°C 55% RH	Controlled temp and humidity 25°C 55% RH	Controlled temp and humidity 42°C 15% RH Constant head 2.5 cm of water	Controlled temp. and humidity 25°C 55% RH
	Sidewall	Unrestrained			N/A			Unrestrained	Restrained Rigid metal screw-	Restrained Rigid plastic screw-	Restrained Rigid plastic screws
	Bottom	Controlled temp and humidity 25°C 32, 68, 83, & 97% RH			N/A			No flow	No flow	No flow	No flow
Soil placement conditions		1	2	3	1	2	3				
	Gravimetric water content, ω (%)	18	22	25	20	22	24	34	34	22	26
	Volumetric water content, θ (%)	28	34	33	31	34	32	45	45	34	40
	Dry unit weight, γ_d (kN/m³)	15.0	15.2	15.2	15.2	15.2	15.2	13.0	13.0	15.2	15.1
	Degree of Saturation, S (%)	62	76	61	68	76	83	86	86	76	90
Testing stages	1	Controlled Suction			Equilibration of HDC sensor			Evaporation	Evaporation	Evaporation	Evaporation
	2	N/A			N/A			N/A	N/A	Infiltration	Infiltration
	3	N/A			N/A			N/A	N/A	Evaporation	Evaporation
Variables measured	Soil Water Retention Curve (SWRC)	N/A			N/A			N/A	N/A	Measured (TDR and HDC) 1st Evaporation phase Infiltration phase, & 2nd Evaporation phase	Measured (TDR and HDC) 1st Evaporation phase Infiltration phase, & 2nd Evaporation phase
	Time-mass relationship	Intact specimen Initial mass and mass at 85% Data			N/A			Intact specimen Intermittent mass via laboratory scale	Cracked specimen Continuous mass via load cell	N/A Instrumentation problem	Measured data reported in Fredlund (2006)
	Hydraulic conductivity function for unsaturated soil (K-function)	N/A			N/A			N/A	N/A	Calculated (instantaneous-profiling method) 1st Evaporation phase & 2nd Evaporation phase	Calculated (instantaneous-profiling method) 1st Evaporation phase & 2nd Evaporation phase

3.2.1 Boundary Conditions

The evaporation and infiltration experiments involved compacting soil into circular tubes with rigid sidewalls. Specifically, clear polyvinylchloride (PVC) tubing ranging from 152 mm to 203 mm in diameter and 100 mm to 250 mm in length was used (the circular ends of the tubes were oriented horizontally for the experiments). Three boundary conditions had to be selected for each experiment; one at the top end of the tube, one at the bottom end of the tube, and one at the sidewalls of the tube. The temperature and relative humidity were controlled at the top boundary while the tube was closed at its bottom boundary creating a no-flow boundary. In several of the soil columns screws were used to restrain the soil laterally. Restraints were used in Soil Column 2, Soil Column 3, and Soil Column 4, as will be discussed in Section 3.2.4, 3.2.5, and 3.2.6, respectively. No lateral restraint was used in Soil Column 1.

The suction at boundaries where temperature and relative humidity were controlled was determined using Kelvin's equation (Lu and Likos 2005). Kelvin's equation is typically expressed in terms of total suction, as follows:

$$\Psi_t = -\frac{RT}{\upsilon_{wO}\omega_v}\ln(RH) \qquad \text{Equation 3.1}$$

Where, R = universal gas constant (8.2144 J/mol-K), T = absolute temperature in Kelvin, $\upsilon_{\omega o}$ = saturated vapor pressure of free water in kilopascals at temperature T, and ω_v = molecular weight of water (equal to 18.06 kg/Kmol).

The suction, defined using Kelvin's equation, for relative humidity values ranging from 0 to 100% is shown in Figure 3.3 for temperatures of 0, 20, and 40° C. Over the range of temperatures used during this research component, the effect of temperature on total suction was found to be negligible when compared to the effect of relative humidity.

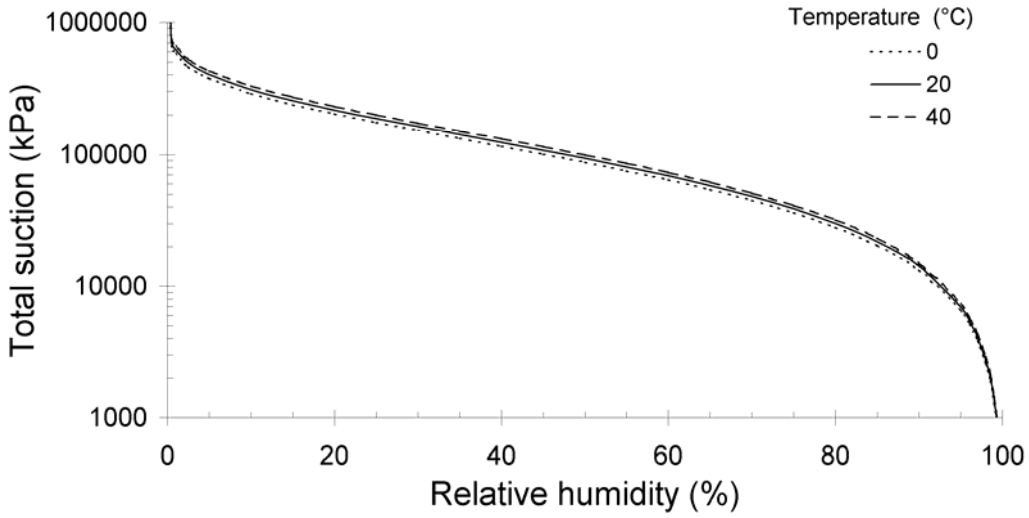

Figure 3.3: Kelvin's equation for total suction plotted for full range of values of relative humidity at various temperatures

The evaluation of soil placement conditions also involved compacting soil into circular tubes with rigid sidewalls. Specifically, a 10 mm length of 2 mm thick aluminum tubing with an inner diameter of 54 mm was used for individual soil samples. Top, bottom and sidewall boundary conditions were selected. The temperature and relative humidity were controlled at the top and bottom boundaries. No form of lateral restraint was used. The suction at the bottom and top boundary conditions was calculated using Kelvin's equation (Equation 3.1) based on measured temperature and the relative humidity for various saturated salt solutions (Greenspan 1976).

3.2.2 Quantification of Suction under Initial Soil Placement Conditions

Soil conditions immediately after compaction operations affect the magnitude of suction within the soil. This "initial suction" affects water flow within an embankment. Two experiments were conducted to evaluate the effects of soil placement on the magnitude of the initial suction. One experiment was conducted to evaluate the effect of relative humidity on moisture movement after soil placement, while another experiment was conducted to measure the initial suction for different soil placement conditions.

To evaluate the effect of relative humidity as a boundary condition, soil samples were compacted using three different placement conditions and were allowed to reach equilibrium under four different values of relative humidity. Different saturated salt solutions were used to maintain relative humidity values of 33%, 68%, 84%, and 97%. The saturated salt solutions used in this experiment and the total suction value corresponding to the relative humidity based on Equation 3.1 for a temperature of 25°C are shown in Table 3.3.

Table 3.3 Suctions for saturated salt solutions

Saturated aqueous salt solution	Relative humidity, RH (%)	Suction, ψ (kPa)
Magnesium chloride	32.8	153009
Cupric chloride	68.4	52102
Potassium Chloride	84.3	23365
Potassium Sulfate	97.3	3755

Soil was compacted at gravimetric water contents dry and wet of optimum. The soil was compacted into a stack of four 10 mm high and 54 mm inner diameter aluminum tubes. Rings from individual stacks were then separated with a wire saw to obtain four specimens of the same initial water content and dry unit weight (Figure 3.4). A soil specimen from each compaction water content group were each placed atop a geonet, stacked atop one another, and placed atop a plastic pedestal in each of the four relative humidity environments involving airtight jars containing different saturated salt solutions (Figure 3.5). The geonet layer atop which each soil specimen was placed was 5 mm thick and was used to ensure that the all of the upper and lower boundaries were exposed to the same relative humidity. After 850 hours, the specimens were removed and placed in an oven to measure their gravimetric water content. The measurements of gravimetric water content obtained in this experiment are discussed in Section 4.1.

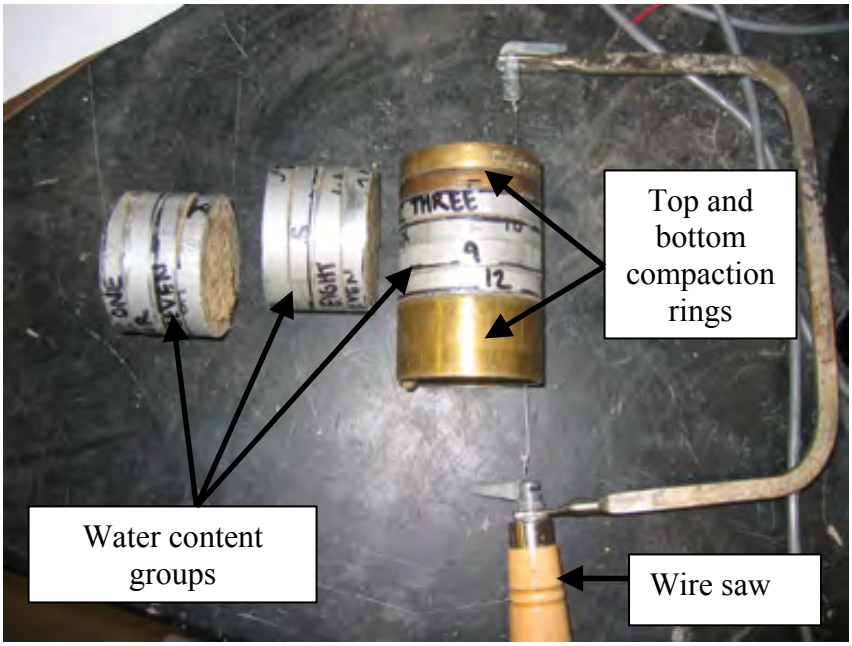

Figure 3.4: Trimming of compaction water content groups for relative humidity experiment

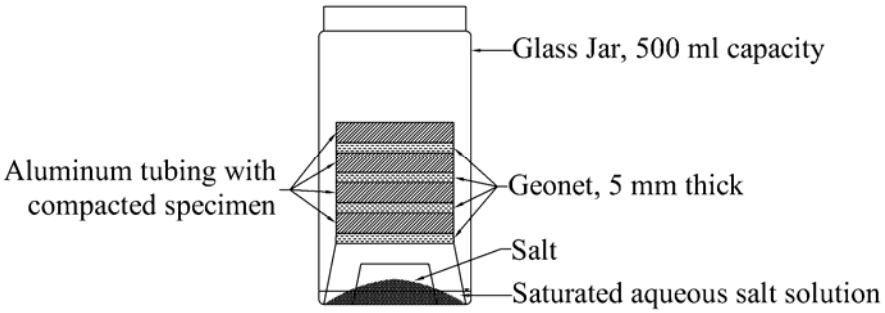

Figure 3.5: Compacted specimens in glass jar containing saturated aqueous salt solution

In the second experiment, HDU probes were used to measure the suction in specimens placed under different soil placement conditions. Soil was compacted into a standard Proctor mold at gravimetric water contents of 20%, 22%, and 24% using standard Proctor compactive effort (ASTM D698). Following the manufacturer's recommended procedure, the HDU probes were submerged in water for 24 hours before being placed in the soil specimens. The cylinder of soil was then extruded and a spade bit was used to form a hole slightly smaller than the outside

diameter of the HDU probe. The HDU probes were then pushed into the soil specimen using hand pressure. The soil cylinders containing the HUD probes were then placed into separate airtight low density polyethylene bags. HDU probe readings were taken at 8-minute intervals until the temperature rise occurring between 2 and 20 seconds of heating did not change by more than 0.01°C between subsequent readings.

3.2.3 Construction of the Soil Columns

A series of soil column experiments was performed to investigate the effect of cracking on the hydraulic properties of unsaturated highly plastic clay. Specifically, four instrumented soil columns were constructed using different boundary conditions. Out of these experiments, the analysis of results of Soil Columns 3 and 4 is the main focus of this research. The construction of Soil Column 3 is similar to the construction of other soil columns used in this research component and is described in detail in Kuhn (2005). A schematic layout of Soil Column 3 is presented in Figure 3.6. Soil Column 4 is nearly identical to Soil Column 3 with the exception that it is 15 cm in height rather than 25. A full description of Soil Column 4 is available in Freilich (2006). Specific differences in the other columns are discussed in Sections 3.2.4 to 3.2.6.

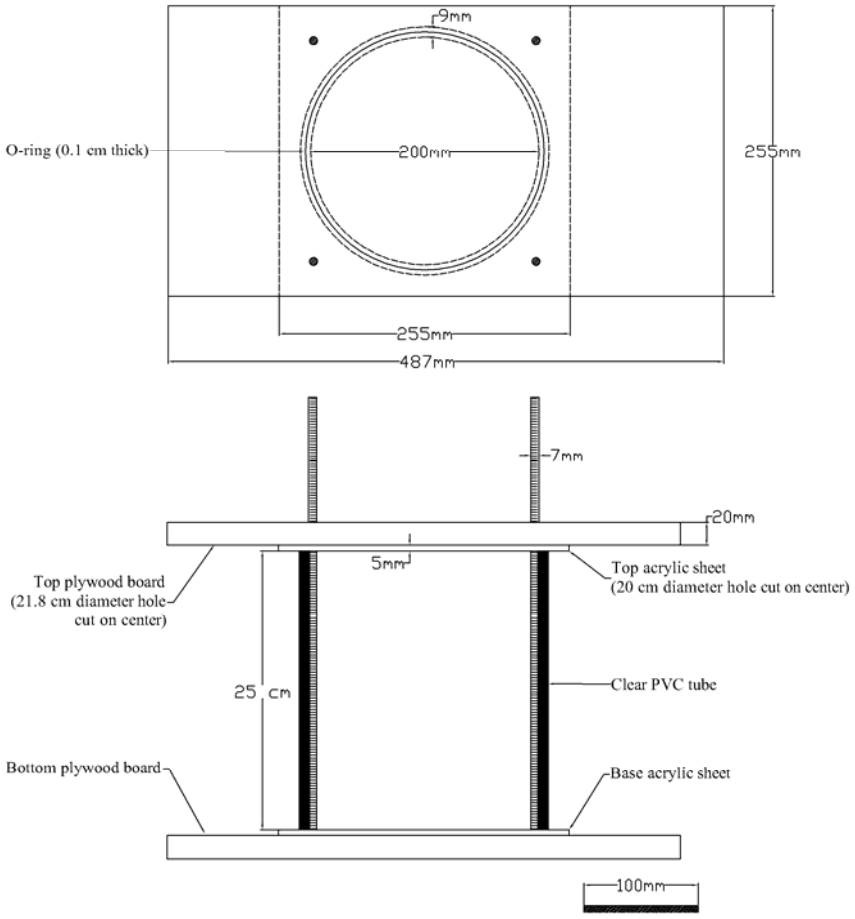

Figure 3.6: Schematic of Column 3

3.2.4 Description of Preliminary Soil Columns

Initial investigations of the effect of cracking on the Hydraulic Properties of Unsaturated Highly Plastic Clay led to the design and use of two preliminary soil columns. Soil Column 1 consisted of a clear acrylic cylinder 225 mm in height and 152 mm in diameter. The soil in this soil column was compacted at a high gravimetric water content of 34% in order to encourage cracking during initial testing. The soil column was instrumented with TDR probes to measure volumetric water content and HDU probes to measure suction. TDR and HDU probes were placed at 50 and 100 mm below the top surface of the compacted soil. These sensors groups are referred to as Level A (bottom sensor) and Level B (top sensor). The elevation of the sensors actually changed as the soil shrunk or swelled. The TDR probes were placed into the soil layer before compaction. The HDU probes were inserted into the sides of the soil column after compaction by drilling a hole slightly smaller than the probe and inserting the probe with hand pressure. The weight of the entire soil column was measured periodically by placing the entire soil column and apparatus on an electronic balance accurate to ± 5 grams.

Digital photos of the top surface and sides of the soil column were taken periodically. As will be detailed in Section 4.2.1, the soil was unrestrained laterally and volumetric changes caused the specimen to detach from the sidewalls, which led to subsequent closing of cracks that initially developed.

A fan was used to blow air across the top of the soil column to control the temperature and relative humidity at the top boundary. The ambient temperature of the laboratory, measured using a thermometer, ranged from 20 to 25° C. The ambient relativity humidity, measured with a humidity gauge, ranged from 40 to 50%. The total suction at the top boundary obtained using Equation 3.1 was approximately 100,000 kPa. Because separation of the specimen from the sidewalls was not prevented, Soil Column 1 is referred to as a "laterally-unrestrained" soil column.

Soil Column 2 was used to investigate the rate of evaporation from a cracked clay specimen. To avoid separation between the soil and sidewalls (as in Soil Column 1), Soil Column 2 incorporated measures to minimize separation of the soil from the column walls. This soil column was 203 mm in diameter and 40 mm in height. The soil in Soil Column 2 was compacted at 34% gravimetric water content to a dry unit weight of 13.0 kN/m^3 (Table 3.2). This corresponds to a degree of saturation of 86% and a volumetric water content of 45%. Sheet metal screws with a 2.9 mm inner diameter and 3.5 mm outer diameter were driven through 2.8 mm diameter pilot holes in the column sidewalls and 20 mm into the soil to minimize separation of the soil from the sidewalls during drying. The screws were placed at intervals of 22.5° around the perimeter of the soil column and at 5 mm intervals of height above the base of the soil column (Figure 3.7). The metal screws provided lateral restraint but were fixed rigidly against vertical movement along the sidewalls. Soil Column 2 is referred to as a "rigid laterally-restrained" soil column. Soil Column 2 is believed to have provided a better representation of field conditions by allowing desiccation cracks to remain open, rather than having cracks close during drying as observed in Soil Column 1.

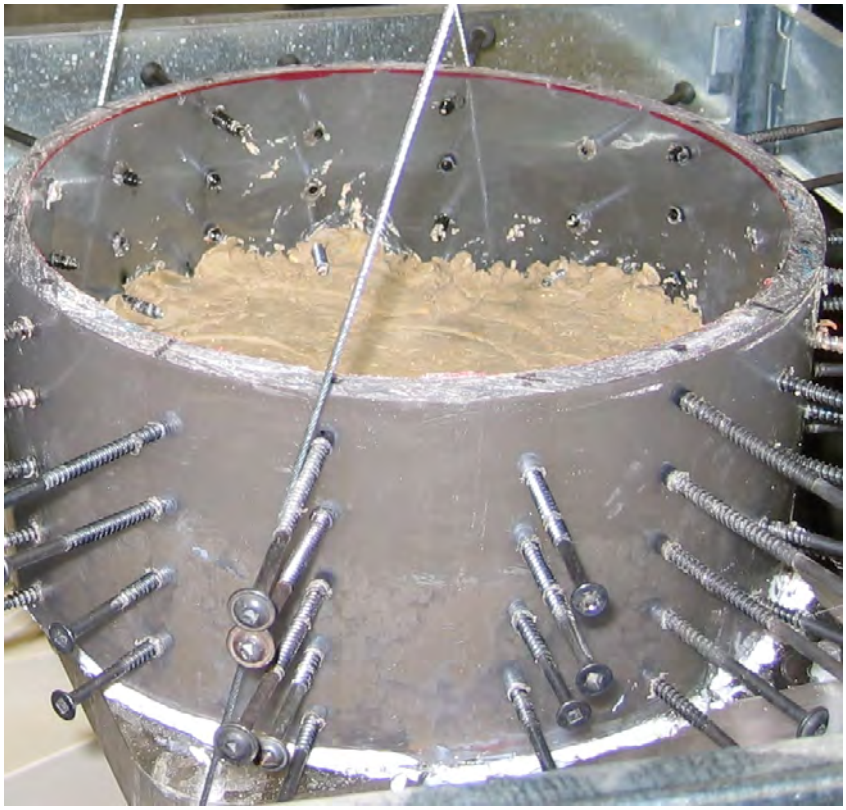

Figure 3.7: Soil Column 2

3.2.5 Description of Soil Column 3 and Soil Column 4

The third and fourth soil columns were constructed to measure water content and suction with time while keeping the specimen from separating from the sidewalls. The design of Soil Columns 3 and 4 combined the water content and suction monitoring capabilities of Soil Column 1 with the prevention of sidewall separation achieved in Soil Column 2. Soil Column 3 is 203 mm in diameter and 250 mm in height. Soil Column 4 was constructed after testing of Soil Column 3 was concluded. Because the upper two sensor layers in Soil Column 3 provided sufficient data for evaluation of the SWRC and K-function of cracked Eagle Ford clay, Soil Column 3 was constructed to a height of 250mm in order to expedite testing. It should be noted that Column 4, as referred to in this document, is not the same as Column 4 referenced in Kuhn (2005). Soil Column 4 as described in this document was tested after Kuhn (2005) was submitted to the university. An illustration of Soil Column 3 is shown in Figure 3.8.

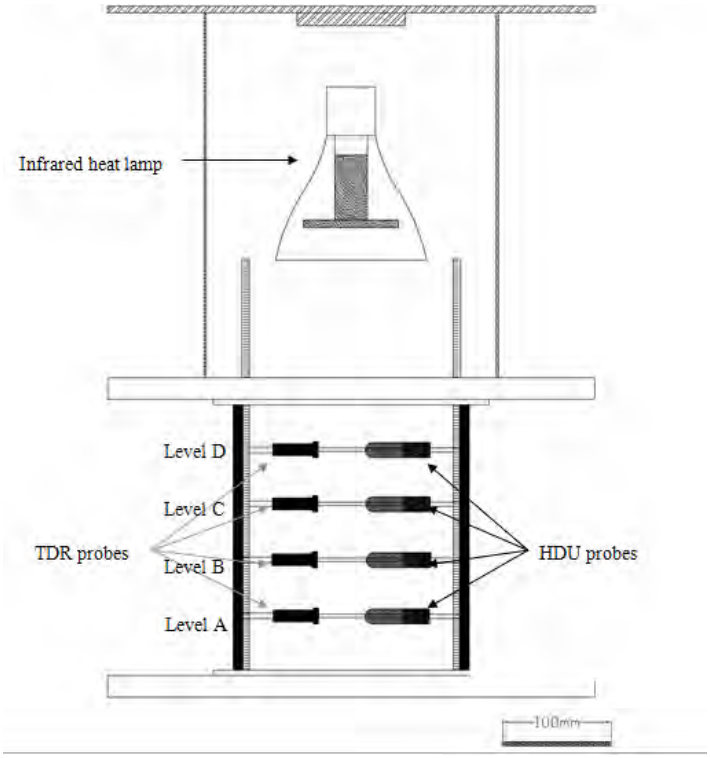

Figure 3.8: Instrumentation setup for Soil Column 3 drying phases

The soil in Soil Column 3 was compacted dry of optimum at 22% gravimetric water content and the soil in Soil Column 4 was compacted wet of optimum at 26% gravimetric water content (Table 3.2). Plastic dry-wall screws were used in Soil Columns 3 and 4 in the place of the metal screws used in Soil Column 2. The plastic dry-screws used in this research component are model 25310 manufactured by ITW Buildex (Itasca, Illinois). The screws are 41 mm in length with a 7 mm inner diameter and 13 mm out diameter. Plastic screws were used to avoid the possible corrosion that could occur with metal screws. Holes slightly smaller than the diameter of the head of the plastic dry wall screws were pre-drilled every 45° around the perimeter of the soil column, starting 30 mm above the base of the soil column and continuing every 50 mm up the side of the soil column. The holes were covered with reinforced packing tape prior to compaction. After compaction, the packing tape was removed and the plastic screws were screwed in the column. The head of the plastic dry wall screw, which was exposed on the outside of the soil column, was then covered with a layer of silicone sealant. Soil Columns 3 and 4 are referred to as "rigid laterally-restrained" soil columns.

For Soil Column 3, TDR and HDU probes were placed at elevations of 50, 100, 150, and 200 mm, referred to as Levels A, B, C and D, respectively (Figure 3.8). For Soil Column 4, TDR and HDU probes were placed at elevations of 50 and 100 mm. The actual elevation of the probes changed as the soil shrank or swelled. As in Soil Column 1, the TDR probes were placed into the soil layers before compaction and HDU probes were placed into the column after compaction. A plan view of the TDR and HDU probes as placed into the soil column is shown in Figure 3.9.

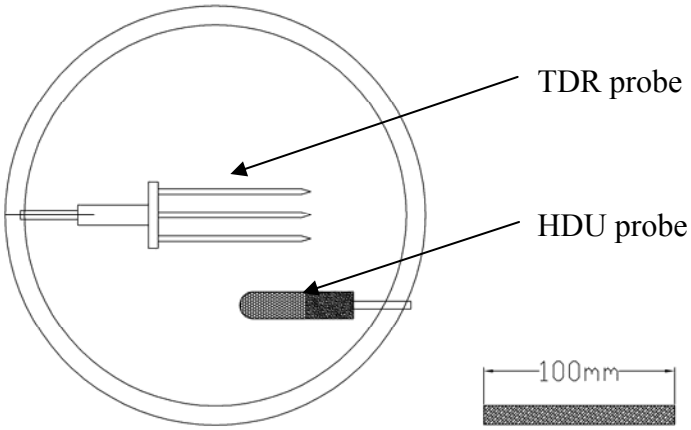

Figure 3.9: Plan view of Soil Column 3 instrumentation

Unlike the experiments for Soil Column 1 and Soil Column 2, which involved a single evaporation stage, testing of Soil Columns 3 and 4 included three stages (evaporation, infiltration, and a second evaporation). A schematic representation of the sequences of evaporation (Stages I and II), infiltration (Stages III, IV and V), and a second evaporation (Stages V and VI) in Soil Column 3 is summarized in Figure 3.10. A fan was used to blow air across the top of the soil specimen and to expedite evaporation (Figure 3.10: Stage I). For Soil Column 3, a constant temperature of 32.2 ± .5° C was maintained using an infrared heat lamp attached to a temperature controller. For Soil Column 4, an infrared heat lamp was not used and instead the ambient temperature was measured throughout testing. The temperature controller used in this research component is a single stage electronic temperature controller manufactured by Ranco North America (Plain City, Ohio). The temperature controller measured the temperature directly above the soil surface with a thermocouple and used this to switch the heat lamp on or off as needed. Digital photos of the top surface and side of the soil column were taken during both the first and second stages of evaporation. During infiltration into Soil Column 3, a 50 mm long clear PVC tube with o-ring grooves cut at both ends was constructed by the methods described in Section 3.2.3. This "infiltration collar" was then placed atop the soil column and a constant head of 25 mm relative to the soil surface was applied to induce infiltration from the top boundary (Figure 3.10: Stage III). The constant head apparatus used for this purpose included a mariotte bottle (Figure 3.11). Due to the large diameter of the mariotte tube and the slow flow rate, a nominal vacuum was applied at the top of the mariotte tube to pull air through the center tube. The elevation of water in the reservoir was recorded with time. Infiltration of Soil Column 4 was conducted by manually maintaining a constant head of water above the soil surface and measuring the amount of water dispensed into the column with time. The methodology and rationale used in maintaining a constant head for Soil Column 4 in this manner appears in Freilich (2006).

The results obtained from Soil Column 3 and 4 are the main focus of this report, as data obtained from Column 3 and 4 are used to determine the hydraulic properties of the unsaturated and cracked compacted Eagle Ford clay during drying, wetting and a second stage of drying.

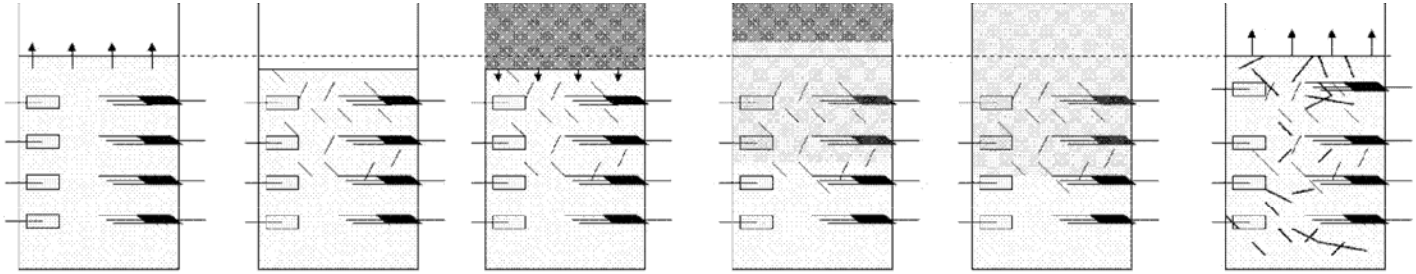

Stages					
I. Start 1st evaporation	II. End 1st evaporation	III. Start infiltration	IV. After 100 hours of infiltration	V. After 1000 hours of infiltration	VI. 2nd evaporation
Summary description					
A 25 cm high specimen was compacted 2% dry of optimum. A fan was then blown across the soil surface to start evaporation.	After 400 hours of evaporation the suction and water content at sensor levels C & D reached steady values constant. Small cracks were visible at the soils surface and the surface had settled 0.1 cm.	A constant head of 2.5 cm was applied at the upper boundary to start infiltration. The soil swelled from 24.9 cm in height to 27.7 cm in height during the first 18 hours of infiltration.	After 100 hours of infiltration an initial wetting front reached the base of the column and a second wetting front reached mid height.	After 260 hours of infiltration, the soil specimen swelled to the top of the infiltration collar at 32.5 cm elevation. Infiltration was continued until 1000 hours when no further downward movement of the second wetting front was observed.	The infiltration apparatus was removed and the soil above 25 cm elevation was removed. A fan was then used to start the 2nd evaporation phase. Significant cracking occurred during the second evaporation stage. After 1050 hours of evaporation testing was stopped.

Figure 3.10: Soil Column 3 timeline

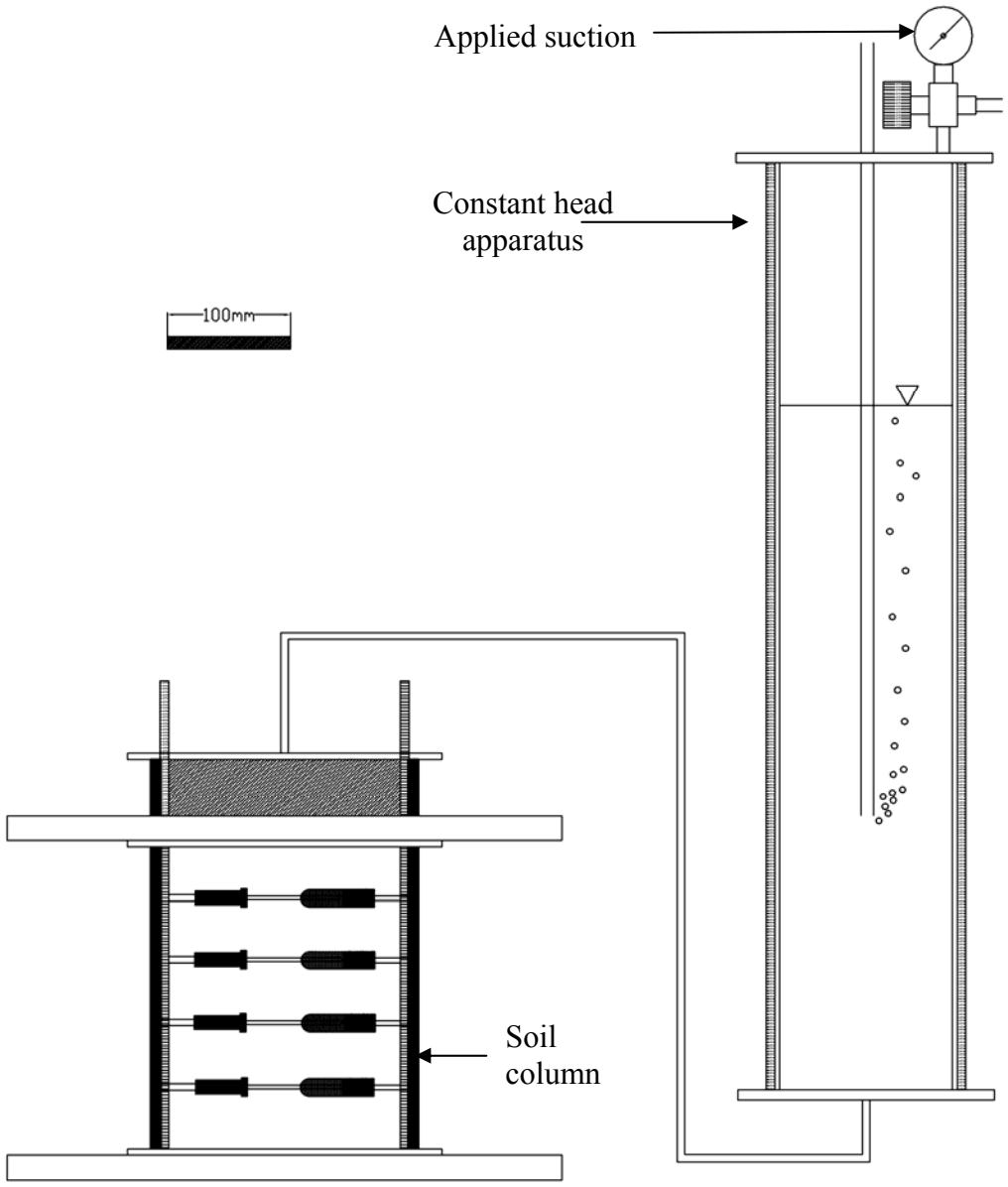

Figure 3.11: Constant head infiltration apparatus for infiltration of Soil Column 3

3.3 Calibration of Time Domain Reflectometry Probes

Background information on time domain reflectometry was presented in Section 2.4.1. This section presents the soil-specific TDR calibrations obtained for this research component. As mentioned, TDR probes can be used to measure the bulk dielectric constant of a soil. The bulk dielectric constant of the soil is strongly affected by its volumetric water content. The measured bulk dielectric constant of the soil is typically converted to volumetric water content using empirical equations. As described in Section 2.4.1, empirical relationships have not been found

to work well for highly plastic clays (Roth et al. 1990). To demonstrate the need for soil-specific calibration, an empirical relationship can be plotted versus values measured for Eagle Ford clay. One commonly used empirical equation was developed by Topp et al. 1980, and is known as "Topp's Universal Equation." The volumetric water content, defined using Topp's Universal Equation, for the square root of the dielectric constant ranging from 1 to 13 is plotted with values measured for Eagle Ford clay in Figure 3.12.

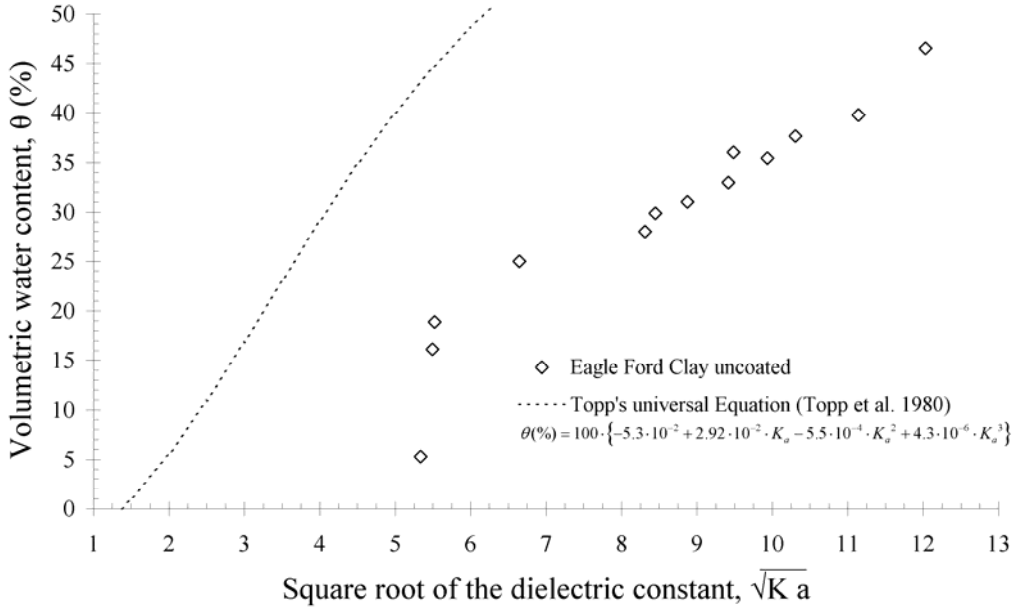

Figure 3.12: The measured and predicted volumetric water content based on measured dielectric constant

The TDR probes and the cable tester used in this research component are manufactured by Soilmoisture Equipment Corporation (Santa Barbara, California). The TDR probes were placed within Eagle Ford clay compacted at gravimetric water contents ranging from 4% to 35 % using standard Proctor compactive effort. Details concerning the calibration procedure are presented in Kuhn (2005). The calibration equations obtained in this research component are shown in Figure 3.13. The calibration data is best represented by a bi-linear relationship. A linear relationship between the square root of the measured dielectric constant and the volumetric water content was determined for volumetric water contents up to 19%. A separate linear relationship for uncoated probes was determined for volumetric water contents greater than 19%.

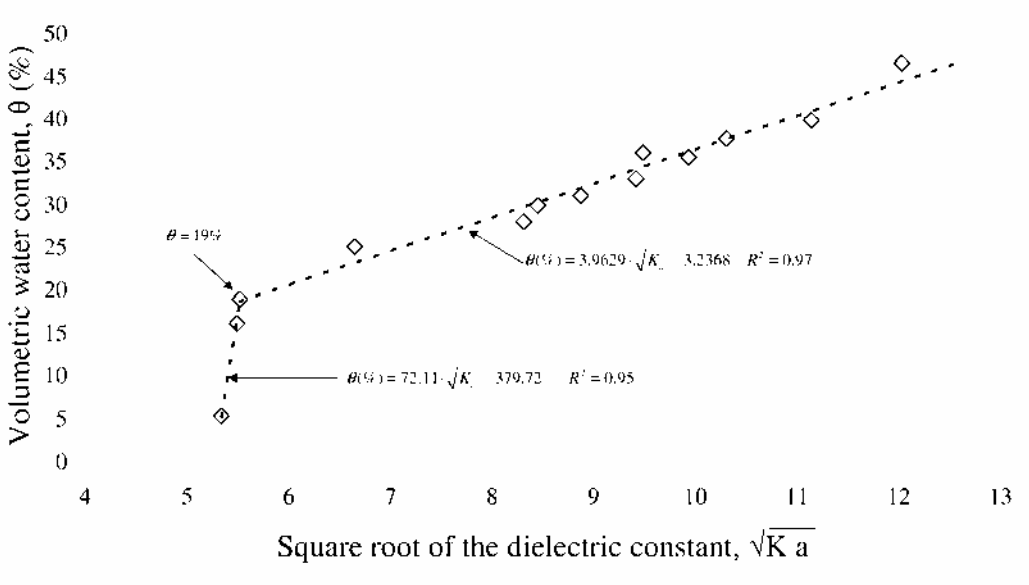

Figure 3.13: Calibrations for coated and uncoated TDR probes in Eagle Ford clay

3.4 Calibration of Heat Dissipation Unit Probes

Background information on heat dissipation unit (HDU) probes was presented in Section 2.4.2. This section introduces an HDU calibration procedure by Flint et al. (2002) and presents the verification of this calibration procedure performed by Kuhn (2005). As mentioned, HDU probes can be used to measure the suction in a soil. A heating element inside the probe is turned on for a period of time and a thermocouple inside of the probe is used to measures the temperature of the probe's porous ceramic body during this time period. The change in temperature that occurs during a selected portion of this time period is defined as the measured temperature rise. The measured temperature rise depends on the thermal properties of the HDU probe and varies with the volumetric water content of the HDU probe and suction of the HDU probe. A calibration relationship consisting of the relationship between temperature rise and suction can be established for individual probes.

The calibration relationship for HDU probes is independent of the soil in which the HDU probe is placed. HDU probes are typically vacuum saturated prior to calibration (Reedy 2004). When the sensor is placed into a soil with suction over 10 kPa (the air entry pressure of the porous ceramic body), water flows out of the HDU probe and into the soil until the suction in the probe reaches equilibrium with the suction in the soil. Measurements of temperature rise taken after the probe has reached equilibrium are then used to determine the suction within the soil.

3.4.1 Calibration of Non-dimensional Temperature Rise

Scanlon et al. (2002) reported that individual HDU probes can be calibrated within 3% accuracy using a procedure proposed by Flint et al. (2002). According to Flint et al. (2002), the temperature rise occurring during heating of the HDU probe can be non-dimensionalized using the maximum and minimum temperature rise for the HDU probe. This calibration procedure must be performed on individual probes as small differences in manufacturing may result in

different maximum and minimum temperature rises during heating (Flint et al. 2002). The calibration procedure involves calculating a non-dimensional temperature rise, *T**, as follows:

$$T^* = \frac{\Delta T_{max} - \Delta T}{\Delta T_{max} - \Delta T_{min}} \qquad \text{Equation 3.2}$$

Where, *T** = non-dimensional temperature rise, ΔT_{max} = minimum temperature rise, ΔT_{min} = maximum temperature rise, and ΔT = measured temperature rise. Flint et al. found that the non-dimensional temperature rise was not probe specific. The following equation, proposed by Flint et al. (2002), was used in this research component:

$$\psi(kPa) = 56.2 \cdot (T^{*-2.22} - 1) \qquad \text{Equation 3.3}$$

Additional details on the calibration procedure are presented in Flint et al. (2002) and Kuhn (2005).

3.4.2 Verification of the Calibration of Non-dimensional Temperature Rise

The calibration procedure proposed by Flint et al. was validated in this research component to gain confidence in using non-dimensional temperature rise to calculate suction (Equation 3.2; Equation 3.3). Specifically, the calibration procedure proposed by Flint et al. was validated by saturating HDU probes and using axis translation to impose suction values of 55 and 148 kPa. Also, an unsaturated aqueous solution of sodium chloride was used to impose suction values of 300 and 454 kPa. Details concerning these verification procedures can be found in Kuhn (2005).

The measured temperature rise for HDU probes under different suctions induced by using axis translation and unsaturated aqueous solution of sodium chloride are shown with in Figure 3.14. Temperature rise as a function of suction is plotted in the figure using Flint et al.'s (2002) calibration equation. Good agreement was found between measured values of temperature rise and values predicted by Flint et al.'s (2002) calibration procedure. Accordingly, Flint et al.'s (2002) calibration equation was deemed sufficiently accurate for this research component.

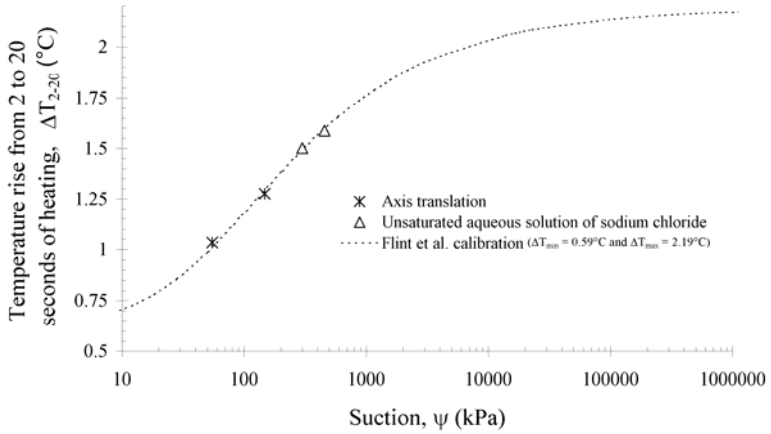

Figure 3.14: Verification of Flint et al.'s calibration procedure

Chapter 4. Results from Experimental Testing Program

The results from the experimental testing program are presented in this chapter. Specifically, and following setup for the experimental testing program was previously discussed in Section 3.2, the suction measurements obtained for soil placement conditions and the instrumentation results from Soil Column 1, 2, 3, and 4 are discussed. The analysis of the results from the experimental testing program will be presented in Chapter 5.

4.1 Evaluation of Suction under Initial Soil Placement Conditions

Two test series were conducted in this research component to evaluate the effects of soil placement conditions on the initial suction. The first test series was conducted to evaluate the effect of relative humidity on moisture movement after initial soil placement. The experimental procedure involved compacting the soil under three different placement water contents (ω = 18.4, 21.6, and 24.6) and subsequently exposing the soil specimens to four different values of relative humidity (RH = 32.8, 68.4, 84.3, and 97.3). A total of twelve specimens were tested in this experiment.

The results obtained in this evaluation are shown in Figure 4.1. The gravimetric water content measured in compacted specimen after 850 hours of exposure to environments with constant values of relative humidity. The results show that the gravimetric water content of all but one specimen decreased with time. The case in which gravimetric water content did not decrease with time corresponds to comparatively high relative humidity (RH = 97%) and samples compacted under comparatively low gravimetric water content (5.6% dry of optimum). Given that suction is a function of volumetric water content, as it typically is for intact porous materials, the gravimetric water content is expected to decrease from its initial value. This indicates that the suction within Eagle Ford clay is expected to increase with time over extended periods of exposure. Consequently, one would expect that water in compacted highly plastic clay embankments is expected to evaporate for relative humidity values less than 97%.

In the second experimental component, HDU probes were used to measure the initial suction for different soil placement conditions. The sensors were inserted into the compacted specimens and reached equilibrium with the surrounding soil suction after approximately 17 hours. This procedure allowed for the measurement of initial suction under different soil placement conditions. Additional measurements of the initial suction for different soil placement conditions were obtained from HDU readings immediately after compaction of the soil columns (Section 4.2).

The resulting measurements of suction and dry unit weight for different soil compaction water contents are shown in Figure 4.2. The suction under soil placement conditions varies over three orders of magnitude for water contents ranging from only 20% to 26.5%. The dry unit weight of the compacted clay for the results shown in Figure 4.2 is approximately the same (ranging from 15.00 to 15.22 kN/m^3). Results indicated that small changes in placement water content produce significant change in suction under soil placement conditions. Consequently, drastic changes in suction take place in the vicinity of the optimum water content. For example, an initial suction of 100,000 kPa was measured for Eagle Ford clay compacted 2.5% dry of optimum and an initial suction of 100 kPa for Eagle Ford clay compacted 2.5% wet of optimum.

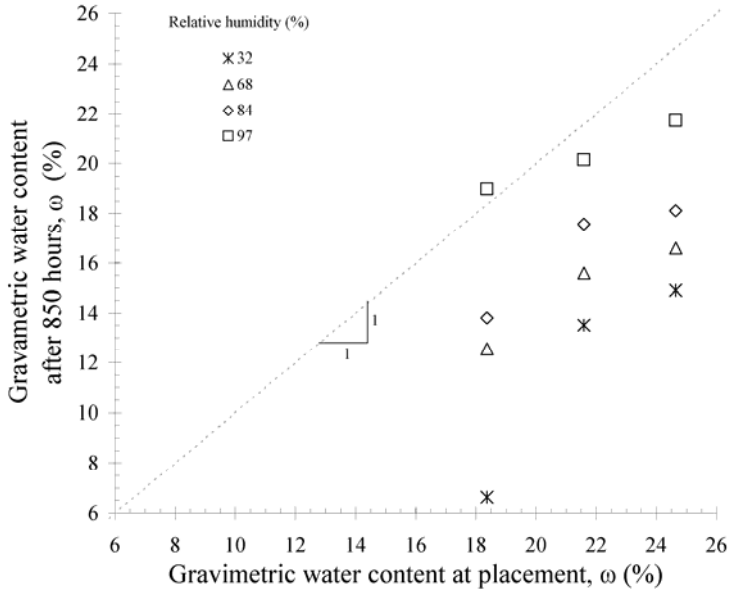

Figure 4.1: Change in gravimetric water content for a sample in a controlled relative humidity environment

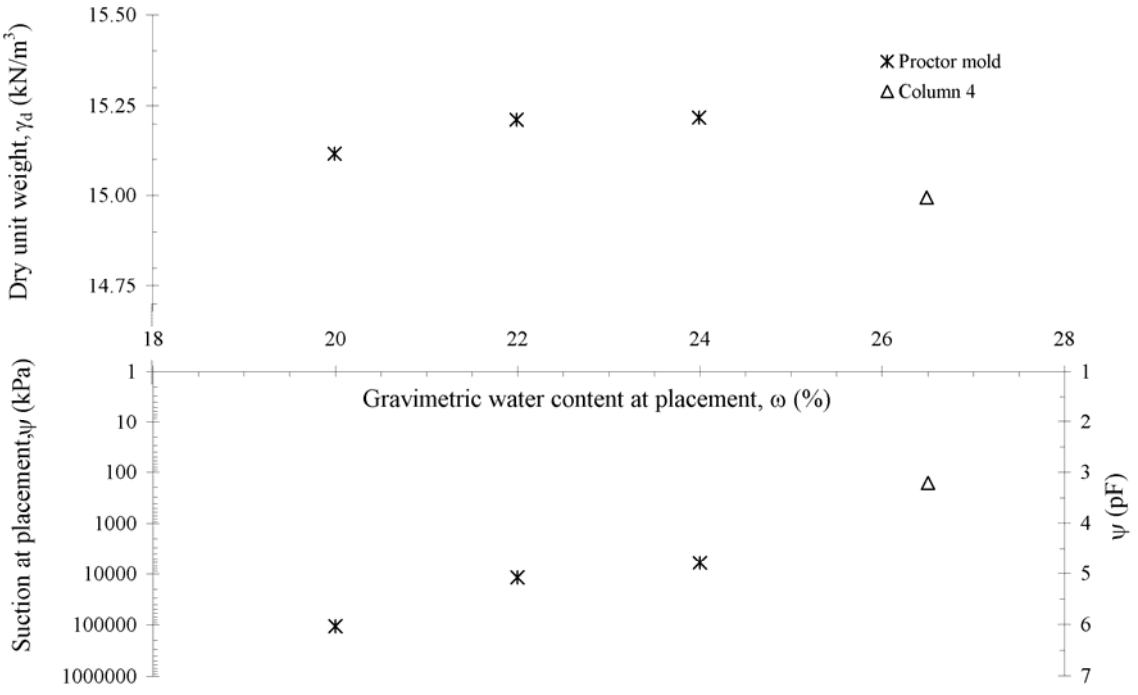

Figure 4.2: Measured suction and dry unit weight for different compaction water contents in Eagle Ford clay

Using the dry unit weight and gravimetric water content, the volumetric water contents were calculated for each specimen. The measured suctions are plotted with the calculated volumetric water contents in Figure 4.3. The results show a significant increase in measured suction with decreasing volumetric water content. The total suction at room temperature and a moderate relative humidity (e.g., 50%) is approximately 100,000 kPa (Equation 3.1). The significance of these results will be discussed further in Section 5.4.1.

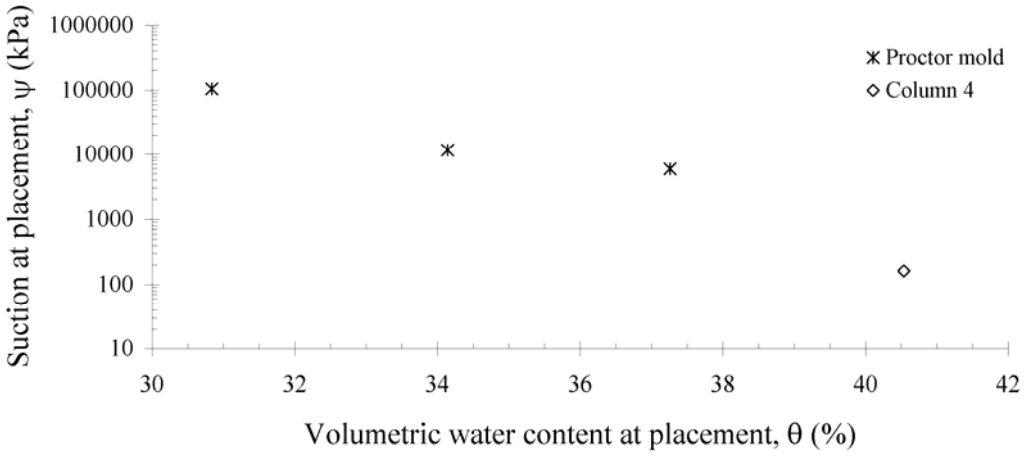

Figure 4.3: Measured suction and volumetric water content for compacted Eagle Ford clay

4.2 Soil Column 1: Laterally-unrestrained Water Balance Column

4.2.1 Visual Observations

The characteristics of Soil Column 1 were described in Section 3.2.4. Digital photos of the soil surface taken during the evaporation stage are shown in Figure 4.4. Geometric cracking patterns were visible on the surface of Soil Column 1 soon after the evaporation stage started. As drying progressed, the intensity of cracking at the surface of the column increased and the soil at the surface of the column became visibly lighter in color. The intensity of cracking continued to increase up to 7.3 hours of drying [see Figures 4.05(a) to 4.05(h)]. After 7.3 hours of drying, the specimen separated from the sidewalls of the soil column [see Figures 4.05(h) to 4.05(i)]. Cracks on the surface of the soil specimen partially closed as the soil specimen separated from the sidewalls of the soil column. The separation between the soil specimen and the column sidewall observed initially at the surface propagated down the soil column during the drying process. No significant changes in the surficial cracking pattern took place from 71 hours to 435 hours of drying, when the drying front reached the bottom of the soil column.

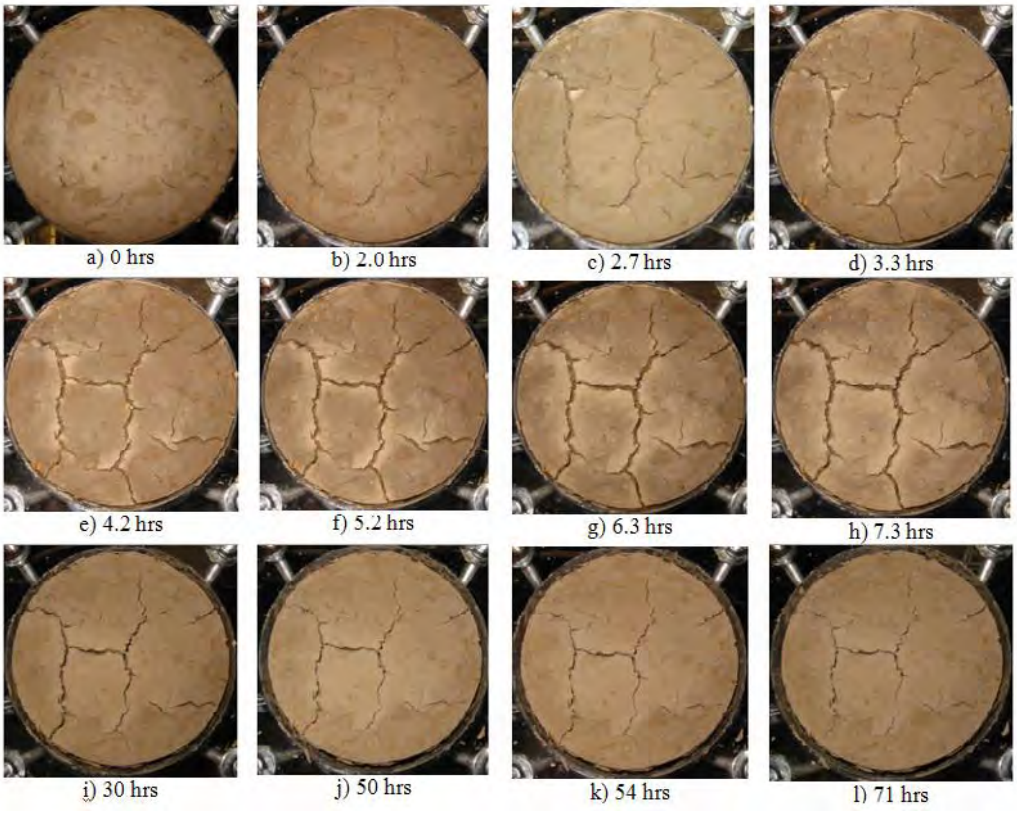

Figure 4.4: Crack formation and closure in Soil Column 1 during drying

Two drying fronts of contrasting water contents were identified based on observed changes in the coloring of the compacted soil along its profile. An image of Soil Column 1 and the two drying fronts, as observed after 48 hours of drying, is shown in Figure 4.5. The first drying (lower front) moving down the soil column was characterized by a darker fringe forming over the as placed soil. The second drying front (upper front) corresponds to the upper boundary of the darker fringe. The reason for these two fronts is speculated to be a reverse capillary break. That is, the upwards flow from the as-placed zone forms a capillary break at the interface with the drier zone. In this case, the hydraulic conductivity of the unsaturated drier zone is less than that of the soil in the darker fringe. This is speculated to lead to water accumulation at the interface between the upper and lower regions. The downward progress of the two drying fronts through the soil column profile was recorded with time, and is shown in Figure 4.6. The average thickness of the intermediate zone was 15 mm (ranging from 10 to 20 mm). The average downward velocity of the drying fronts was approximately of 6×10^{-5} cm/s. The settlement of the soil surface is shown as a function of time in Figure 4.7.

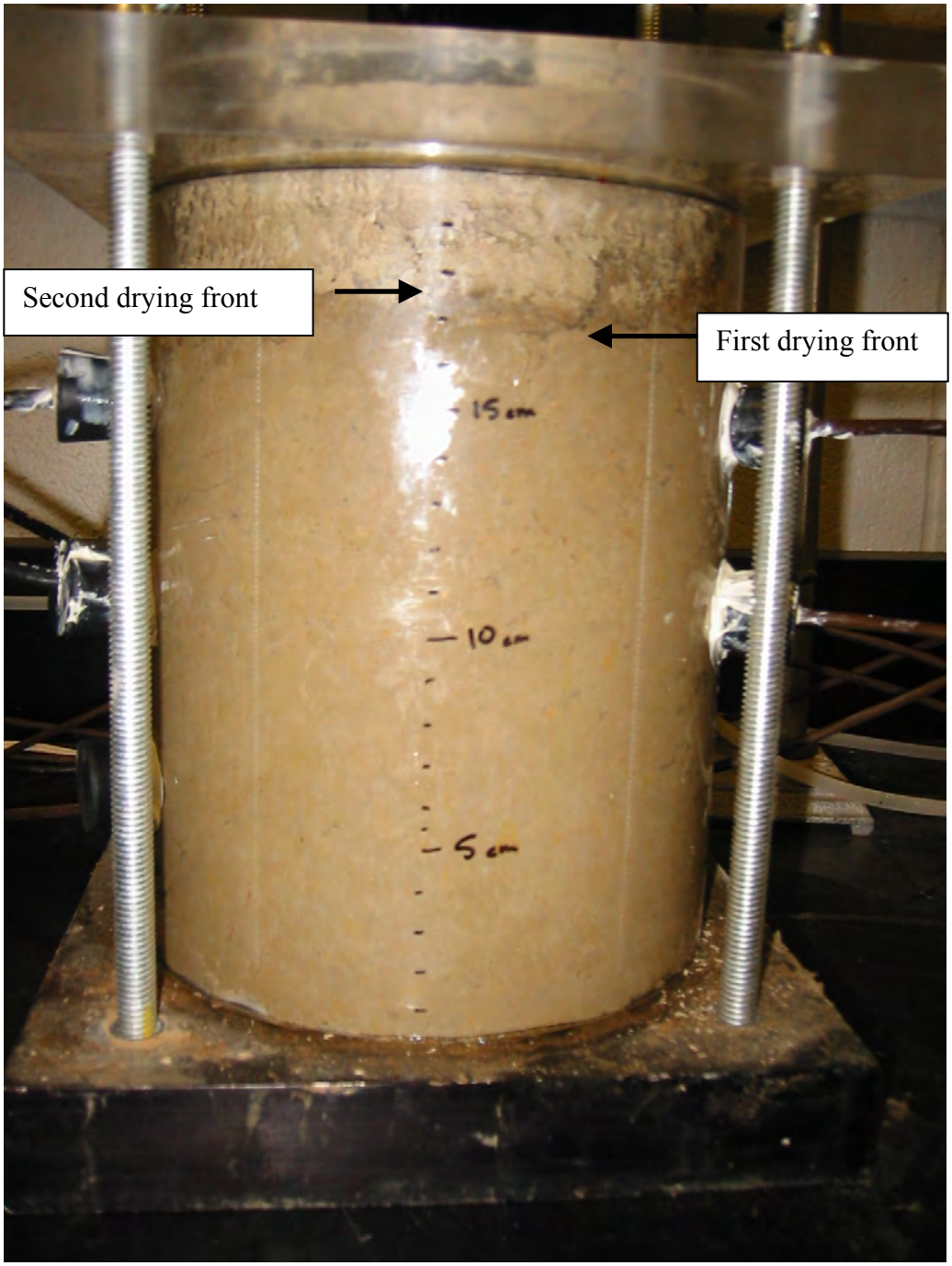

Figure 4.5: Two drying fronts in Soil Column 1 after 48 hours of drying

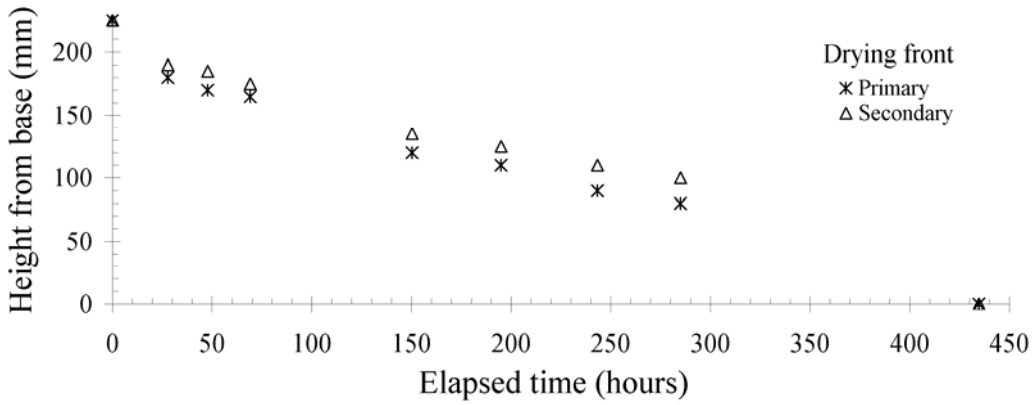

Figure 4.6: Advancement of drying front in Soil Column 1 obtained visually

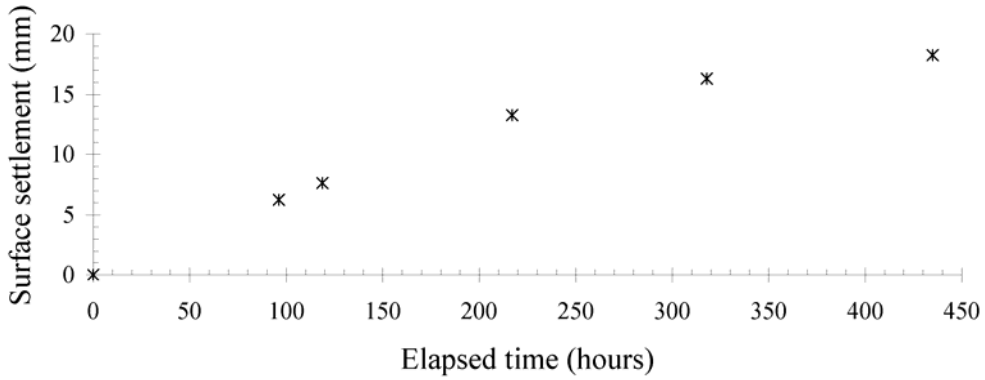

Figure 4.7: Surface settlement in Soil Column 1 obtained using Vernier caliper

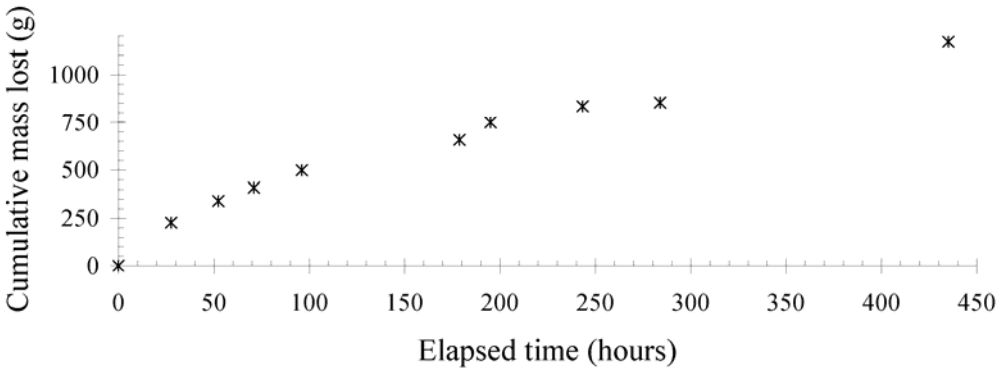

Figure 4.8: Cumulative mass lost in Soil Column 1 obtained using laboratory scale

4.2.2 Measurements

The weight of the soil column system was measured by placing the entire soil column on a laboratory scale at different times. A plot of the cumulative mass loss occurring during evaporation is shown in Figure 4.8.

The volumetric water was measured using uncoated TDR probes. TDR probe measurements from 200 to 284 hours of testing are shown in Figure 4.9. The volumetric water contents at Levels A and B decrease with time. The volumetric water content at Level B (top sensor) started to decrease first and decreased more significantly than the moisture content at Level A as the drying front progressed moved downwards.

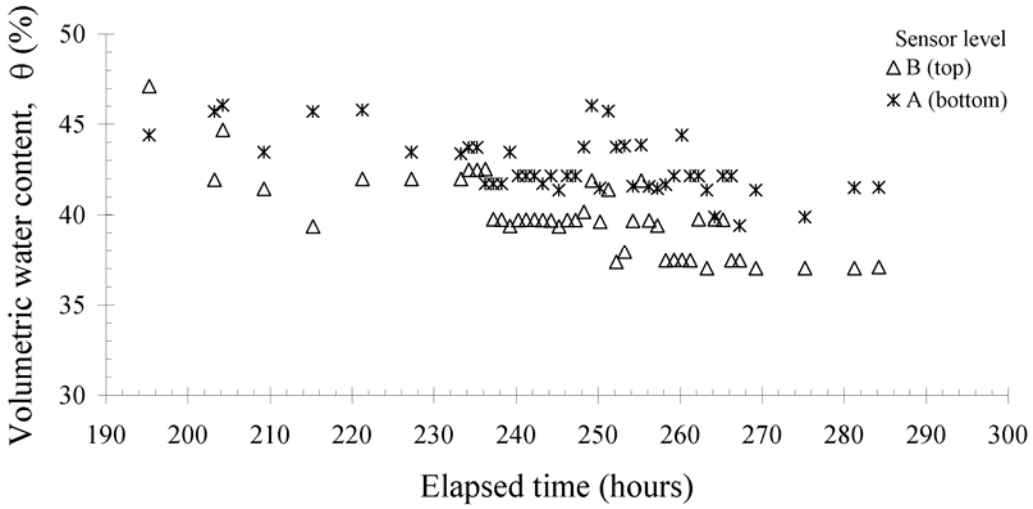

Figure 4.9: Volumetric water content in Soil Column 1 obtained using TDR measurements

Suction was measured using HDU probes placed at levels A and B. Results obtained for the first 125 hours and are shown in Figure 4.10. The suction at both sensor levels increases with time, with the suction at Level B increasing more rapidly than that at Level A.

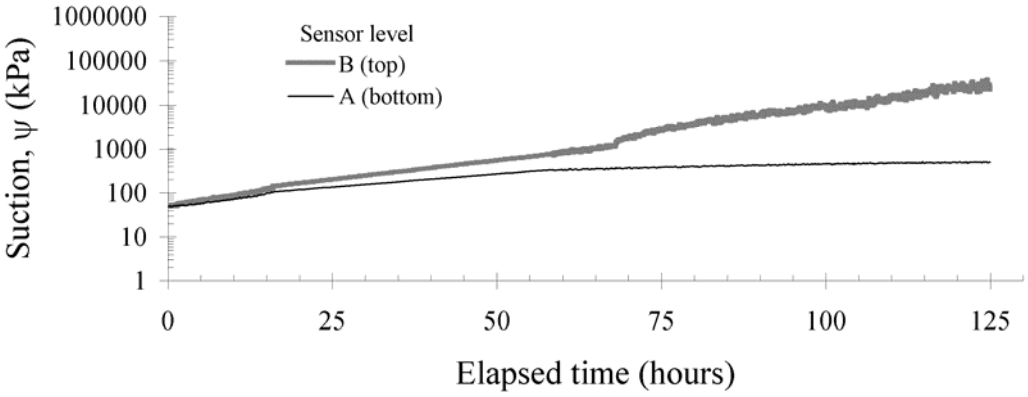

Figure 4.10: Suctions in Soil Column 1 obtained using HDU measurements

4.2.3 Exhumation after testing

At the end of evaporation of water from Soil Column 1, gravimetric water contents were obtained from samples collected every 50 mm from the surface. Two samples were collected at the specimen's perimeter and one was collected at its center at each elevation. The resulting water content profile is shown in Figure 4.11.

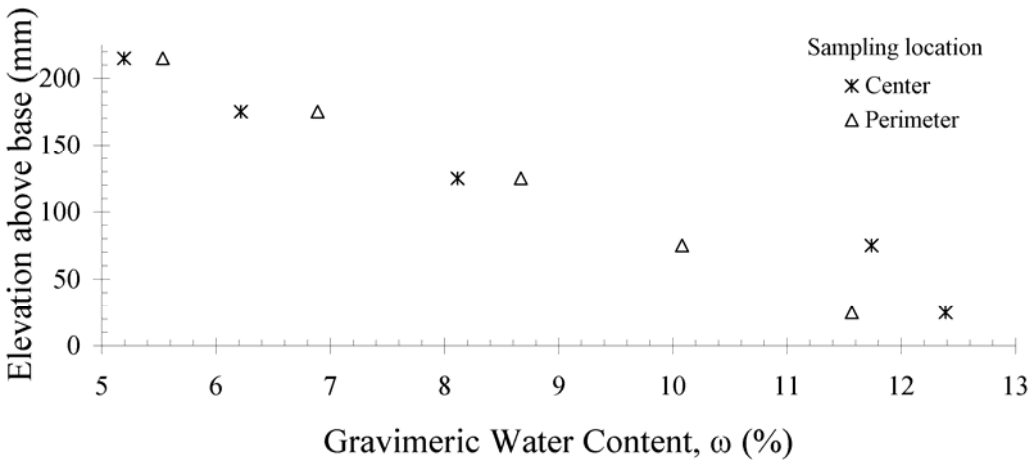

Figure 4.11: Gravimetric water content profile in Column 1 after testing

While dismantling the specimen several interesting features could be noted. For example, cracks that were visible on the surface terminated only 30 mm below the soil surface (Figure 4.12 (a)). The surface at 30 mm depth was irregular with one major crack forming at the side of the specimen and propagating at an angle of approximately 35° downward into the specimen. The bottom half of the cracked portion is shown in Figure 4.12 (b). The soil in the bottom 100 mm of the soil column was found to be essentially intact as shown in Figure 4.12 (c).

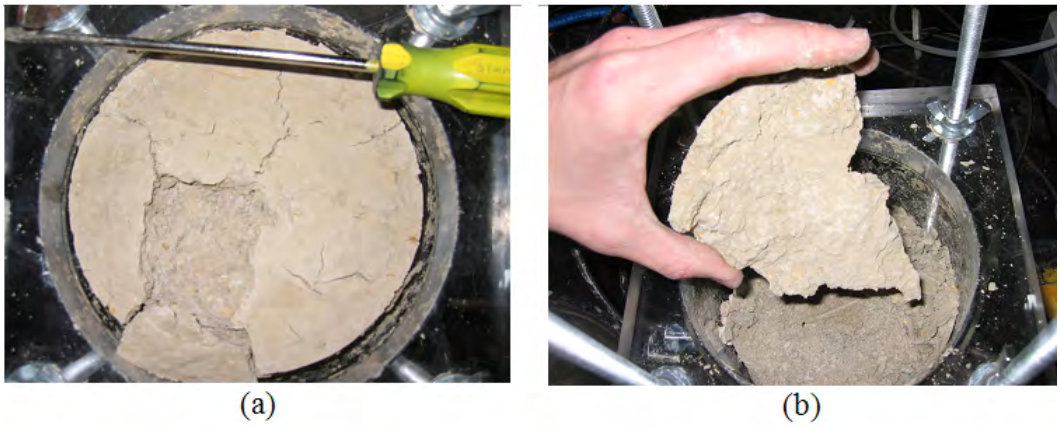

Figure 4.12: Soil Column 1 after testing: (a) Limited cracking; (b) Limited cracking depth; and (c) Intact lower portion

4.3 Soil Column 2: Rigid Laterally-restrained Column

4.3.1 Visual Observations

The characteristics of Soil Column 2 were described in Section 3.2.4. Digital photos of the soil surface of Soil Column 2 taken during the drying process are shown in Figure 4.13. Unlike Soil Column 1, cracks formed on the surface of the Soil Column 2 during drying remained open throughout the entire testing program. A drying front was observed during evaporation and reached the base of the soil column after 65 hours. Unlike Soil Column 1, only a single drying front was observed. The limited height of the soil column may have not allowed for the observation of a second drying front. No sidewall separation was noted, indicating that the restraints were effective. The 40 mm high soil profile settled 4 mm during drying. The average settlement at the side of the soil column was 0.3 mm less than at the center of the soil column as measured with a Vernier caliper. This difference in settlement can be attributed to a combination of sidewall friction and resistance from the screws.

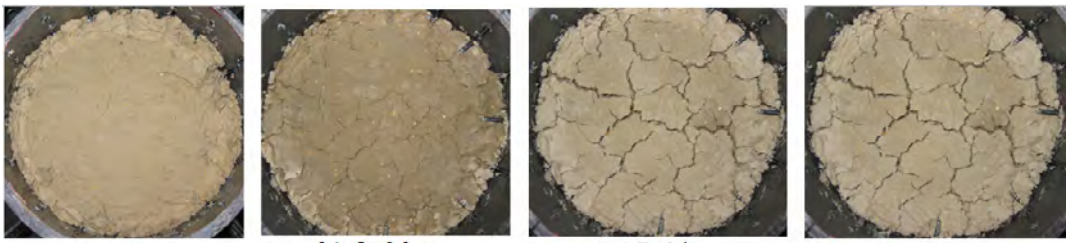

Figure 4.13: Crack formation in Soil Column 2 during drying

4.3.2 Measurements

The weight of Soil Column 2 was continuously measured throughout the experiment by suspending the system and measuring the load using a 22.7 kg capacity load cell within an accuracy of ± 6.8 g. When hanging from the load cell, the column was prone to movements caused by vibrations and air movement in the laboratory. Scatter in weight measurements was as large as ± 4 g. Consequently, readings were taken every 5 minutes and were averaged each hour. The results are presented in Figure 4.14. The rate of cumulative mass loss is observed to decrease with time. Because ambient conditions were the same for Soil Columns 1 and 2, the rate of mass loss can be used to determine the evaporation rates for each soil column as will be discussed in Section 5.3.1.

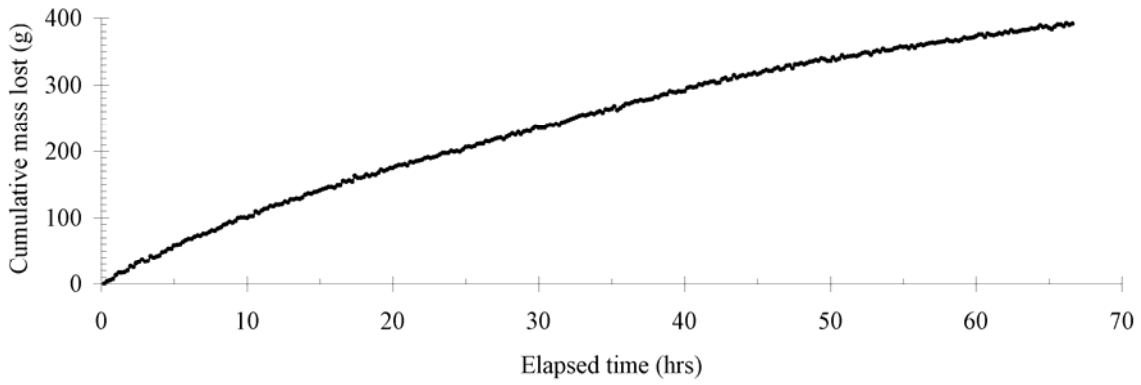

Figure 4.14: Cumulative mass loss from Soil Column 2 obtained using a load cell

4.4 Soil Column 3: Rigid Laterally-restrained Soil Column Compacted 2% Dry of Optimum Water Content

4.4.1 First Evaporation Stage

The characteristics of Soil Column 3 were described in Section 3.2.5. During the first evaporation stage, the volumetric water content measured at the location of the upper two sensors, C and D, changed more significantly than that measured at the location of the lower two sensors (Figure 4.15). The suction measured at sensor levels A and B did not change significantly during the entire first evaporation stage while the suction measured by the sensors C and D increased by two to three orders of magnitude. Within the initial 150 hours of the first evaporation stage, the suction at Level D increased to 100,000 kPa and the suction at Level C increased to 800 kPa (Figure 4.16). The implications of large changes in suction with small changes in volumetric water content are discussed in Section 5.1. During the first evaporation stages only minor cracking was observed (Figure 3.10: Stages I and II). The minor cracking likely resulted from having placed the soil dry of optimum water content. A view of the soil surface after 400 hours of evaporation is shown in Figure 4.17. Minor cracking is visible in the image and only very minimal sidewall separation occurred at the surface of the specimen.

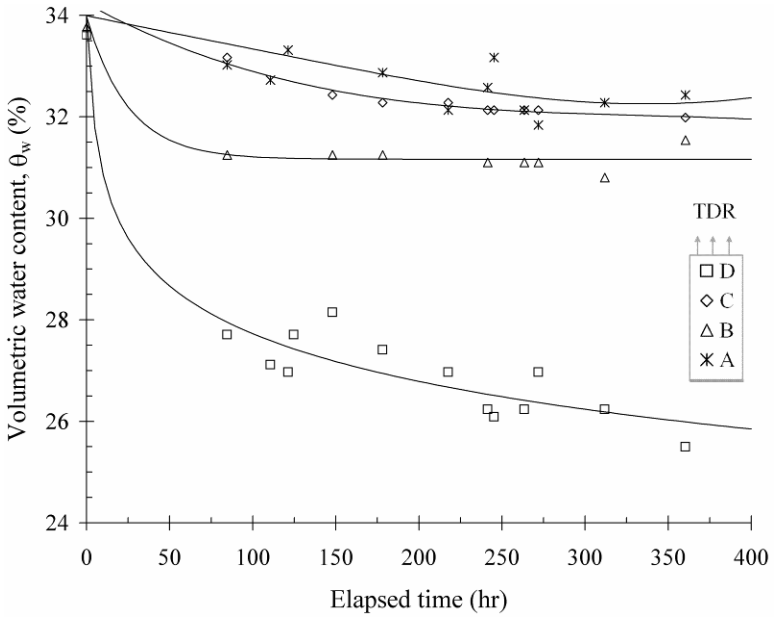

Figure 4.15: Volumetric water contents in Soil Column 3 during first evaporation phase obtained using TDR measurements

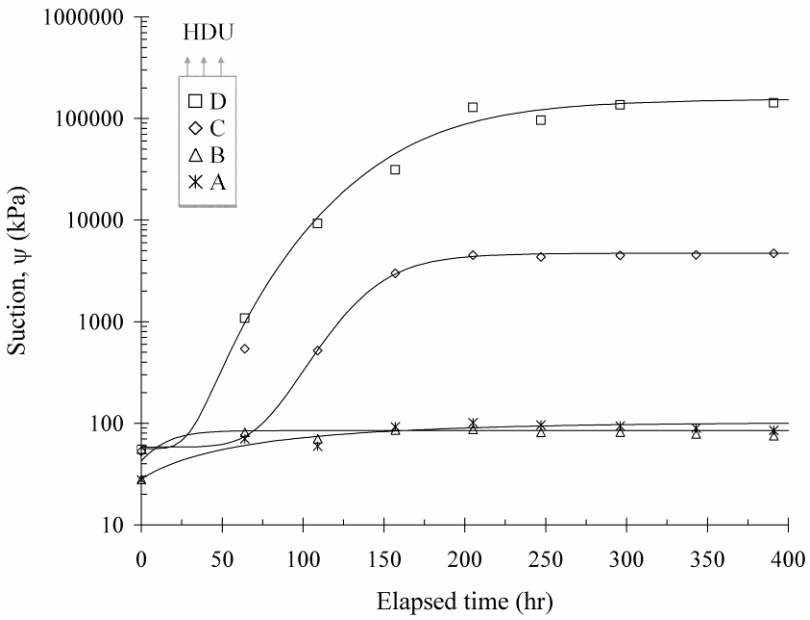

Figure 4.16: Suctions in Soil Column 3 during first evaporation phase obtained using HDU measurements

0 hours 400 hours

Figure 4.17: Surface of Soil Column 3 before and after initial drying phase

4.4.2 Infiltration Stage

After the measured suction reached steady values during the first evaporation stage, an infiltration stage was initiated by placing a constant head of 25 mm of water on the soil surface. A view of Soil Column 3 with the extension attached for infiltration is shown in Figure 4.18. The infiltration rate as a function of time is shown in Figure 4.19. As shown in this figure, the rate of infiltration into the soil column was initially very high and decreased with time (note that the time scale in the figure is logarithmic). The soil column swelled from 249 mm to 277 mm during the first 18 hours of infiltration (Figure 3.10: Stage III). The high initial infiltration rate indicated on Figure 4.19 was due to the high gradient near the interface of ponded water and the underlying unsaturated soil. The wetting front, identified by a change in soil color, reached the base of the soil column after approximately 100 hours of infiltration. In addition, a second wetting front had reached an elevation of 150 mm after 100 hours of infiltration. The progress of the two wetting fronts, as visually observed by changes in soil color is presented in Figure 4.20. After 260 hours of infiltration, the soil specimen swelled to the top of the infiltration collar at an elevation of 325 mm (Figure 3.10: Stage V). Infiltration was continued until 1,000 hours when no further downward movement of the second wetting front was observed.

Figure 4.18: Infiltration setup for Soil Column 3

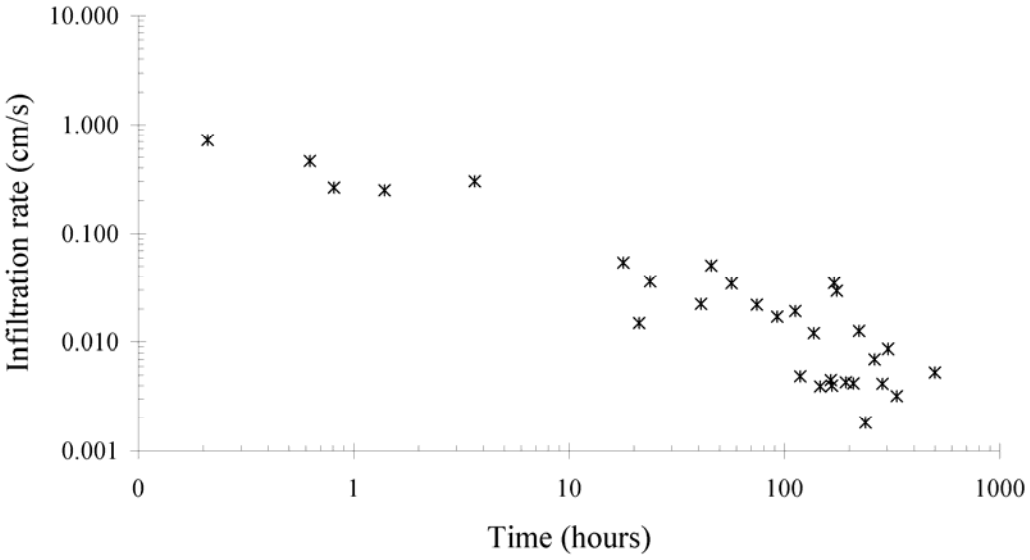

Figure 4.19: Infiltration rate with time for Soil Column 3

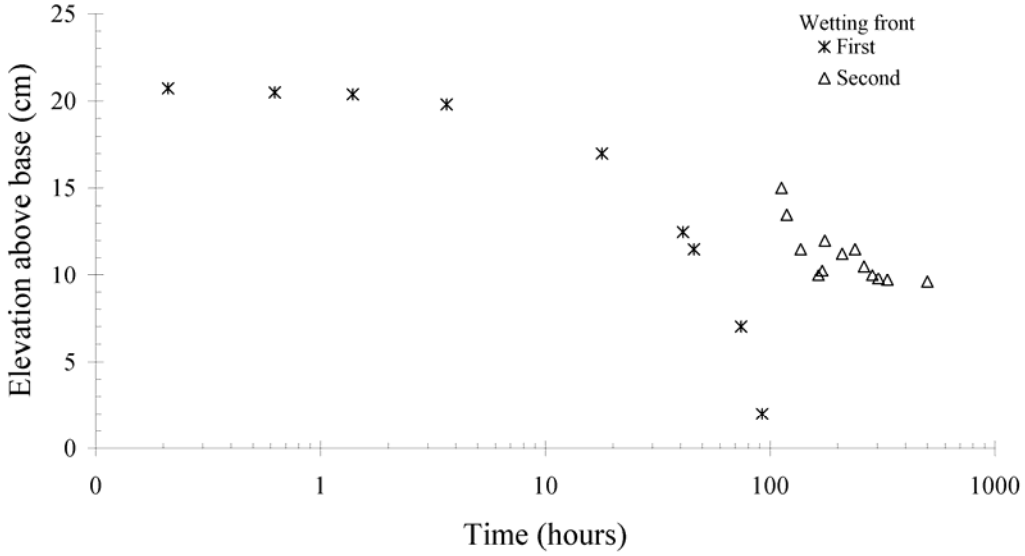

Figure 4.20: Wetting front for column 3 infiltration obtained visually

The volumetric water content and suction measured during infiltration are shown in Figures 4.22 and 4.23. The suction measured at sensor levels C and D decreased within the first few hours of infiltration by one to three orders of magnitude. The suction measured at sensor levels A and B during the infiltration stage did not change significantly. After an initial decrease in suction at levels C and D, the volumetric water content at these levels began to increase significantly. The volumetric water content at level D reached a value similar to that observed at the end of infiltration within the first 3 hours of infiltration. The volumetric water content at level C increased sharply after approximately 800 hours of testing. The volumetric water content at sensor levels A and B increased significantly at approximately 1,200 hours of testing.

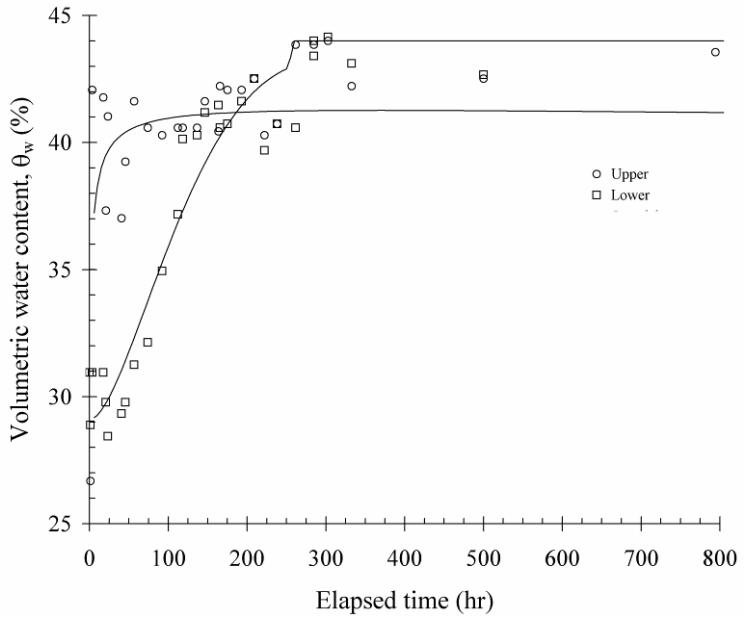

Figure 4.21: Volumetric water content in Soil Column 3 during infiltration phase obtained using TDR measurements

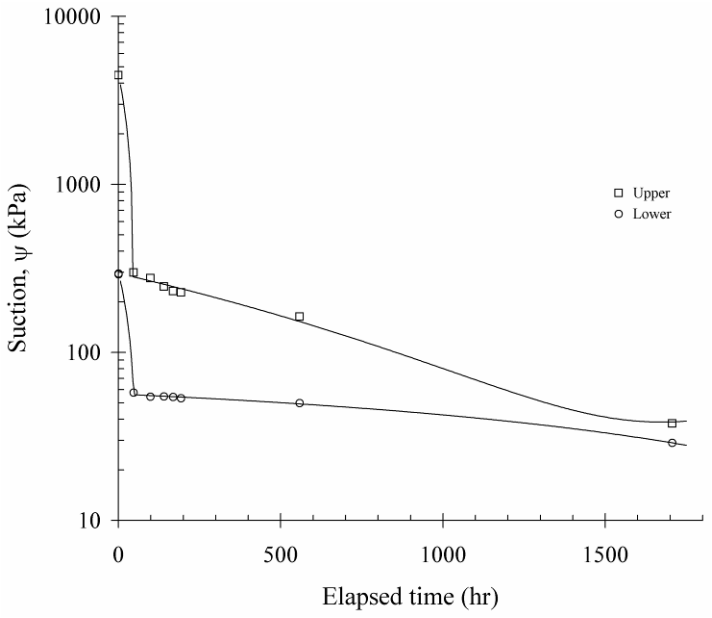

Figure 4.22: Suctions in Soil Column 3 during infiltration phase obtained using HDU measurements

4.4.3 Second Evaporation Stage

A second evaporation stage was started after 1,000 hours of infiltration, when suctions on all levels reached values below 100 kPa (Figure 3.10: Stage VI). Prior to evaporation, soil higher than 250 mm of elevation was removed from the specimen. Soil that had swelled beyond 250 mm of elevation during infiltration was removed because it was above the highest level of plastic screws and would be likely to pull away from the sidewall during drying. The same boundary conditions used during the first evaporation stage were used during the second evaporation stage. Within the first 100 hours of testing the volumetric water content at level D decreased below 20% volumetric water content (Figure 4.23). After 800 hours of evaporation the volumetric water content at Level C had decreased to values that were approximately the same as in Level D. During the second evaporation stage, the suction at Level D increased from 30 to 240 kPa after 1,050 hours of evaporation (Figure 4.24). The suction at Level D remained at values similar to those at Level C (from 40 to 220 kPa). The suction at levels A and B, however, did not increase over 30 kPa throughout the entire second evaporation stage.

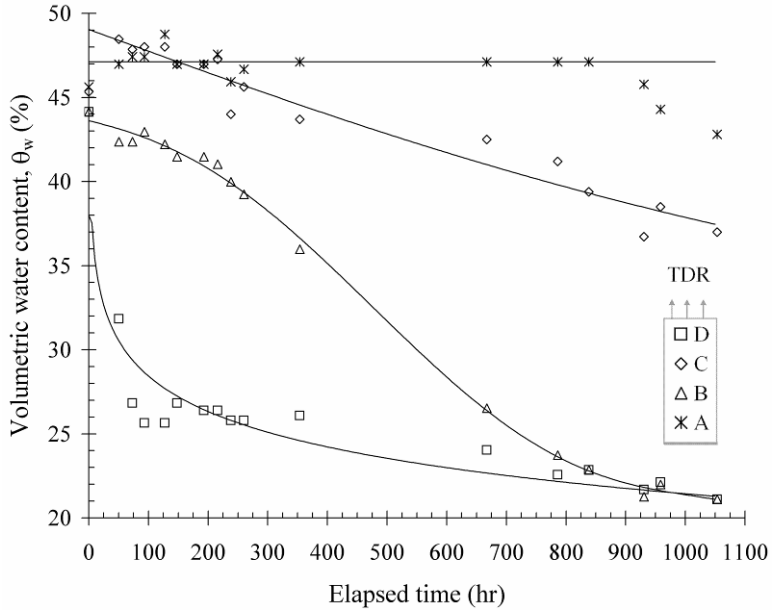

Figure 4.23: Volumetric water content in Soil Column 3 during second evaporation phase obtained using TDR measurements

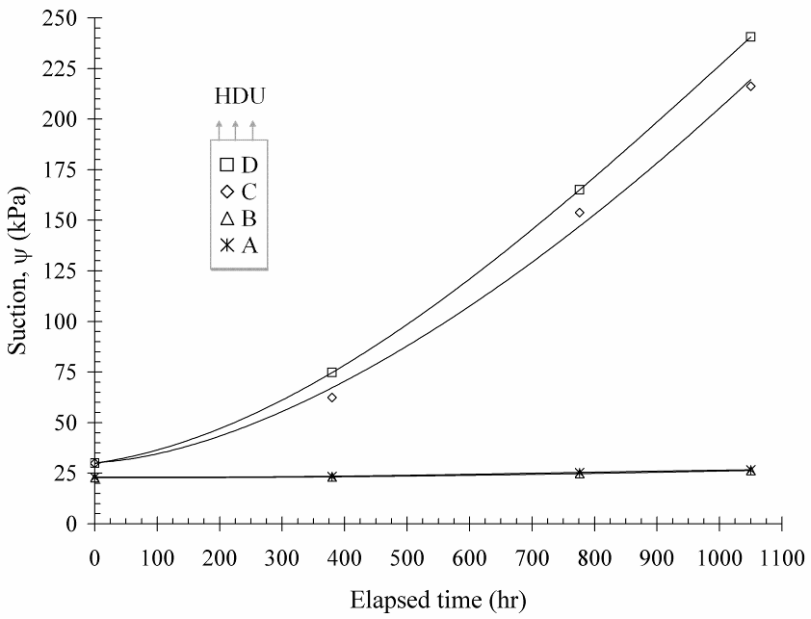

Figure 4.24: Suctions in Soil Column 3 during second evaporation phase obtained using HDU measurements

A view of the drying front obtained during the second evaporation stage is shown in Figure 4.25. Views of the soil surface of Soil Column 3 obtained at the beginning of and after 1,000 hours during the second evaporation stage are shown in Figure 4.26. No significant cracking was visible prior to the second evaporation stage. Swelling that took place during infiltration closed the cracks that had formed during the first evaporation stage. During drying, the top 20 mm of soil pulled away from the sidewalls. Even though an effort was made to remove soil that had swelled above the highest screws during infiltration, it appears as though screws should have been installed closer to the surface of the soil specimen. Yet, cracks formed continuously through the remainder of the specimen immediately below this top 20 mm layer of soil. This was verified when the soil column was dismantled after testing. Significant cracking had developed after 1,050 hours of drying and the surface had settled 20 mm.

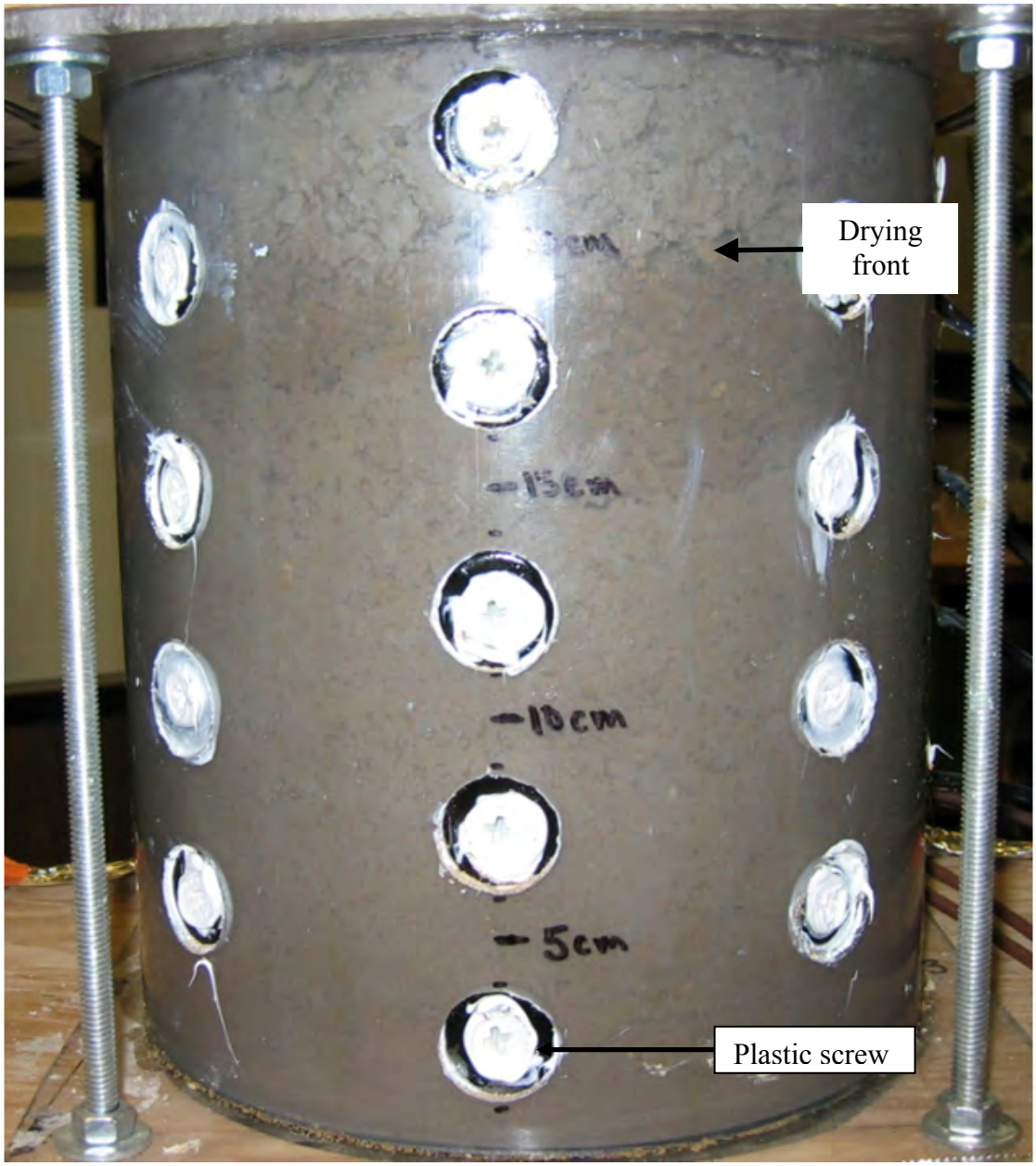

Figure 4.25: Advancement of drying front during second evaporation of Soil Column 3

0 hours 1000 hours

Figure 4.26: Surface of Soil Column 3 before and after second drying phase

4.4.4 Exhumation after testing

At the end of the second evaporation stage for Soil Column 3, samples were collected every 50 mm of depth for determination of gravimetric water contents. At each depth, water content was measured at the center and perimeter of the soil column. The resulting water content profile is shown in Figure 4.27. The gravimetric water content profiles from Soil Column 1, as discussed previously in Section 4.2.3, and the gravimetric water content profile from Soil Column 2 are shown in Figure 4.28. The water content profiles of both columns show that there is virtually no difference between water content measured at the perimeter of the column and water content measured at the center of the column. Also evident in Figure 4.28 is that gravimetric water contents measured in Soil Column 3 are greater than the water contents measured in Soil Column 1 at all elevations.

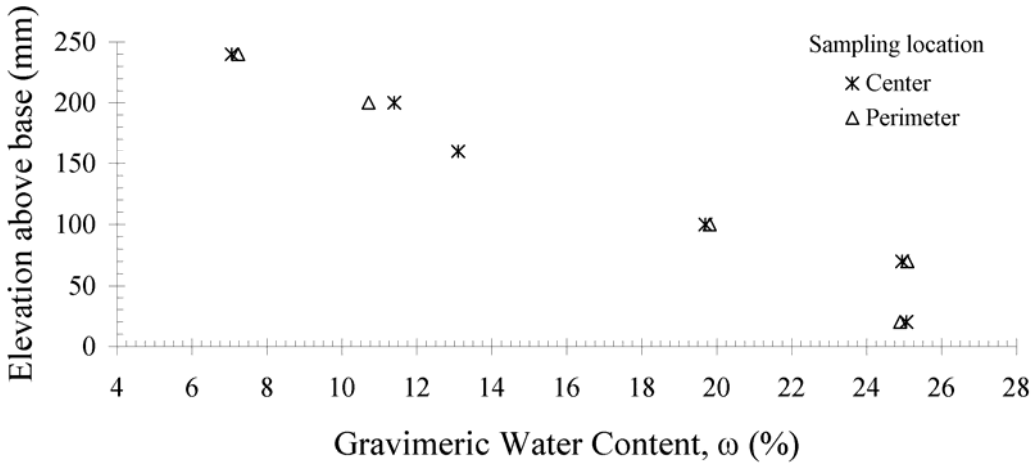

Figure 4.27: Gravimetric water content profile in Soil Column 3 after testing

A view of the instrumentation and cracking at level D is shown in Figure 4.29 as obtained during exhumation of the soil column. The HDU probe for this sensor group is shown imbedded in the soil on the lower left side of the picture. The TDR probe used for this sensor group is in the center of the picture.

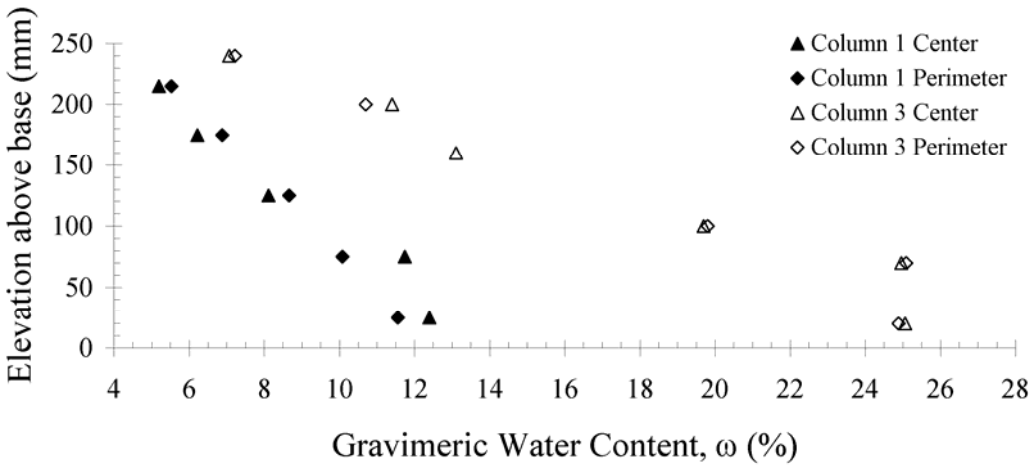

Figure 4.28: Gravimetric water content profiles for Soil Columns 1 and 3 after testing

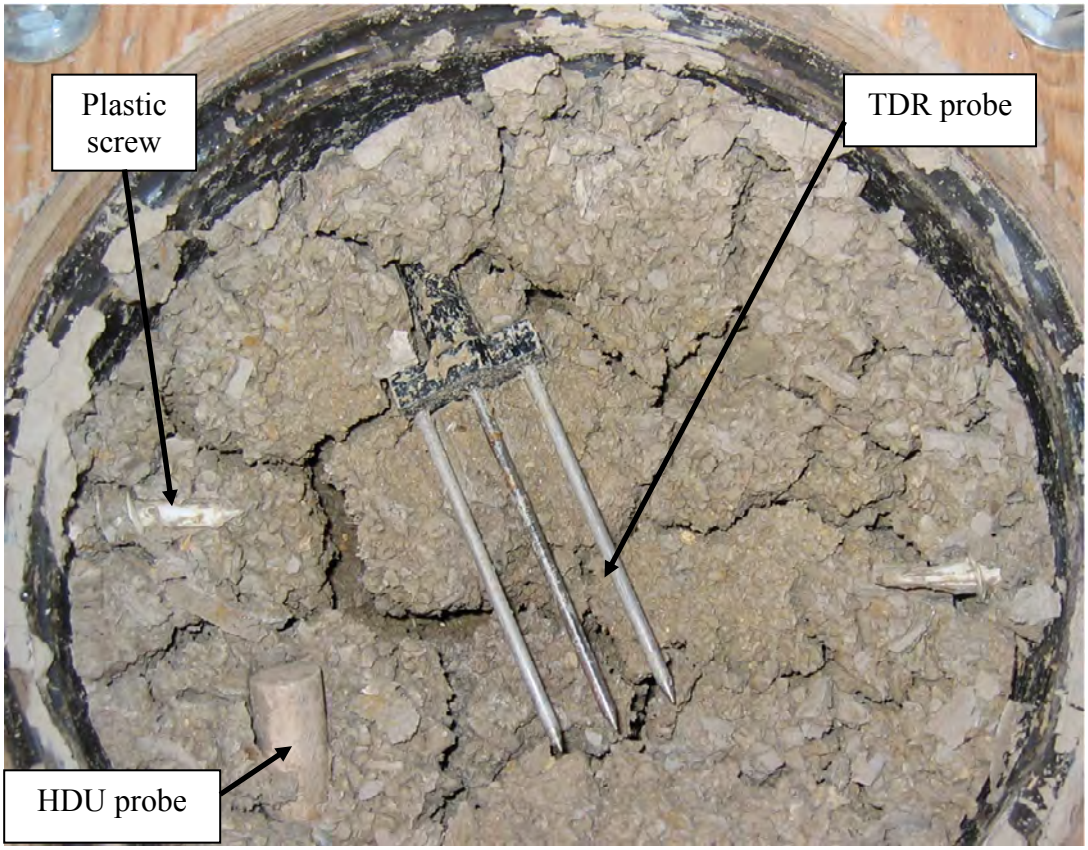

Figure 4.29: Cracking during second evaporation stage, 23 cm elevation, Sensor group D

4.5 Soil Column 4: Rigid Laterally-restrained Soil Column Compacted 2% Wet of Optimum Water Content

4.5.1 First Evaporation Stage

The characteristics of Soil Column 4 were described in Section 3.2.5. A full description of the cracking that occurred in Soil Column 4 is available in Freilich (2006). During the first evaporation stage the volumetric water content at the upper and lower sensor levels decreased more significantly and at a faster rate for the upper layer than the lower layer (Figure 4.30). Likewise, the suction measured at the upper layer was greater than the suction measured at the lower layer (Figure 4.31).

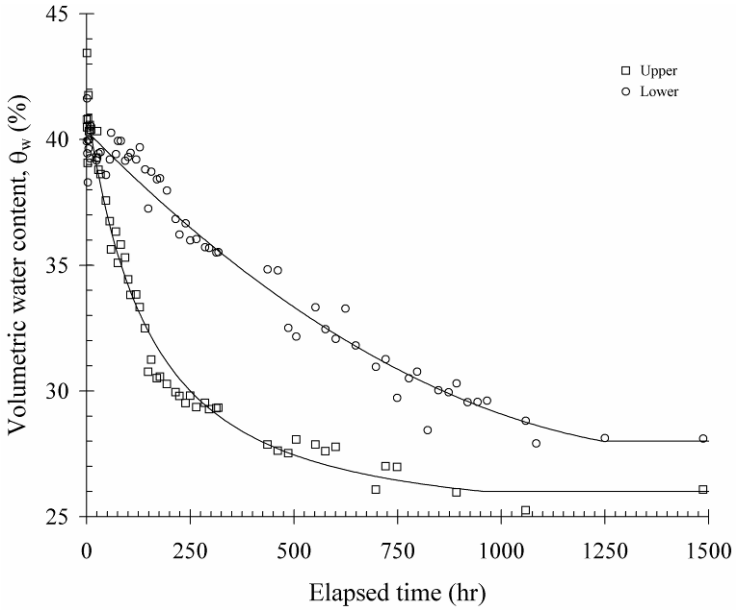

Figure 4.30: Volumetric water contents in Soil Column 4 during first evaporation phase obtained using TDR measurements

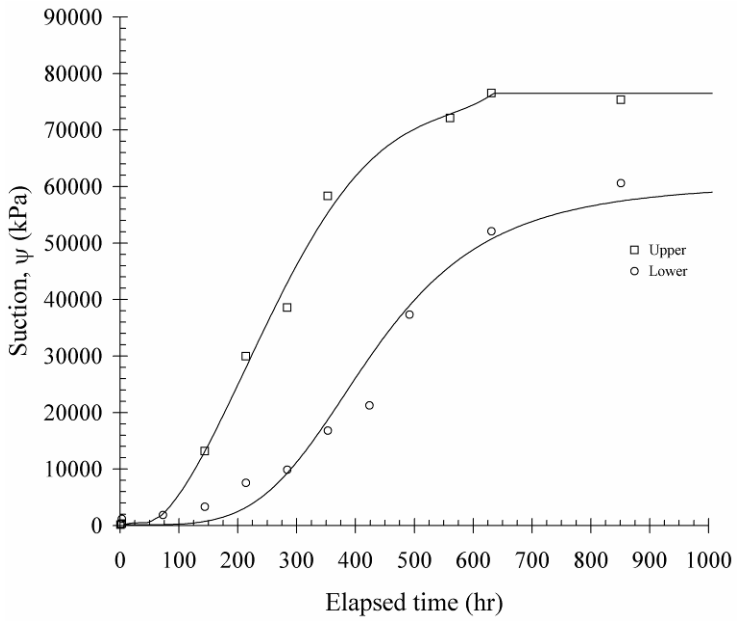

Figure 4.31: Suctions in Soil Column 4 during first evaporation phase obtained using HDU measurements

4.5.2 Infiltration Stage

The volumetric water contents measured during infiltration are shown in Figure 4.32. It is evident that a rapid increase in volumetric moisture content occurred at the upper instrumentation layer. The increase in volumetric moisture content observed at the lower layer was significantly more gradual. Likewise, the suction measured at the upper layer decreased to less than 10 kPa before any significant number of measurements of suction could be taken. The suction at the lower level did, however, decrease significantly more slowly and is shown in Figure 4.33. For the lower layer of instrumentation, the suction value at the beginning of testing was taken as the measurement of suction prior to wetting. Because of an instrument malfunction, data was not recorded until approximately 130 hours of infiltration. Between 150 and 300 hours of testing a gradual decrease in suction can be noted.

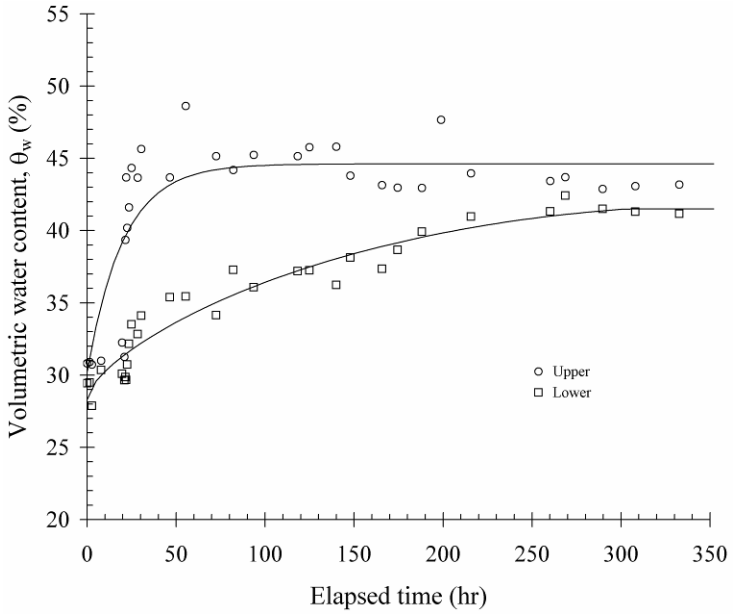

Figure 4.32: Volumetric water content in Soil Column 4 during infiltration phase obtained using TDR measurements

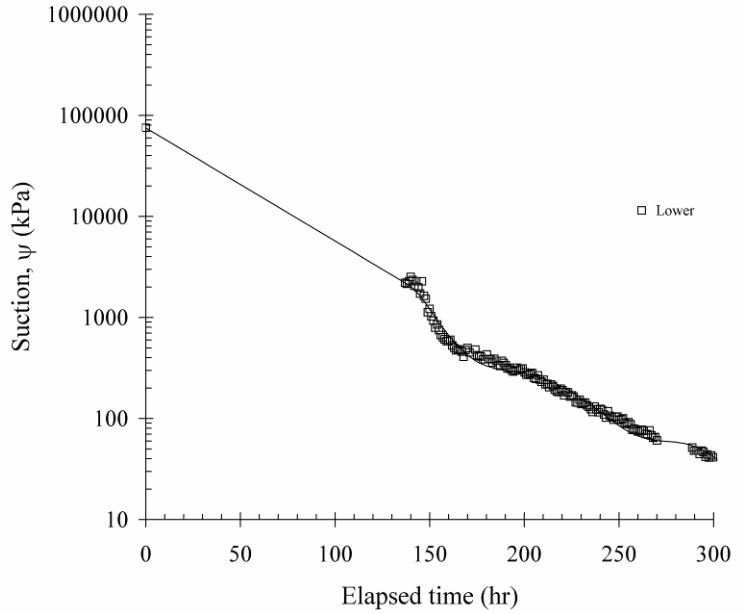

Figure 4.33: Suctions in Soil Column 4 during infiltration phase obtained using HDU measurements

4.5.3 Second Evaporation Stage

A second state of evaporation was started when volumetric moisture contents measured at the upper and lower levels ceased to change significantly with time. The change in volumetric moisture content with time is shown in Figure 4.34. As observed during the wetting phase, a sharp change in volumetric moisture content with time was observed for the upper layer, while a more gradual change in volumetric moisture content with time was observed for the lower layer. The same associated rapid and graduate changes can be observed for the change in suction with time at the upper and lower instrument levels as presented in Figure 4.35. The cracking pattern observed in Soil Column 4 during the second evaporation stage was not significantly different than that observed in Soil column 3.

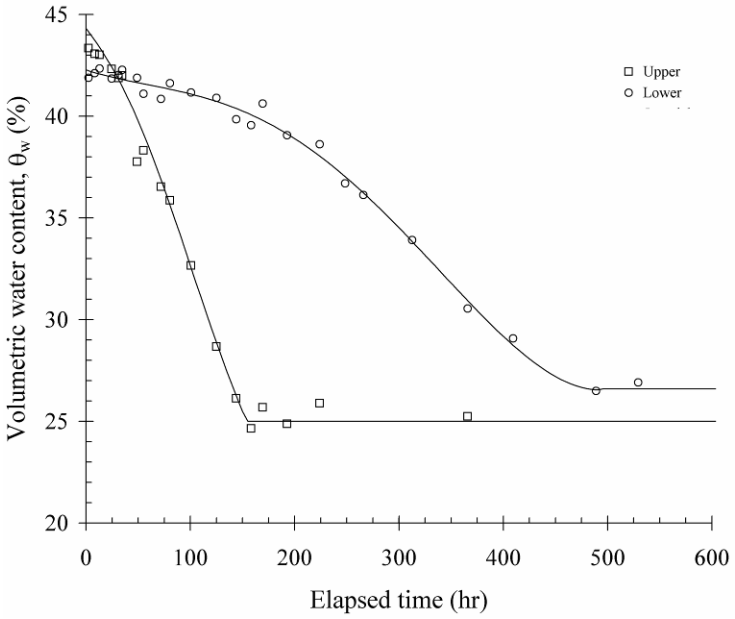

Figure 4.34: Volumetric water content in Soil Column 4 during second evaporation phase obtained using TDR measurements

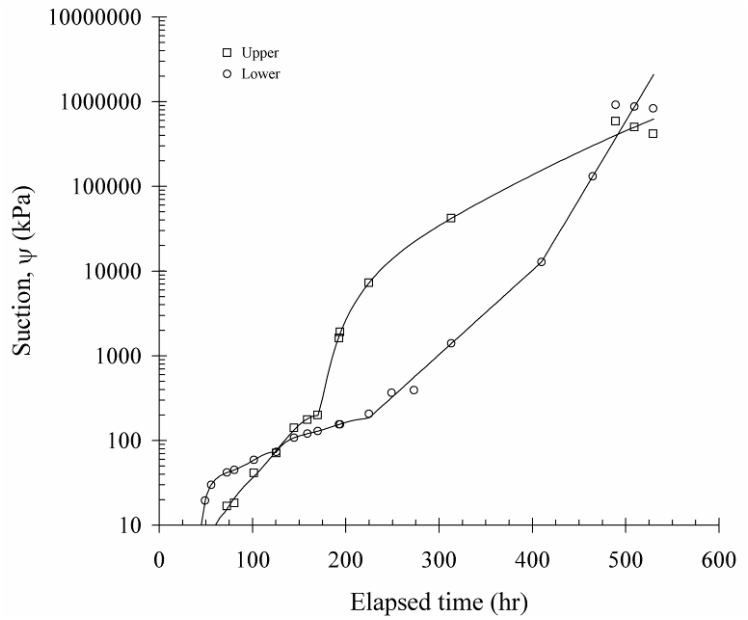

Figure 4.35: Suctions in Soil Column 4 during second evaporation phase obtained using HDU measurements

Chapter 5. Analysis of the Data for Eagle Ford Clay

5.1 SWRC and K-function models

The Soil Water Retention Curves (SWRCs) and Hydraulic Conductivity Functions (K-functions) were determined for Soil Column 3 and 4 using the volumetric water content and suction time histories presented in sections 4.4 and 4.5 of this report. As shown in section 4.4 and 4.5, smooth functions were fit to the data series in order to approximate values of volumetric water content and suction at all times of testing. This has two major advantages. First, this avoids interpreting small scatter between subsequent instrument readings as fluctuations in volumetric water content and suction. Small changes between subsequent readings are expected and are likely due to the precision of the TDR system used in this study. The second advantage of fitting smooth functions to the data is that it allows for the determination of a continuous SWRC and K-function rather than point wise calculations.

In an alternate approach, Kuhn (2005) and Freilich (2006), interpolated values of volumetric water content for times where values of suction are known. This approach was chosen since a greater number of volumetric water content readings were available than suction measurements and thus the interpolated values of volumetric water content were likely to be more accurate. This resulted in a limited number of pairs of volumetric water content and suction and thus a soil water retention curve consisting of several points. In order to better represent the shape of the SWRC, Kuhn (2005) and Freilich (2006) used two common SWRC models, van Genuchten (1966) and Brooks-Corey (1980), in their analysis of volumetric water content and suction data collected from Soil Columns 3 and 4. The use of any SWRC models will be avoided in this report. Details concerning SWRC models and interpretation of the results of using SWRC models for data gathered from Soil Column 3 and 4 can be found in Kuhn (2005) and Freilich (2006), respectively.

5.2 Effect of Cracking on Water Retention Characteristics

The results of Soil Column 3 testing and Soil Column 4 testing were examined to determine the effects of cracking on the SWRC. The SWRC could be determined for each testing stage because smooth functions, as shown in section 4.4 and 4.5 were fit to the data series in order approximate values of volumetric water content and suction at all times of testing. The SWRC and K-function are reported for both an upper layer and lower layer of instrumentation. The upper layer represents instruments at 5 cm and 10 cm below the surface of the soil for both Column 3 and Column 4. As mentioned, Column 4 had four levels of instrumentation but changes in volumetric water content and suction measured at the lower two instrumentation levels were not used for analysis because these changes were small relative to changes measured at the upper two levels (Kuhn, 2005).

The resulting SWRCs for Soil Column 3 are shown in Figure 5.01. The shape of the SWRC during the first evaporation phase is relatively flat, with suction changing significantly over a small range of volumetric water content values. This shallow slope of the SWRC is consistent with that reported in the literature for highly plastic clays (Tinjum et al. 1997; Miller et al. 2002). The SWRC measured at the upper layer lies just below the SWRC measured at the lower layer. Cracking observed during the first drying phase is likely responsible for this shift in

the SWRC. The SWRC obtained for the wetting phase presents significantly larger values of volumetric water content than observed during the first drying phase. This difference can be attributed to the fact that the soil was initially unsaturated, was compacted 2% dry of optimum, and swelled during the infiltration phase increasing the ratio of soil to water at a given value of suction. The SWRC measuring during the second drying phase is different than the SWRC measured during the first infiltration phase and during the wetting phase. While hysteresis of the SWRC may have contributed to the different drying paths observed during wetting, it is also possible that cracks formed during the first stage of evaporation may have changed the water holding characteristics of the soil. When the SWRC from the evaporation stages are compared it may also be noted that there is a significant increase in the slope of the SWRC between phases. Finally, the SWRC measured for the upper layer during the second drying phase indicates lower values of suction at a given value of volumetric water content. This shift in suction values might indicate a greater degree of swelling in the upper layer and may reflect the greater degree of cracking observed in the upper soil layer.

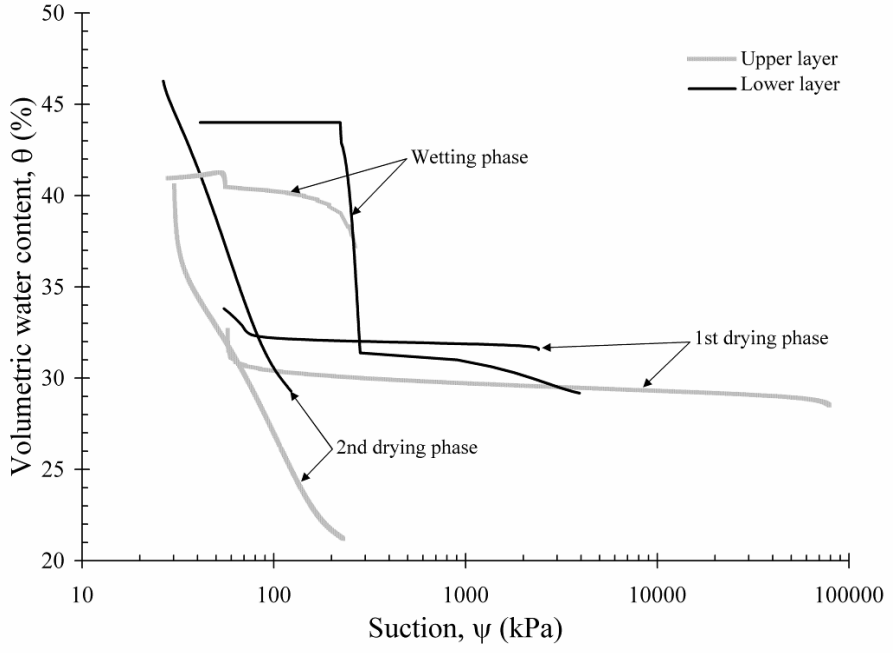

Figure 5.1: Soil water retention curves for Soil Column 3, soil compacted 2% dry of optimum

The SWRC determined for Soil Column 4 is shown in Figure 5.02. The SWRC measured for the 1st drying phase has a higher volumetric moisture contents than Soil Column 5 at lower values of suction. This difference is due to the fact that Soil Column 4 was prepared with soil moisture conditioned to 2% wet of the optimum water content for standard proctor compaction. Accordingly, the initial volumetric water content of the soil in Soil Column 4 was higher than Soil Column 3. The wetting phase SWRC measured for Soil Column 4 is not that significantly different than the 1st drying phase. Unfortunately, the SWRC for the upper layer could not be determined during infiltration since the volumetric water content increased at such a rate that the soil reached its final volumetric water content before a suction measurement could be made after

the initial suction measurement. Since the wetting curve for the lower layer reaches approximately the initial volumetric water content of the soil specimen at compaction, it may be concluded that swelling of the soil for the lower layer may not have been too significant. Alternatively, it may be concluded that the soil, under the imposed water head, did not reach a higher degree of saturation than at the time of compaction.

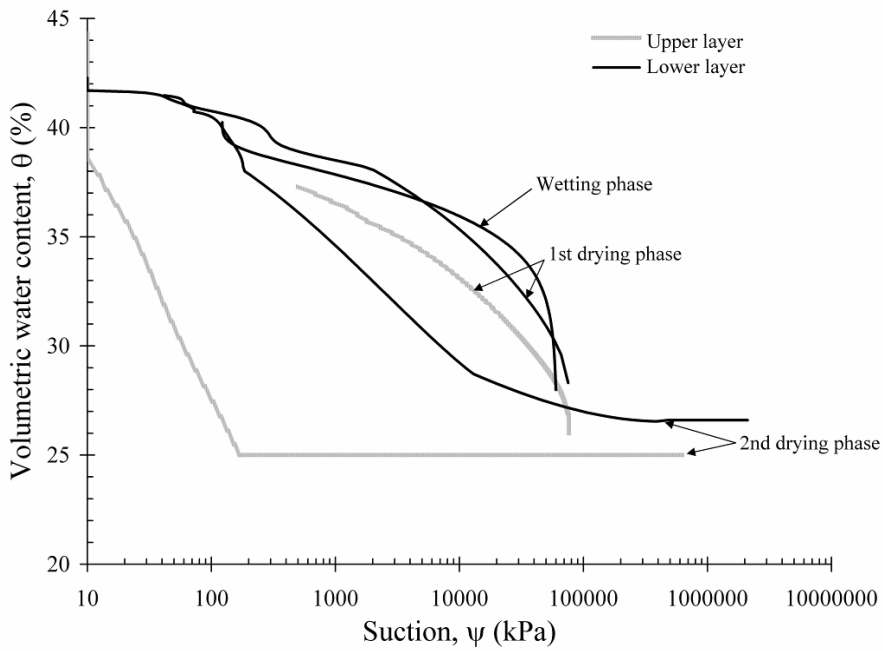

Figure 5.2: Soil water retention curves for Soil Column 4, soil compacted 2% wet of optimum

The SWRCs for Soil Column 3 and 4 are plotted together in Figure 5.3 in order to determine the effect of a drying phase, a wetting phase, and a second drying phase upon the shape of the SWRC. When volumetric water contents for the first evaporation stage and the infiltration stage are compared for low suction values (e.g., lower than 100kPa), the values of volumetric water content measured during the infiltration stage are significantly larger. This increase in volumetric water content was presumably caused by swelling. As noted earlier, this effect was more significant in Soil Column 3 where the soil was prepared at a water content 2% dry of optimum. During the second evaporation stage, the volumetric water content values at suctions higher than 100 kPa are less than the volumetric water content values measured during the first evaporation stage and the infiltration stage. The changes in the SWRC suggest that soil that underwent cracking cannot sustain comparatively high values of suction unless the volumetric water content decreases to a value significantly lower than the volumetric water content measured during the first evaporation stage (e.g., $\theta < 20\%$).

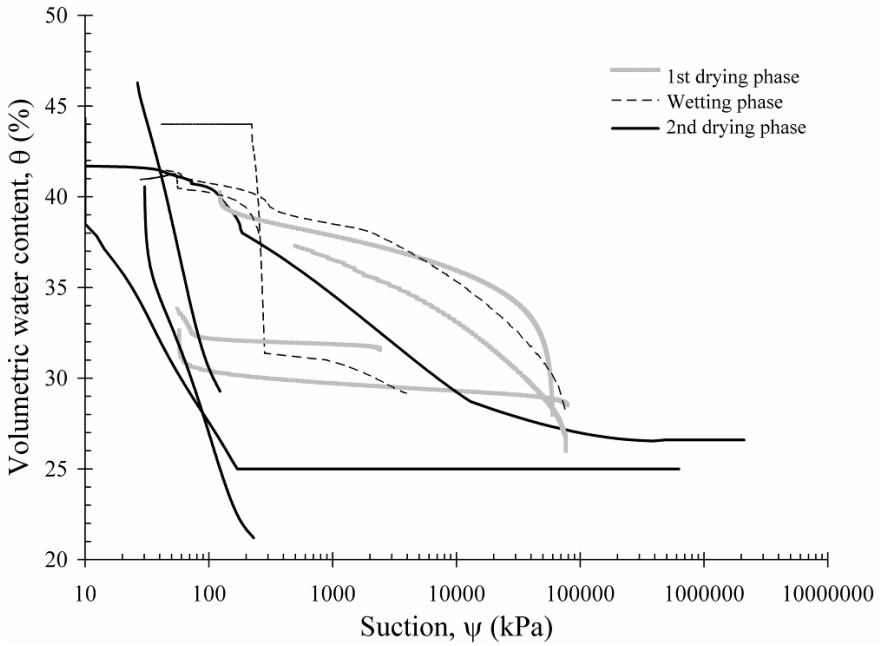

Figure 5.3: Soil water retention curves for the soil specimens, compacted 2% dry and wet of optimum

Data from both the first and second evaporation stages show well defined, yet different SMRCs. A downward shift in the SMRC at suctions greater than 100 kPa is evident when comparing the SMRC from the first evaporation stage (intact stage) with the SMRC from the infiltration stage. These results indicate that layers with different SMRCs can exist in a soil profile that is affected by surficial cracking. Consequently, to model the hydraulic response it may be necessary to consider a multilayered system with significant contrasts in hydraulic conductivity. It should be noted that the presence of multiple layers with contrasting hydraulic conductivities may have significant implications in slope stability analysis.

5.3 Effect of Cracking on the Rates of Evaporation and Infiltration

5.3.1 Rate of Evaporation for Intact and Cracked Clays

The evaporation rates from Soil Columns 1 and 2 can be compared since they were compacted to the same target conditions (gravimetric water content, dry unit weight) and dried under the same boundary conditions. Screws were, however, used to restrain the soil laterally in Soil Column 2. Cracking observed during testing was limited to the surficial soil portion in Soil Column 1, while deeper cracks developed in Soil Column 2. Cracking that had been limited to the top of the soil in Soil Column 1 developed throughout the soil in Soil Column 2. Since cracking developed throughout the soil in one column, but not the other, water loss with time from these two columns provides some quantitative basis for evaluating the effect of cracking on the evaporation rate.

To compare Soil Columns 1 and 2, the volume of water loss was normalized by dividing the cumulative water loss by the surface area of the soil column. The results are plotted in Figure

5.4 as a function of time. The cumulative evaporation measured for Soil Column 2 was approximately twice the value obtained from Soil Column 1.

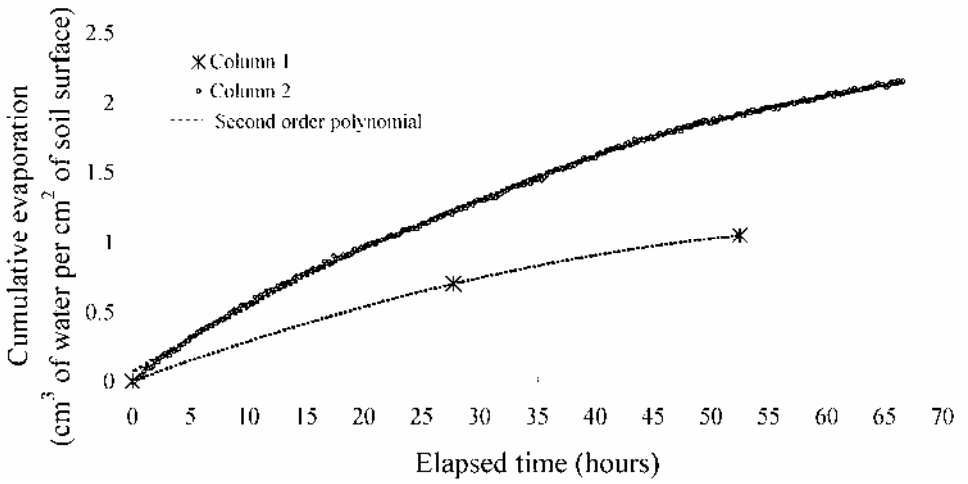

Figure 5.4: Cumulative evaporation from Column 1 and Column 2

The evaporation rate corresponds to the slope of the cumulative mass loss per area shown in Figure 5.4. Because cumulative water loss was determined using a laboratory scale for Soil Column 1, only three data points were available within this time period for Soil Column 2. To compare evaporation rates from Soil Column 1 and Soil Column 2 a second order polynomial was fit to the data from Soil column 1 as shown in Figure 5.4.

The evaporation rates for Soil Columns 1 and 2 are compared in Figure 5.5. To show the contrast in evaporation rates between Soil Column 1 and 2, the evaporation rate from Soil Column 2 was divided by the evaporation rate from Soil Column 1 and the resulting ratio of evaporation rates is shown in Figure 5.6. The initial evaporation rate from Soil Column 2 was greater than two times that from Soil Column 1. The ratio of evaporation rate from Soil Column 2 to Soil Column 1 decreases to the end of testing. It should, however, be noted that Soil Column 1 was 200 mm in height and Soil Column 2 was only 40 mm in height. It is possible that the rate of evaporation from Soil Column 2 was affected towards the end of drying as the drying front came closer to the no-flow boundary condition at the base of the column. Comparing evaporation rates from Soil Column 1 and 2 indicate that the initial rate of evaporation from a compacted soil can double with cracking.

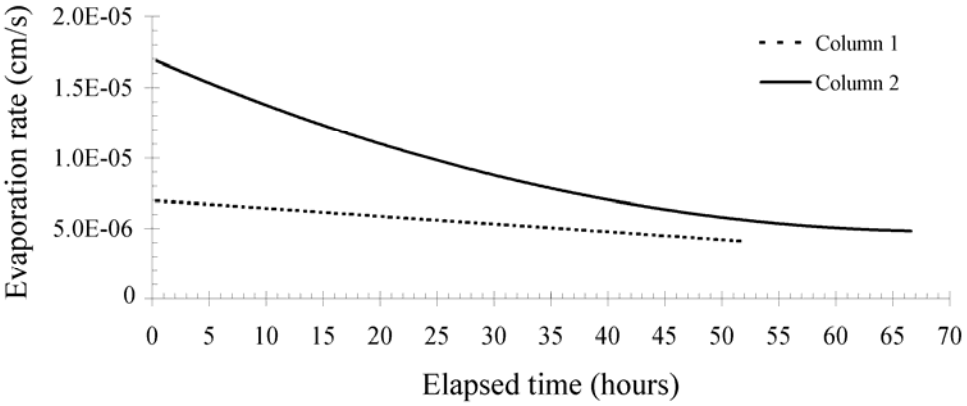

Figure 5.5: Evaporation rates from Soil Column 1 and Soil Column 2

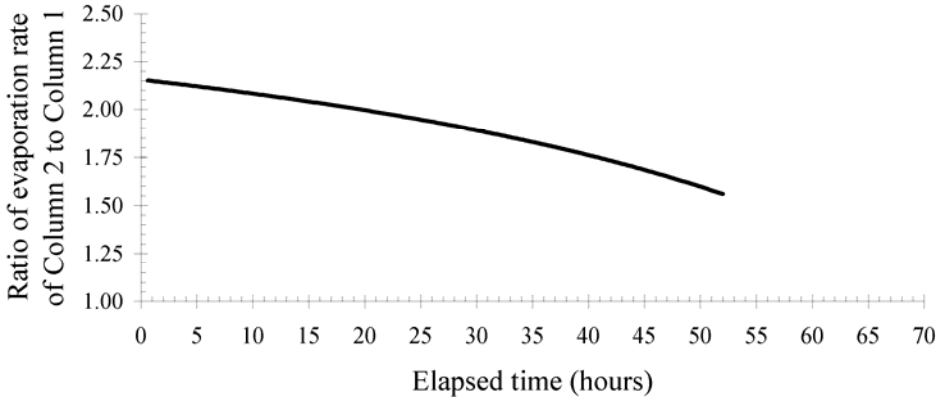

Figure 5.6: Ratio of evaporation rates from Soil Column 1 and Soil Column 2

5.3.2 Determination of the K-function from Soil Column 3 Results

The K-function was determined using the instant profiling method (Daniel 1983; Wendroth et al. 1993; Meerdink et al. 1996). The instant profiling method involves calculating the K-function of a soil profile during infiltration or evaporation using measured suctions and volumetric water contents. Darcy's Law is assumed valid for the instant profiling method. The instant profiling method involves calculating the hydraulic conductivity of a material for a given rate of flow of water, Q_w, and a measured hydraulic gradient, i.

In the case of an unsaturated material, the hydraulic conductivity of the material relative to water, K_{rw} can be estimated as follows:

$$Q_w = -K_{rw} \cdot i \cdot A \qquad \text{Equation 5.05}$$

$$q_w = -K_{rw} \cdot i \qquad \text{Equation 5.06}$$

$$K_{rw} = -\frac{q_w}{i} \qquad \text{Equation 5.07}$$

The flow of water is transient during the column experiment carried out in this research component. Consequently, the volumetric water content and suction changed with time and location throughout the specimen. For soil column experiments involving evaporation, the volumetric water content generally decreased while the suction increased with time at a given elevation.

The following describes the methodology for analyzing data from a soil column containing four levels of instrumentation (i.e., Soil Column 3). The analysis is just as applicable for a soil column containing two levels of instrumentation (i.e., Soil Column 4). An explanation for explicitly analyzing data from a soil column with two instrument levels can be found in Freilich (2006.)

For the analysis of data for Soil Column 3 during the evaporation stages, the column was split into five regions (Figure 5.7). Suction and volumetric water content were measured at levels A through D. The values of suction and volumetric water content at Level O (bottom boundary) were extrapolated at each time step from the values of suction and volumetric water content measured at Levels A and B for time *t* and *t-1*.

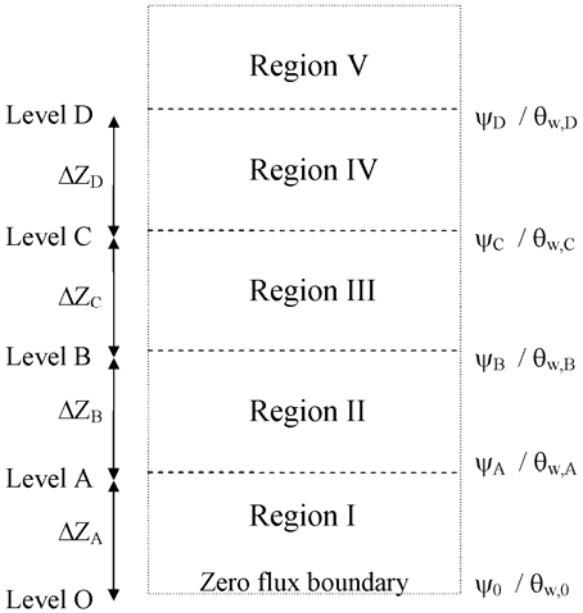

Figure 5.7: Regions for instant profiling analysis for evaporation of water from Soil Column 3

A no-flow boundary was used at the base of the soil columns for all of the experiments conducted in this research component. Accordingly, the volume of flow occurring across Region I of Soil Column 3 during evaporation corresponds to a change in the water storage of Region I. The volume of flow occurring in Regions II, III, IV, and V involves determination of the cumulative change in water storage in the underlying regions.

If time *t-1* is a time less than t, then the quantity of flow occurring through Region I between time *t-1* and time *t*, equals the difference in volume of water in Region I between time *t*, $V_{w,t}$, and time t-1, $V_{w,t-1}$. The rate of flow equals the volume of flow divided by the length of the time step, Δt, as follows:

$$Q_w = \frac{\Delta V_w}{\Delta t} = \frac{V_{w,t} - V_{w,t-1}}{\Delta t} \qquad \text{Equation 5.08}$$

Although the volume of flow leaving Region I was not measured, values of volumetric water content at Level A were measured and the volumetric water content at Level O was extrapolated. Accordingly, the volumes at times t and *t-1* can be calculated from the measured volumetric water contents at the respective times, as follows:

$$V_{w,t} = V_{total} \cdot \frac{V_w}{V_{total}} = V_{total} \cdot \theta_w = A \cdot \Delta Z_{A,t} \cdot \frac{\theta_{w,t,0} + \theta_{w,t,A}}{2} \qquad \text{Equation 5.09}$$

$$V_{w,t-1} = A \cdot \Delta Z_{A,t} \cdot \frac{\theta_{w,t-1,0} + \theta_{w,t-1,A}}{2} \qquad \text{Equation 5.10}$$

Assuming that no volume change occurs between *t-1* and *t*, the height of Region I, ΔZ_A, can be considered constant. Combining Equation 5.09 and 5.10 and normalizing by the cross sectional area of the soil yields the average rate of flow between *t-1* and *t*, q_w, as follows:

$$Q_w = A \cdot \Delta Z_A \cdot \frac{\left(\theta_{w,t,0} - \theta_{w,t-1,0}\right) + \left(\theta_{w,t,A} - \theta_{w,t-1,A}\right)}{2\Delta t} \qquad \text{Equation 5.11}$$

$$q_w = \Delta Z_A \cdot \frac{\theta_{w,0}\big|_t^{t-1} + \theta_{w,A}\big|_t^{t-1}}{2\Delta t} \qquad \text{Equation 5.12}$$

The hydraulic gradient acting across Region I between time *t-1* and *t* must be determined to calculate the hydraulic conductivity. The change in total head can be defined by estimating the change in total suction, where total suction is the sum of osmotic potential and matric suction. Osmotic potential is assumed to be constant (i.e., independent of water content). Accordingly, this analysis assumes that osmotic suction has no effect on the total hydraulic gradient. Thus, flow is driven solely by matric suction and gravimetric head. During evaporation, flow causes an increasing suction at the upper portion of Region I which should overcome gravity, which is represented by a negative unit gradient. The change in matric suction occurring across Region I is the average of the change in matric suction occurring at time *t-1* and time *t* as follows:

$$i = \frac{\partial h}{\partial l} = \left(\frac{\partial \psi}{\Delta Z_A} - 1\right) = -\left(\frac{\left(\psi_{t,A} - \psi_{t,0}\right) + \left(\psi_{t-1,A} - \psi_{t-1,0}\right)}{2 \cdot \Delta Z_A} - 1\right) \qquad \text{Equation 5.13}$$

Substituting Equation 5.12 and 5.13 into Equation 5.07 yields an estimate of the hydraulic conductivity in Region I between times *t-1* and time *t*, as follows:

$$K_{rw,I,t} = \frac{q_w}{i} = \frac{\Delta Z_A \cdot \frac{\theta_{w,0}\big|_t^{t-1} + \theta_{w,A}\big|_t^{t-1}}{2\Delta t}}{\left(\frac{\left(\psi_{t,A} - \psi_{t,0}\right) + \left(\psi_{t-1,A} - \psi_{t-1,0}\right)}{2 \cdot \Delta Z_A} - 1 \right)}$$ Equation 5.14

The K-ψ and K-θ relationships can then be defined using the suction and volumetric water content values corresponding to the average values in Region I (levels O and A) at times *t-1* and *t*, as follows:

$$\psi = \frac{\psi_{t-1,0} + \psi_{t-1,I} + \psi_{t,0} + \psi_{t,I}}{4}$$ Equation 5.15

$$\theta = \frac{\theta_{w,t-1,0} + \theta_{w,t-1,I} + \theta_{w,t,0} + \theta_{w,t,I}}{4}$$ Equation 5.16

The same process for computing the flow rate and hydraulic gradient can be conducted for Regions III and IV. For each region, the volume of flow from underlying regions needs to be added to the volume of flow for that respective region. The changes in suction occurring during the first evaporation stage in Soil Column 3 (between 0 and 64 hours) are shown in Figure 5.8. The corresponding changes in volumetric water content that occurred during the same evaporation stage (between 0 and 64 hours) are shown in Figure 5.9. As discussed next in section 5.3.3, this information was used to define the K-function of Eagle Ford Clay.

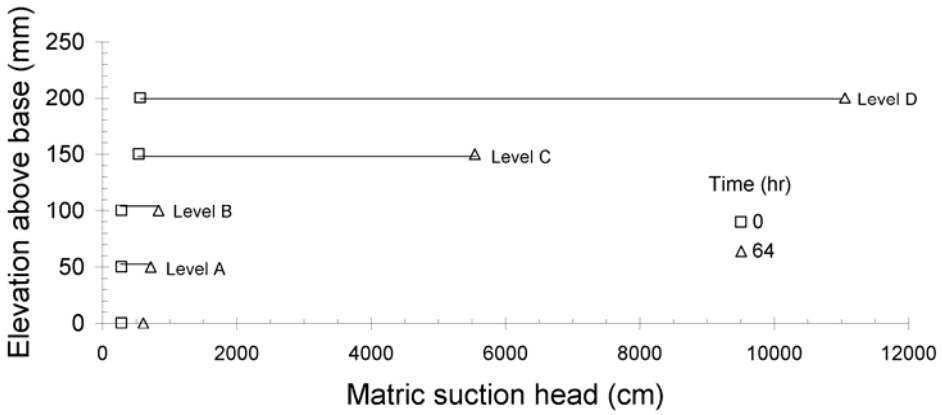

Figure 5.8: Matric suction during the time step of the first evaporation phase of Soil Column 3

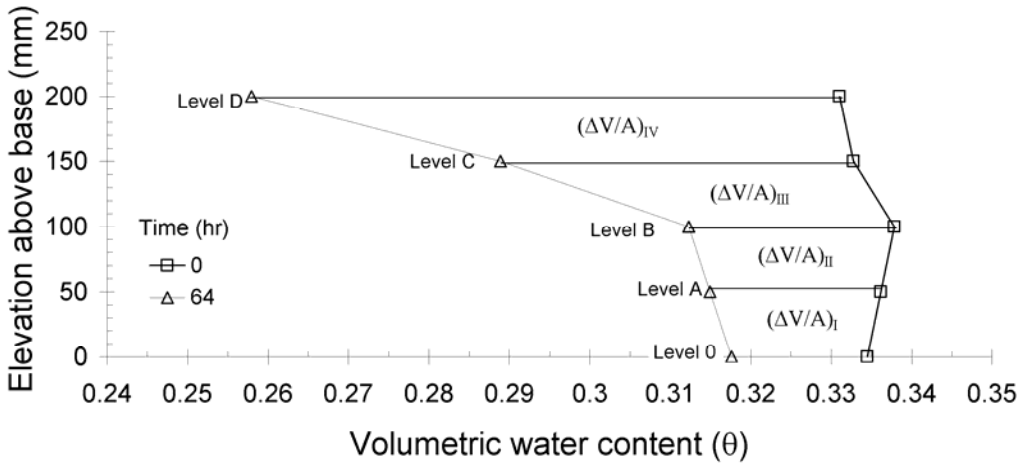

Figure 5.9: Volumetric moisture content during the time step of the first evaporation phase of Soil Column 3

5.3.3 Effect of Cracking on the K-function

The K-function was determined for the first and second evaporation stage of Soil Column 3 following the methodology outlined in Section 5.3.2. In order to use the methodology outlined in 5.3.2, it is necessary to know the height of instrumentation during the experiment. During the first and second evaporation stages for Soil Column 3 and Soil Column 4, the settlement of the specimen was on the order of 10 mm. Consequently, the height of instrumentation for the first evaporation stage for both Columns was taken as the elevation at installation. The elevations of instrumentation for the second evaporation stage were measured after the second evaporation stage, when the column was exhumed. The K-function was not calculated during infiltration into Soil Column 3 and 4 because the distance between instrumentation levels could not be measured during swelling.

The hydraulic conductivity functions determined for Soil Column 3 are shown in Figure 5.10. It is evident that there is a shift in the hydraulic conductivity function from the first to the second drying phase. During the second drying phase, suction values at high as observed during the first drying phase were not observed until near the close of the experiment. Furthermore, the measured range of hydraulic conductivity increased by approximately three orders of magnitude form the first to the second drying phase. It can, however, be noted that the hydraulic conductivity function measured during the first and second drying phases have approximately the same slope. This may indicate that although the k-function has shifted significantly, the change in hydraulic conductivity with change in suction in a log-log relationship does not change significantly with a cycle of wetting and drying.

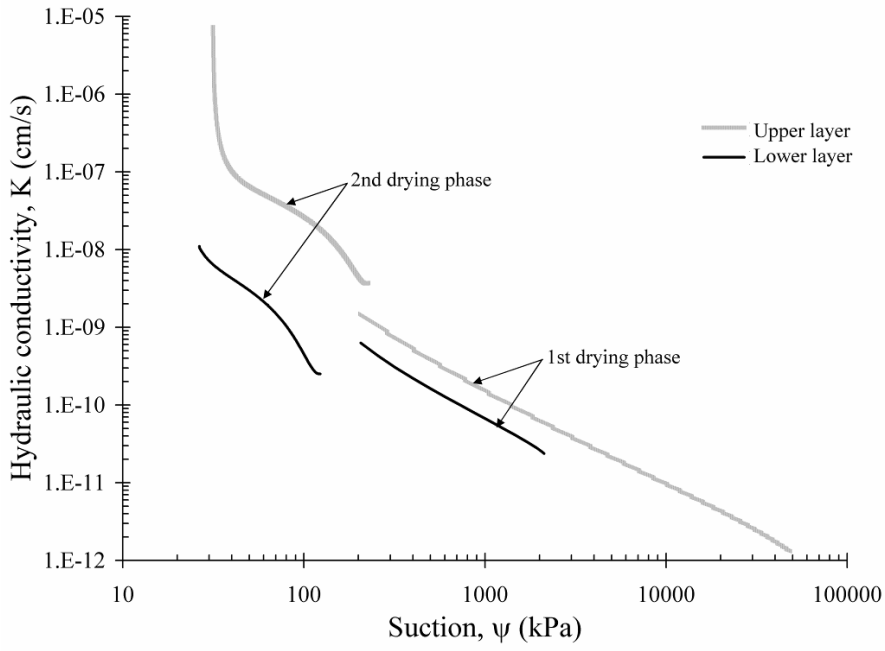

Figure 5.10: Hydraulic conductivity function for the Soil Column 3, compacted 2% dry of optimum

The hydraulic conductivity functions determined for Soil Column 4 are shown in Figure 5.11. Unlike Soil Column 3, where the measured range of hydraulic conductivity increased by approximately three orders of magnitude from the first to second drying phase, the measured range of hydraulic conductivity did not change significantly. When noting the difference between SWRCs for upper and lower during the first and second drying phases, it is evident that the SWRC for the upper layer does not change significantly from the first to second drying phase. The SWRC for the lower layer does, however, change significantly. For a given value of suction, the measured hydraulic conductivity of the lower layer for the first drying phase is approximately one order of magnitude greater than the measured hydraulic conductivity of the lower layer for the second drying phase.

In order to evaluate the effect of a cycle of wetting and drying on the shape of the SWRC for soil compacted 2% dry and 2% wet of optimum water content, the data presented in Figure 5.10 and 5.82 is plotted together in Figure 5.12. As prior noted, the K-function measured during the second drying phase indicates higher measured hydraulic conductivities at a given suction level for the second drying phase than the first drying phase.

The combined effects of cracking occurring during the first evaporation stage, swelling occurring during the second evaporation stage, and cracking occurring during the second evaporation stage led to significant changes in the K-function of Eagle Ford clay. These changes in the K-function lead to an increase in the rate of evaporation and infiltration and may affect slope performance as will be discussed in the subsequent section.

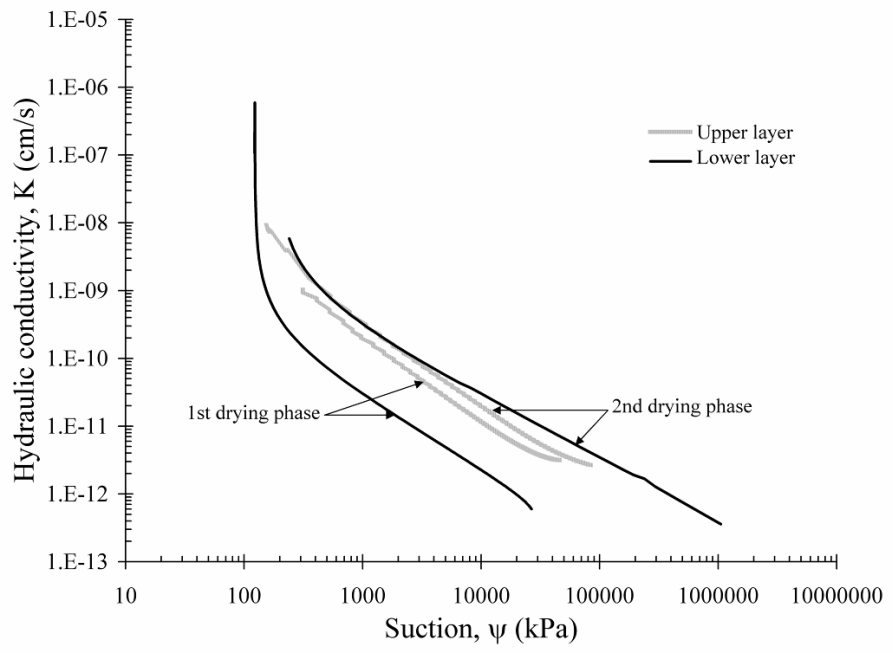

Figure 5.11: Hydraulic conductivity function for Soil Column 4, compacted 2% wet of optimum

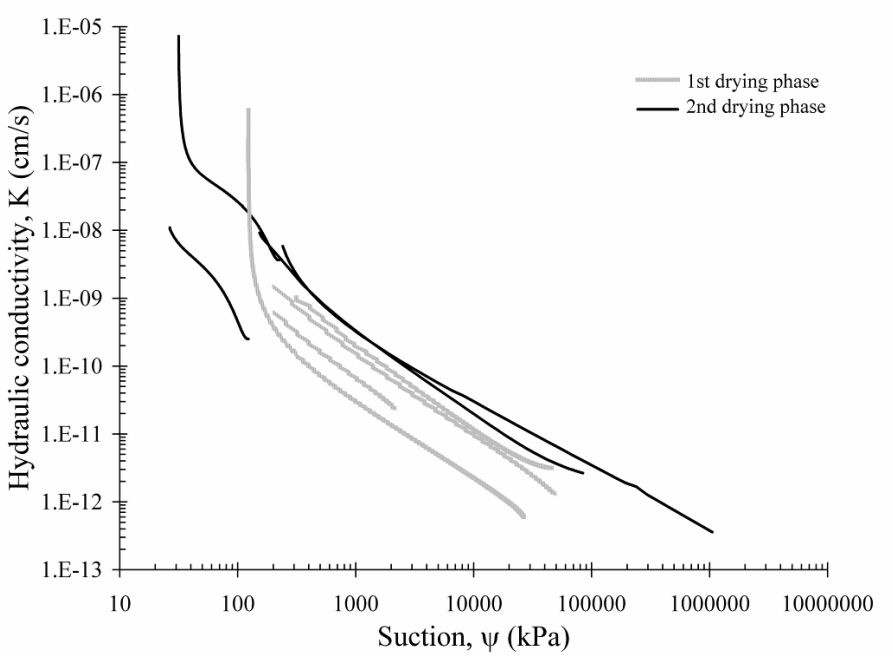

Figure 5.12: Hydraulic conductivity function for Soil Columns 3 and 4, compacted 2% dry and wet of optimum, respectively

5.4 Significance of Experimental Results

The prediction of slope failures in highly plastic clays has been a concern of TxDOT. Recognizing the causes of these failures will allow TxDOT to design and construct embankments using highly plastic clay fill in a manner that will limit the extent and number of slope failures. The improved design and construction of embankment using highly plastic clays will therefore reduce the need for and costs associated with slope maintenance. While water infiltration and development of cracks may not be the only causes of these slopes failures, they are probably among the main causes. The significance of experimental results collected in this research component on the stability of highly plastic clay embankments is discussed in this section.

5.4.1 Significance of Experimental Results on the Stability of Highly Plastic Clay Slopes after Discrete Precipitation Events

The results of this research component indicate that cracking changes the shape of the SWRC and the K-function of highly plastic clays. These changes have the potential to affect slope performance because they lead to significant increases in rates of water infiltration and evaporation. They also lead to the development of contrasting hydraulic conductivities during both the infiltration and evaporation processes.

The beneficial aspects of negative pore water pressures in slope stability are generally not considered in design because negative pore water pressures can be lost due to water infiltration. While this has been a commonly accepted design approach, this research component reveals that cracking significantly changes the SWRC of highly plastic clay. As a result, comparatively high suction values may not develop unless the soil reaches significantly low volumetric water contents. This loss in suction may be particularly detrimental to the surficial stability of slopes, where suction can lead to a significant increase in the factor of safety against shallow slope failure. The factor of safety increases significantly for shallow slope failures because the shear strength component provided by suction is significant at low stress levels.

The experimental results showed a significant increase in the hydraulic conductivity of unsaturated highly plastic clay due to cracking. Accordingly, the rate of infiltration into the slope may increase leading to destabilizing conditions of flow. An increase in saturated hydraulic conductivity with cracking was also reported in past research (Boyton and Daniel 1980; Sims et al. 1996; and Albrecht and Benson 2001). If the depth of cracking is uniform, then there is also a potential for the development of distinct layers with significantly different SWRCs and hydraulic conductivities. The existence of layers of contrasting hydraulic conductivities in highly plastic clays is supported by the multiple SWRC needed to fit the wetting path at different elevations in Soil Column 3 (Figure 5.02). Such multilayered configurations may conceivably lead to the generation of positive pore water pressures at the interface between the cracked and intact zones.

5.4.2 Significance of Experimental Results on the Long Term Stability of Highly Plastic Clay Slopes

The long-term stability of highly plastic clay slopes has been speculated to depend on long term changes in suction within clay slopes, which may be the product of long term exposure of the slope to the environment (Aubeny and Lytton 2003). In this case, the average weather conditions rather than the seasonal precipitation events should be quantified. Following the discussion of the effects of average weather conditions, the boundary conditions for infiltration

and evaporation in highly plastic clay slopes are discussed. Specifically, boundary conditions typical for the state of Texas, boundary condition used for this testing program, and boundary conditions assumed by Aubeny and Lytton (2003) are evaluated in this section. Additionally, expected differences between the development of cracks in the field and laboratory, resulting from differences in field and laboratory boundary conditions, are discussed. As previously discussed (see Figure 3.07), the effect of temperature on suction is minor when compared to the effect of relative humidity for the range in temperature used in this research component and typical of the state of Texas. Accordingly, the focus of this evaluation is on the average relative humidity conditions to which clay slopes are exposed.

The range in atmospheric relative humidity values is very broad for the state of Texas. A map of annual mean relative humidity values throughout the state of Texas at 6 a.m. and 6 p.m. is shown in Figure 5.13 (Arbingast et al. 1976). A modified version of the relative humidity map (Arbingast et al. 1976) showing the suction of soil that reached equilibrium with atmospheric conditions characterized by a mean annual relative humidity values representative of conditions in Texas is shown in Figure 5.14. Suction values were calculated using Equation 3.1 and assuming an average temperature of 20°C. It is evident that the broad range in relative humidity values results in a broad range in suctions across Texas. The majority of surficial clays in Texas fall within the eastern half of Texas (Olive et al. 1989). Suction values in the eastern half of Texas range approximately from 14,000 kPa to 107,000 kPa.

Although the range in values of calculated suction is very broad for the state of Texas, the rate of evaporation is not controlled by the atmospheric relative humidity. Instead, the movement of water is controlled by gradients in temperature and relative humidity across the soil-atmosphere interface (Tindall 1999). In the experimental testing program conducted as part of this research component, a fan was used to move air across the soil-atmosphere interface to maintain a constant relative humidity. In the field, however, the air velocity above the air-soil interface may not, be sufficiently large enough to maintain the relative humidity at the soil-atmosphere interface equal to the relative humidity in the atmosphere. Although, the relative humidity at the soil-atmosphere interface may differ from the atmospheric relative humidity, the atmospheric relative humidity provides a preliminary estimate of the maximum expected suction at the interface.

Results obtained in this research component indicate that evaporation occurs for relative humidity values below 97% (i.e., suctions greater than 3,800 kPa) in Eagle Ford Clay placed within three percent of optimum water content with standard Proctor compactive effort. These results indicate that a long-term evaporation process is expected to take placed for embankments constructed using typical soil placement conditions and for average relative humidity values in Texas.

The boundary condition used in the laboratory can be compared to field boundary conditions. The suction at the top boundary of Soil Column 3 was 108,000 kPa (Equation 3.1). When compared to average suction values for Texas (Figure 6.2), the suction imposed at the top boundary of Soil Column 3 is at the upper limit of suctions calculated from relative humidity values. Accordingly, the rate of evaporation measured in the laboratory should be towards the upper limit of the rate of evaporation expected in the field.

Aubeny and Lytton (2003) assumed a scenario in which the long-term process involves continued decrease of suction (i.e., infiltration) from the surface into the slope. A diffusion coefficient was measured in the laboratory and used to model suction with time in the field. Flow was assumed to occur from the bottom of cracks into the slope. The suction at the bottom of the

cracks was reported to range from 10 to 100 kPa and the suction under soil placement conditions was assumed ranging between 300 and 1000 kPa. The results from this research component, however, indicate surface suctions ranging from 14,000 to 162,000 kPa (Figure 5.02) for average conditions in Texas and the suction under soil placement conditions ranging between 100 and 100,000 kPa (Figure 5.13:). The long term flow process involves continued desiccation (i.e., increase in suction) with time. Accordingly, the boundary conditions proposed by Aubeny and Lytton (2003) do not seem to be realistic.

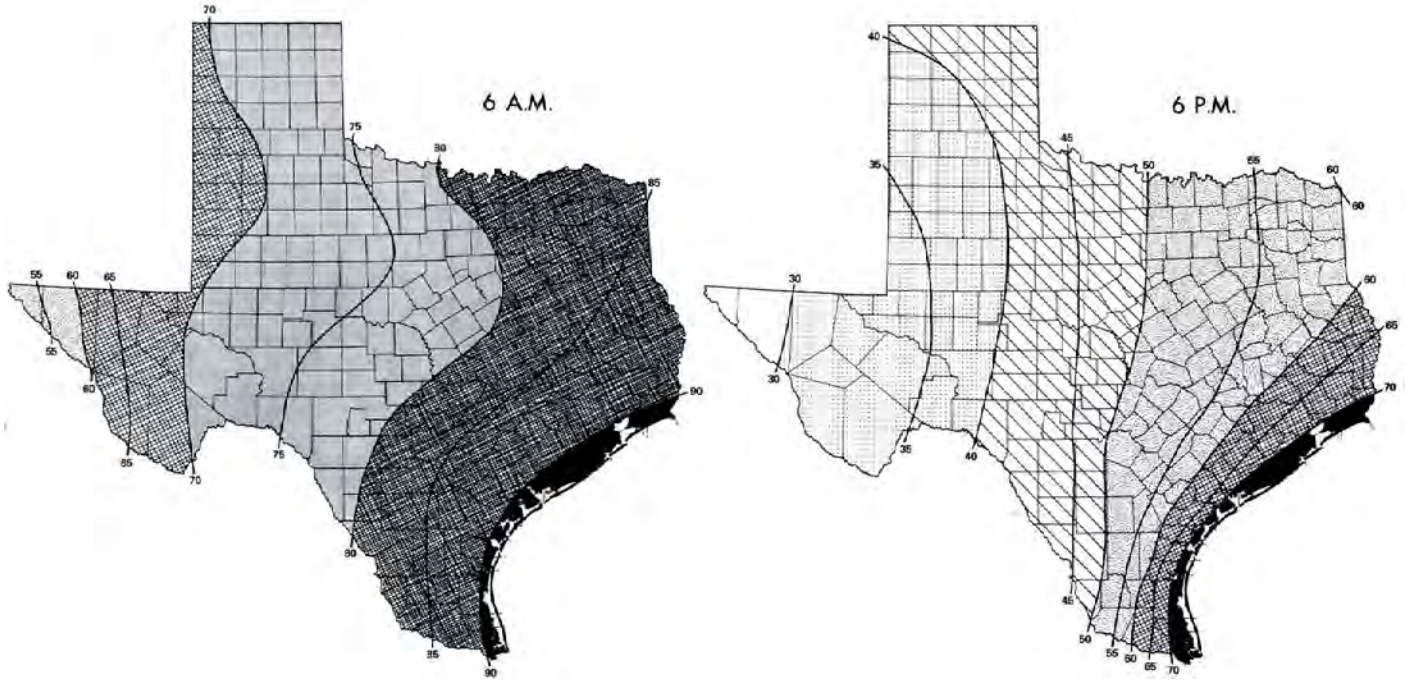

Figure 5.13: Mean annual relative humidity (Arbingast et al. 1976)

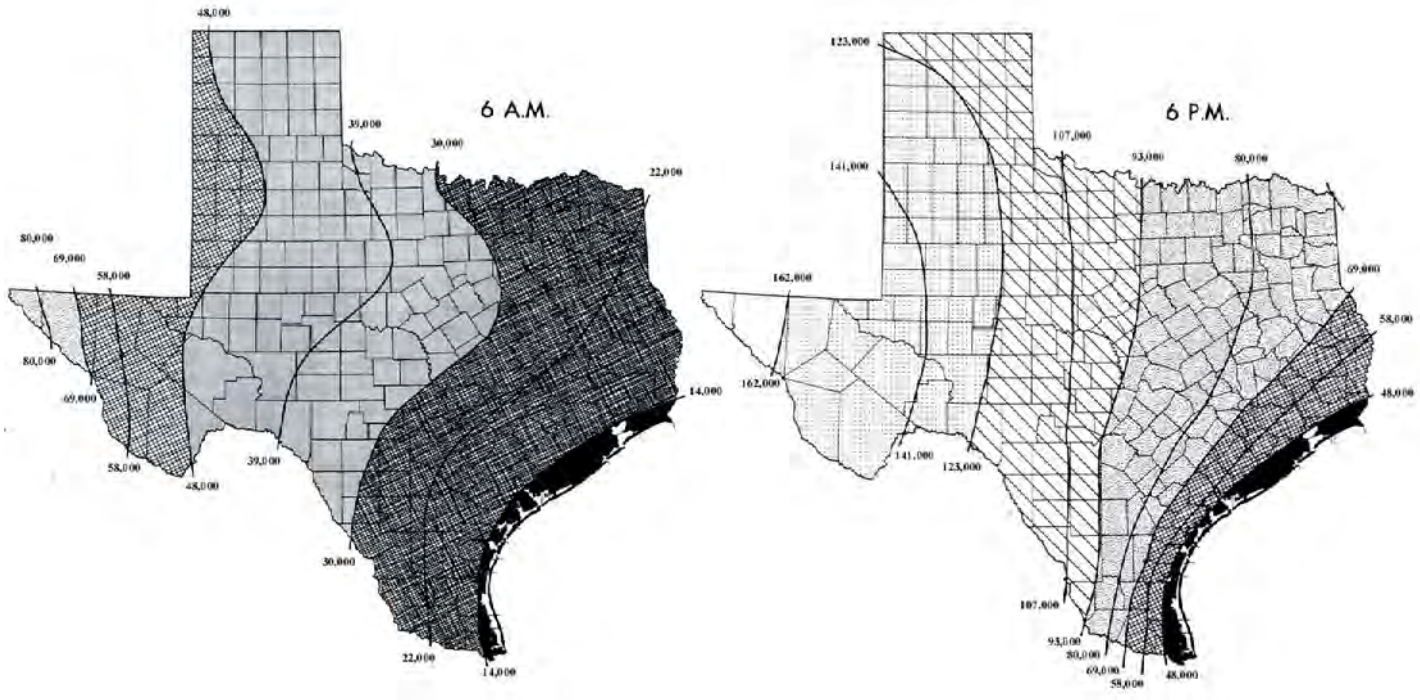

Figure 5.14: Equilibrium suction in kPa for 18.3°C calculated using Kelvin's equation (modified from Arbingast et al. 1976)

5.4.3 Recommendations for Future Evaluations

The results of column testing conducted in this research component indicate that cracking significantly affects the SWRC and K-function of Eagle Ford clay. Cracking results in a change in the SWRC and an increase in the hydraulic conductivity of the highly plastic clay. Accordingly, measures should be taken to reduce the amount of cracking occurring in compacted highly plastic slopes to limit the extent and number of failures. Techniques that could be considered in the design of highly plastic clay embankments to limit the amount of cracking include: (1) control of soil placement conditions; (2) retarding cyclical water movement in and out of the slope (e.g., by using concrete or asphalt covers); and (3) increasing surficial strength and reducing the cracking susceptibility by using fiber reinforcement. Other measures that can be taken to limit the extent and number of failures include control of surface water. The techniques include: (1) internal drainage to prevent the development of positive pore water pressures; (2) use of soil cover systems; and (3) control of surface water runoff from the slope.

Chapter 6. Conclusions and Recommendations for Future Study

A series of evaporation and infiltration experiments were conducted on compacted Eagle Ford clay to investigate the effect of cracking on the hydraulic properties of unsaturated highly plastic clays. The following conclusions are drawn:

- A long-term evaporation process (i.e., increase in suction) is expected for typical embankment soil placement conditions and typical weather conditions in Texas. Specifically, evaporation occurs for relative humidity values below 97% in highly plastic soil placed within three percent of optimum water content with standard Proctor compaction effort. Accordingly, while specific precipitation events may lead to instability due to sudden infiltration, suction within the soil embankments is expected to increase with time due to continued exposure.

- Small changes in placement water content produce significant changes in initial suction. For example, the initial suction for Eagle Ford Clay compacted 2.5% dry of optimum is 100,000 kPa while the initial suction is only 100 kPa if the soil is compacted 2.5% wet of optimum.

- The use of screws for lateral restraint in soil column experiments used to investigate water movement in highly plastic clays proved useful as it keeps soil cracks open throughout the drying process and provides representative field conditions.

- The evaporation rate in highly plastic clays compacted wet of optimum was found to be twice as high after crack development than the evaporation rate from intact clay.

- The shape of the soil-water retention curve of highly plastic clays is significantly affected by the development of cracks. Specifically, the slope of the soil water retention curve, the change in volumetric water content with increasing suction, was found to increase after cracking.

- The relationship between the hydraulic conductivity and the volumetric water content of unsaturated Eagle Ford clay is significantly affected by cracking. No clear trend between hydraulic conductivity and volumetric water content was found after cracking. Instead, the hydraulic conductivity of unsaturated Eagle Ford clay after cracking can be represented by hydraulic conductivities ranging from 2×10^{-10} cm/s to 3×10^{-7} cm/s for volumetric water content values ranging from 20% to 50%. This suggests that cracking controls flow, which is apparently independent of the volumetric water content of the soil.

- Soil profiles of highly plastic clay affected by cracking are expected to have layers of different hydraulic properties. That is, the hydraulic response of exposed slopes constructed with highly plastic clay should possibly be considered a multilayered system with significant contrasts in soil water retention characteristics and hydraulic conductivity values.

The experimental testing program carried out in this research prompts several recommendations for future studies on the effect of cracking on the hydraulic properties of highly plastic clay. Specifically, future research is recommended on instrumentation, soil-profile testing, new testing devices, and alternative testing methods to complement the results of instant profile testing.

The instrumentation of the soil columns was a challenging aspect of this research component. One of the major drawbacks of time domain reflectometry (TDR) measurements in highly plastic clays is that continued measurement of volumetric water content is difficult when using uncoated TDR probes. As discussed in Section 3.3, the TRASE program (Soil Moisture Equipment Corp., Santa Barbra Ca.) does not report the time between reflected pulses for measurements in highly plastic clays with uncoated probes. As a result graphical interpretation is required, which is time consuming and compromises the frequency by which readings can readily be made. TDR calibrations conducted as part of this research component showed clear reflections with both uncoated as well as coated probes. This suggests that a computer program could be developed to determine the time between reflections. This would facilitate the measurement of volumetric water content without the need for coating.

Regarding soil column testing, additional investigations could be conducted using a laboratory scale capable of holding the weight of testing apparatus. This would facilitate analysis of the water-balance within the column during evaporation and infiltration.

Future soil-profile testing could also include larger scale testing in order to minimize the effect of sidewall boundaries on the development of cracking. Also, different upper boundary conditions during infiltration and evaporation could also be considered. For example, a constant flow rate could be used during infiltration instead of a constant head of water relative to the soil surface. Different relative humidity values and temperatures could be selected at the upper boundary condition during evaporation. Additional investigation of the sidewall boundary condition would also be beneficial.

In order to verify the results of soil-profile testing, alternate techniques could be used to evaluate infiltration and evaporation processes. For example, the soil water retention curve of highly plastic clay used in soil-profile testing could be determined using hanging column apparatus, pressure plate apparatus, and/or centrifuge methods. Also, the hydraulic conductivity of unsaturated highly plastic clay could be investigated using a pressure plate apparatus and/or a geotechnical centrifuge.

Appendix A. Calibrated Model for Determination of Suction and Recommended Field Suction Values

A.1 Hydraulic Properties for Cracked Clays

In order to estimate expected values of suction with depth for field conditions, a vertical profile of highly plastic clay was modeled using the finite element flow program SVflux. The hydraulic properties used in modeling cracked highly plastic clay were established in Section Chapter 5. of this report. The soil water retention curve and hydraulic conductivity functions are based on laboratory studies of Kuhn (2005) and Freilich (2006). The soil water retention curve and hydraulic conductivity function used for this study are shown in Figure A.1. The soil water retention curve and hydraulic conductivity functions were measured during the drying of cracked highly plastic clay. These hydraulic properties are used in this study to represent both the change in volumetric water content with changes in suction that occur during both wetting and drying.

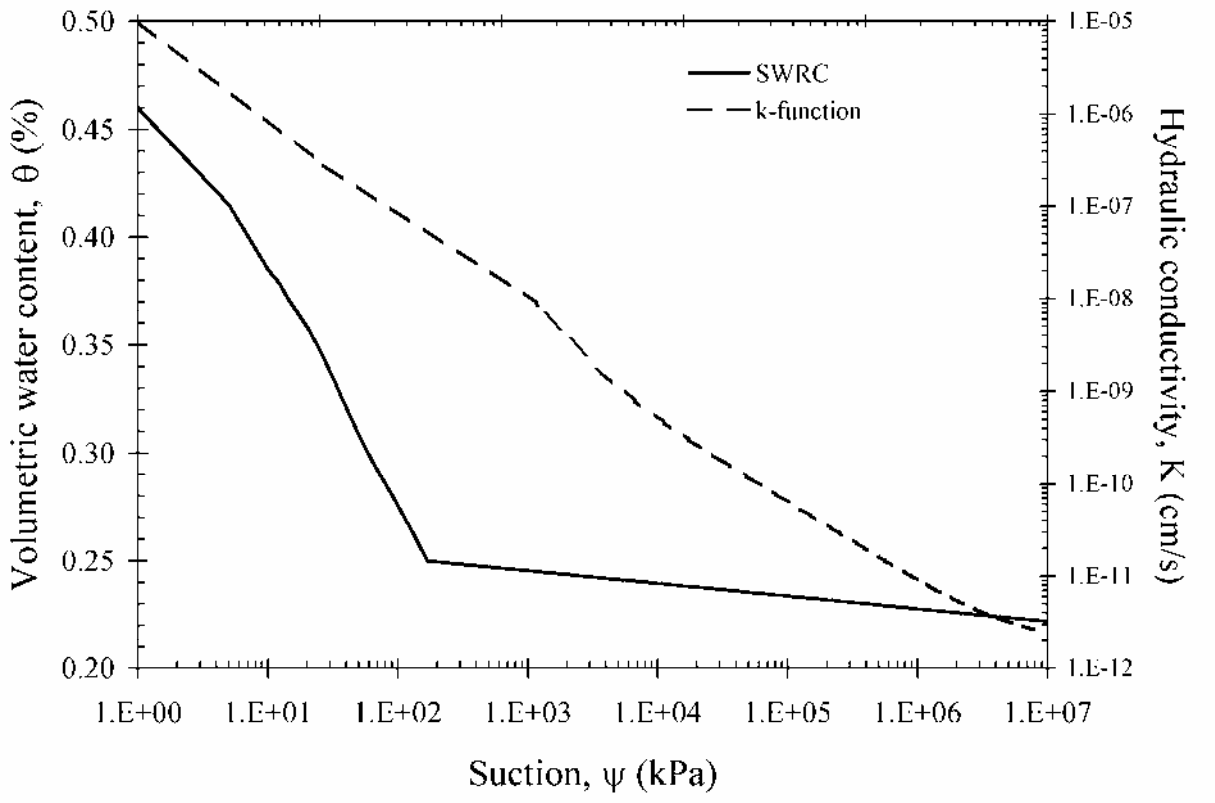

Figure A.1 Hydraulic conductivity function and Soil water retention curve for cracked highly plastic clay compacted 2% wet of optimum water content

A.2 Depth of moisture fluctuations

An important aspect of this study is defining the seasonal fluctuations in suction within a soil profile. The range of these fluctuations in suction are dependent on fluctuations in water content and decrease with increasing depth into a soil profile. At a certain depth these fluctuations in suction will be small enough that they may be considered to have little effect on moisture movements within the soil. The depth where fluctuations in suctions are minimal can be referred to as the depth of wetting and drying. The depth of moisture fluctuations for a generic soil profile is shown as a boundary in 0.

Moisture fluctuations within the soil cause volumetric strains. These volumetric strains lead to cracking of the soil. Aguettant (2006) measured changes in shear strength properties with moisture fluctuations and Kuhn (2005) measured changes in hydraulic properties with moisture fluctuations. Accordingly the depth of moisture fluctuations, as shown in 0, is likely to be associated with a depth at which there is a contrast in strength and hydraulic properties of soil overlying and underlying this boundary.

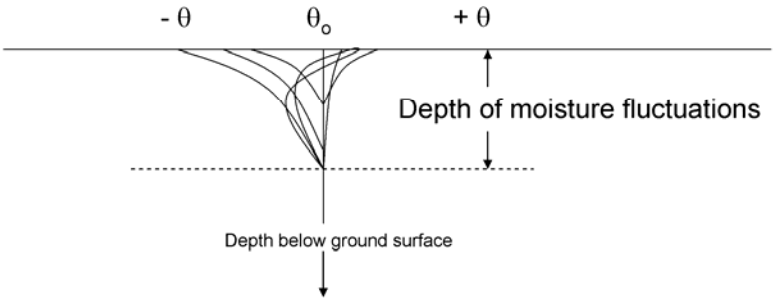

Figure A.2 The depth of moisture fluctuations within a soil profile

The same moisture content profile fluctuations that occur in moisture profile on level ground should also expected to occur in slopes. The difference between infiltration into an earthen slope and infiltration into level ground is the runoff. Assuming a uniform depth of moisture fluctuations along the width of the slope, the zone of moisture fluctuations is represented in 0. As noted in 0, the soil below the zone of moisture fluctuations is likely intact or defined by its initial compaction conditions since it has not been exposed to significant wetting and drying.

The moisture fluctuations in the zone of moisture fluctuations will likely result in a discontinuity in shear strength and hydraulic characteristics at a particular depth. The variation in hydraulic properties with depth was evaluated by Kuhn (2005). In this study, changes in hydraulic properties of the soil were found to occur more rapidly at shallow depths where moisture contents fluctuated more significantly.

Since the depth of moisture fluctuation is thought to control the shear strength and hydraulic properties of compacted highly plastic clays after placement it is investigated in this report. The results of analysis of the depth of moisture fluctuations are used in a slope stability analysis presented in Appendix B. and an evaluation of the recurrence rates of slope failures in Appendix C.

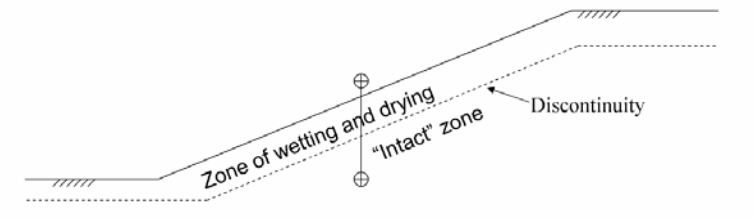

Figure A.3 The depth of moisture fluctuations within a soil slope

A.3 Modeling procedure

The analysis of depth of moisture fluctuations in cracked highly plastic clay was conducted using the finite element flow program SVflux. SVflux is a component of the software suite SoilVision. For the analysis, a one-dimensional finite element flow model with a 6 meter profile was used. The top boundary of the model was specified as a flux boundary where temperature, precipitation, potential evapotranspiration, and relative humidity were input in order to determine the flux into the soil profile. Simulations using weather conditions for both Austin and Houston were used. Records of temperature, precipitation, and potential evapotranspiration for Austin and Houston were obtained from the Texas Evapotranspiration Network, as shown in Figures A.4, A.5, and A.6. The average quarterly relative humidity values for Austin and Houston were obtained from the HELP model and are shown in 0. The bottom boundary was specified as a seepage face boundary condition and was placed 6 meters below the upper boundary as to not effect moisture fluctuations at shallow depths.

The finite element flow model for Austin and Houston weather conditions and the prior mentioned hydraulic properties of cracked highly plastic clay was run for a simulation time of 30 years. The model was run twice for each city, once with out accounting for runoff and once while accounting for runoff. At the beginning of the simulation a suction of 10 kilopascals was specified for the entirety of the six meter profile. By the end of the 30 year simulation an annual pattern of suction and volumetric water content profile changes with time was established based on the input weather and hydraulic parameters. This pattern of suction and water content profile change will be used in the following analysis to approximate the depth of wetting and drying.

The two components of the SoilVision suite which were used in this analysis are SVFlux and FlexPDE. SVflux is used to create the finite element mesh and input the boundary conditions and output parameters. The A screenshot from SVFlux is shown in 0. FlexPDE is the program used to solve the input parameters from SVFlux. FlexPDE is visible to the user during execution of an input file and a screenshot taken from the end of a simulation is shown in 0.

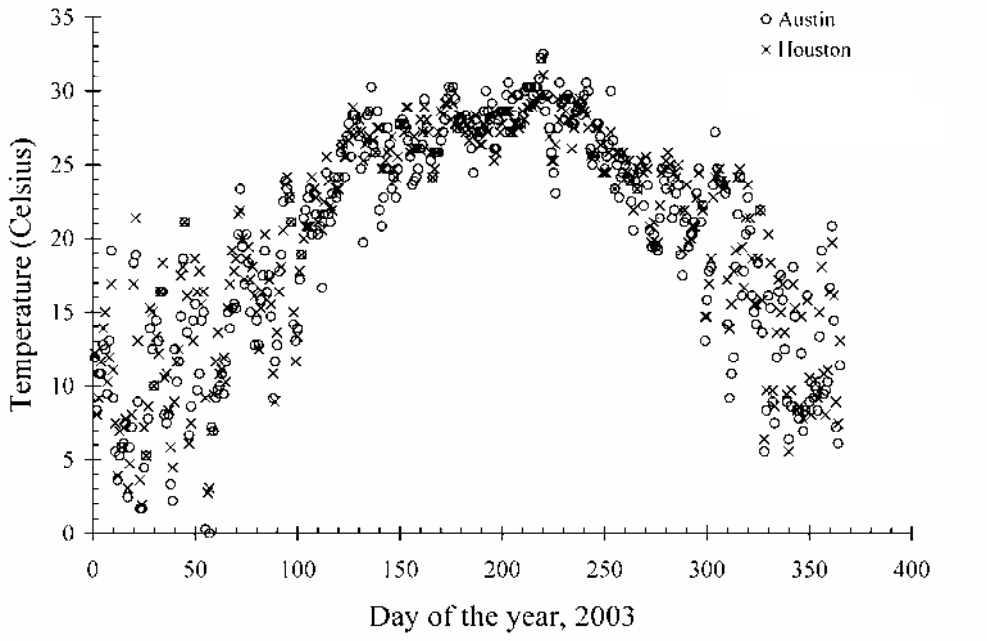

Figure A.4 Daily temperate inputs for Austin and Houston simulations

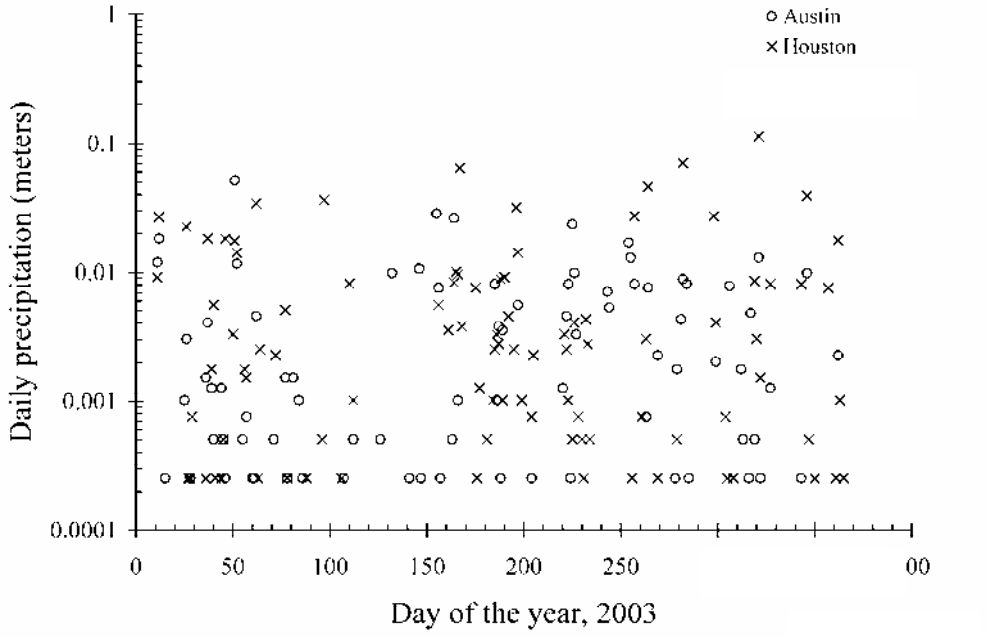

Figure A.5 Daily precipitation inputs for Austin and Houston simulations

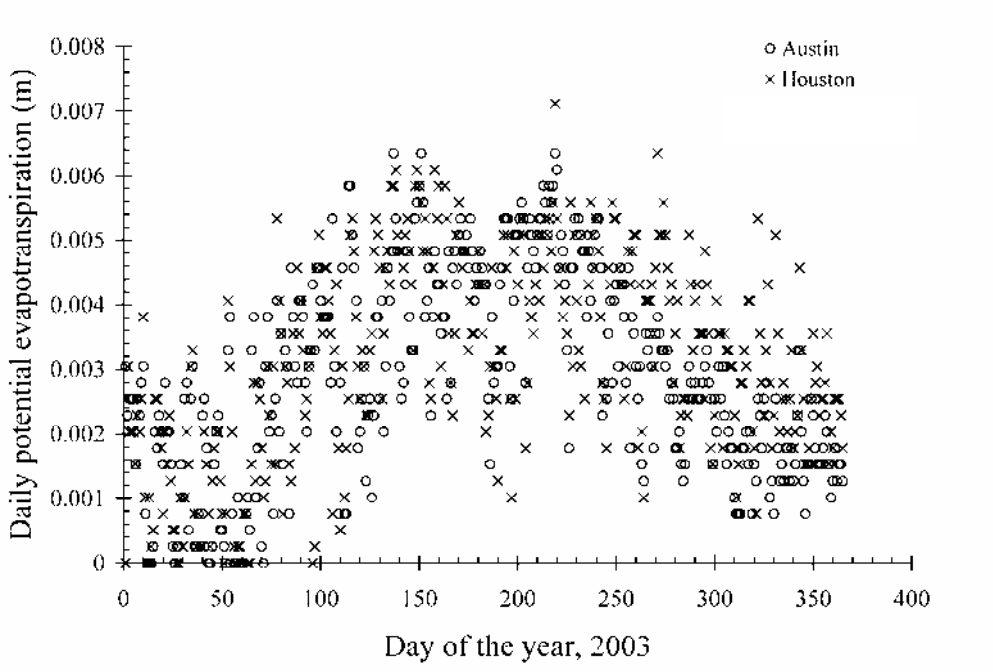

Figure A.6 Daily potential evaporation inputs for Austin and Houston simulations

Table A.1 Quarterly relative humidity inputs for Austin and Houston simulations

Quarter	Austin Relative humidity (%)	Houston relative humidity (%)
1st	66	74
2nd	70	76
3rd	66	77
4th	67	77

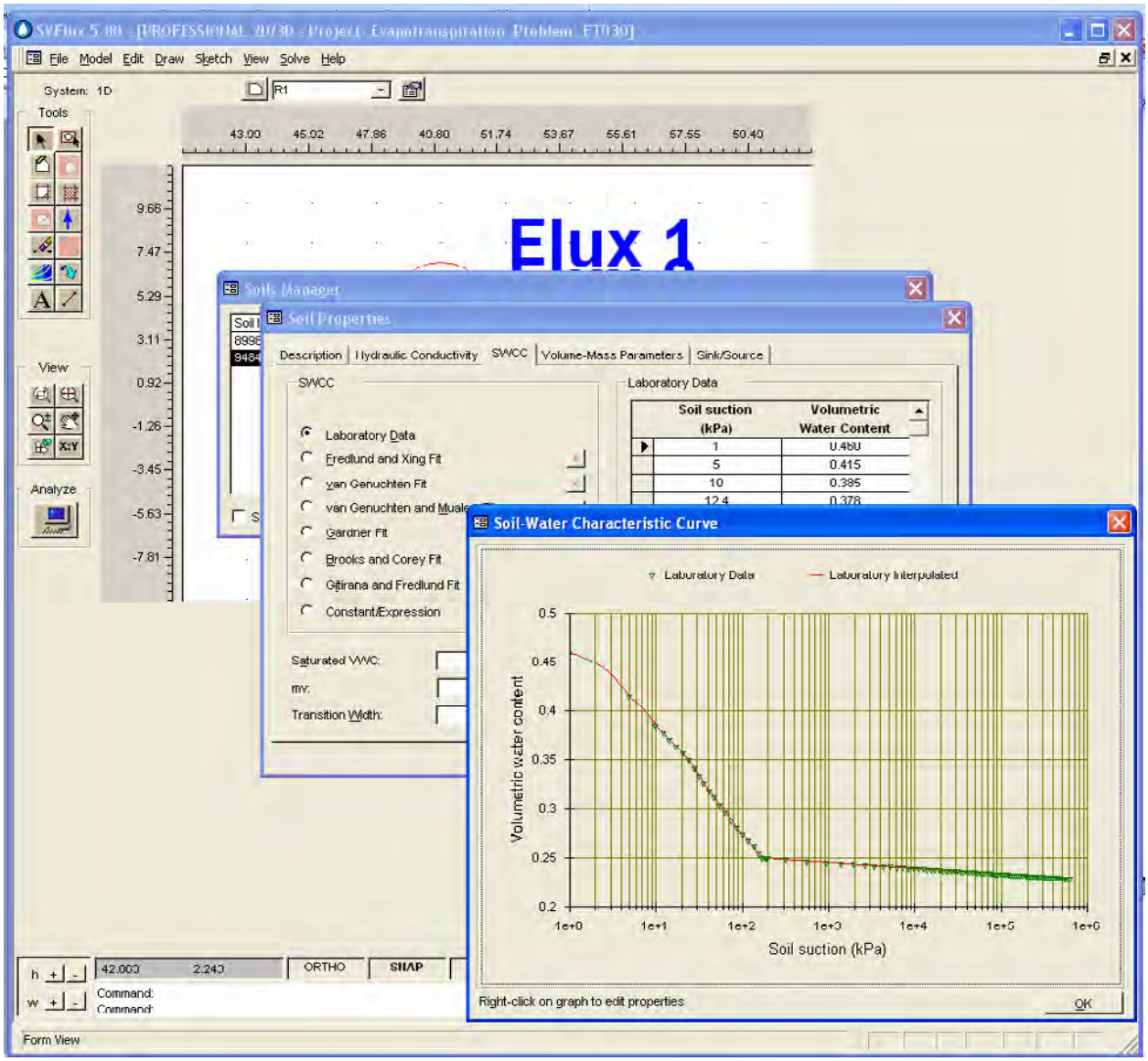

Figure A.7 Screenshot from SVflux5

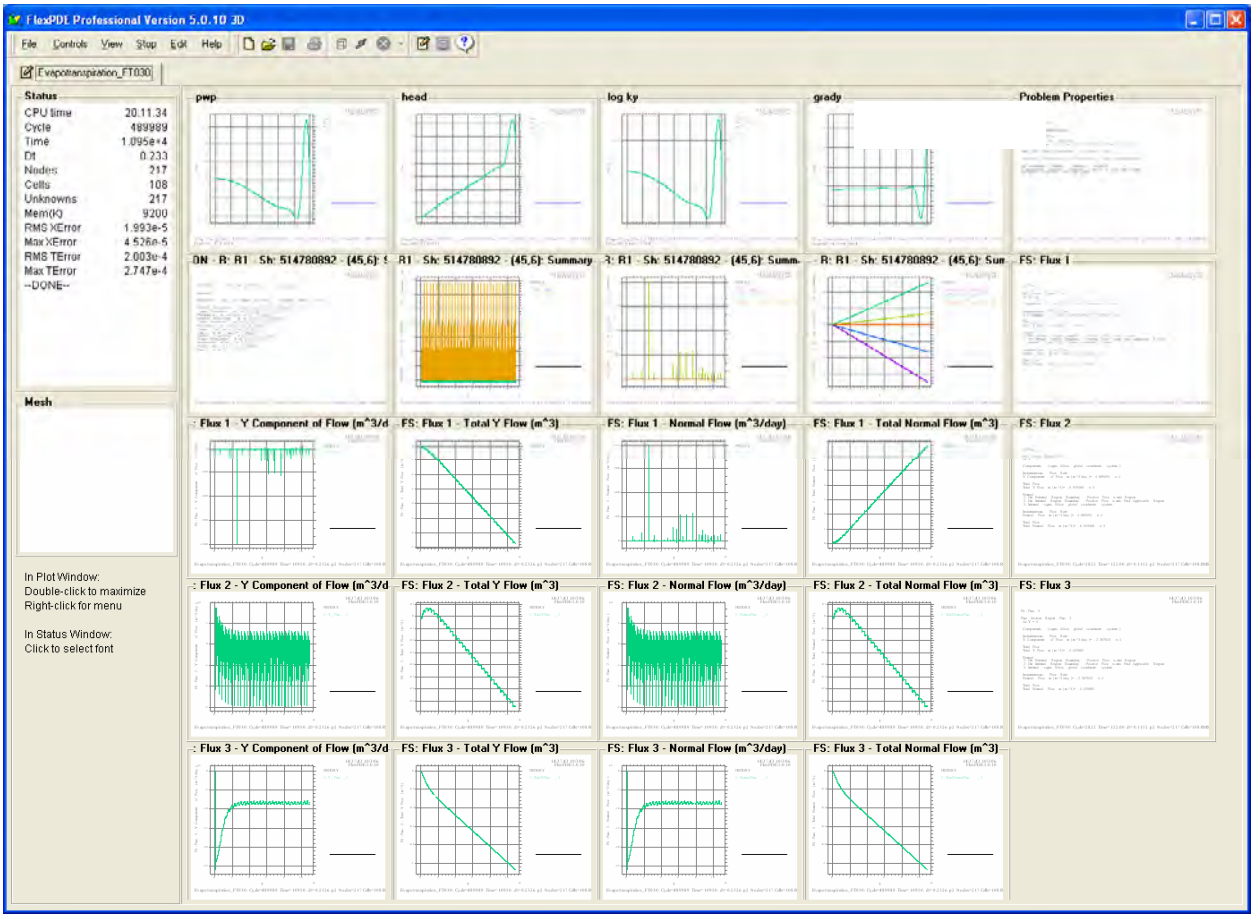

Figure A.8 Screen shot from FlexPDE

A.4 Results of analysis

The 30-year simulation of weather patterns for Austin and Houston resulted in a regular annual pattern of moisture and suction profiles. The values of moisture content and suction throughout the 29th year of the simulation can be found in Figures A.21 to A.24 for the first 3 meters of the modeled profile.

The variation in moisture and suction profiles for Austin and Houston are shown for the 29th simulation year in Figures A.9 through A.12. The grey contours in these figures represent bi-monthly moisture and suction profiles modeled for Austin and Houston. The darker lines represent the lower bound, median, and upper bound values of volumetric water contents and suctions modeled for Austin and Houston.

In order to evaluate the effect of incorporating runoff into the model the simulation was run for both Austin and Houston accounting for runoff. For Austin, the resulting variation of the volumetric water content profile was not distinguishable from the simulation that did not account for runoff. For Houston, however, the resulting variation of the volumetric moisture content profile was similar in shape but was shifted to the left as shown in 0. When suction profiles are compared for Houston modeled with and without runoff (0), the suctions predicted with runoff

are greater than those predicted without runoff. In order to avoid over predicting values of field suction, the Houston model without runoff will be used in further comparisons.

The resolution for precipitation events input into the analysis was daily precipitation. It is therefore possible that runoff may be greater than predicted if a higher resolution were used for the simulation. That is, high intensity, short-duration storms may exceed the infiltration capacity of the soil very rapidly. Nonetheless, based on the analysis for Houston with and without runoff it is likely that this will result in a shift of the volumetric water content and suction profiles without dramatically change their shapes. Accordingly, the shape of the volumetric water content and suction profiles resulting from this simulation should be considered representative of the shape of expected field profiles in Houston given the hydraulic parameters of the modeled soil.

A comparison between volumetric water content and suction profiles for Austin and Houston are shown in Figures A.13 and A.14. For both Houston and Austin, the minimum values of volumetric water content with depth are approximately constant by a depth of 3 meters. At this depth, the variation in suction is minimal. For Austin, the field suction that should be expected at 3 meters of depths is on the order of 300 kPa. For Houston, the field suction that should be expected at depth is an order of magnitude smaller than that on the order of 40 kPa. Field suction values at depths shallower than the depth of moisture fluctuation can not be recommended since cracking may lead to water flow that may bypass the soil. This can further be examined in Figures A.17 and A.18, where a cumulative frequency plot of suction with depth is presented for Austin and Houston.

In order to determine the depth of moisture fluctuations from the analysis, histograms and cumulative frequency plots for volumetric water content with depth were established for both Austin and Houston (Figures A.19 and A.20). Based on the results of the analysis, it appears as though the depth of moisture fluctuation occurs at a point between 1 and 1.5 meters of depth. This point may also be seen in 0 which compares moisture content profiles in Austin and Houston it is apparent that there is a zone with distinctly higher volumetric water contents beginning at approximately 1.1 meters of depth. This zone is also apparent for Houston, but is not as severe. Accordingly, a depth of moisture fluctuation of 1.1 meters is defined as representative of the depth of moisture fluctuations for both Austin and Houston for highly plastic clay with the characteristics of Eagle Ford clay.

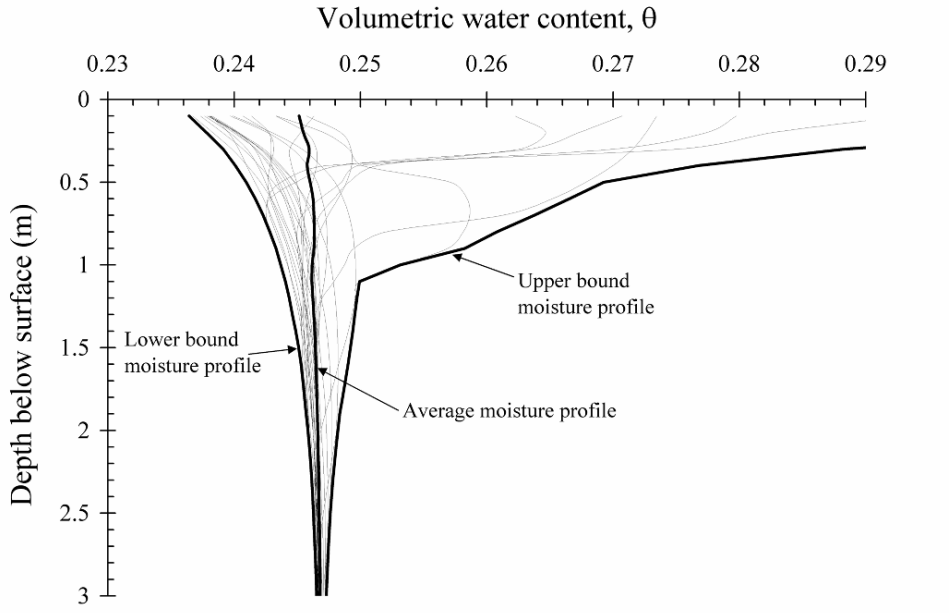

Figure A.9 Predicted variation of volumetric water content profile over the course of a year for Eagle Ford clay under Austin, TX weather conditions

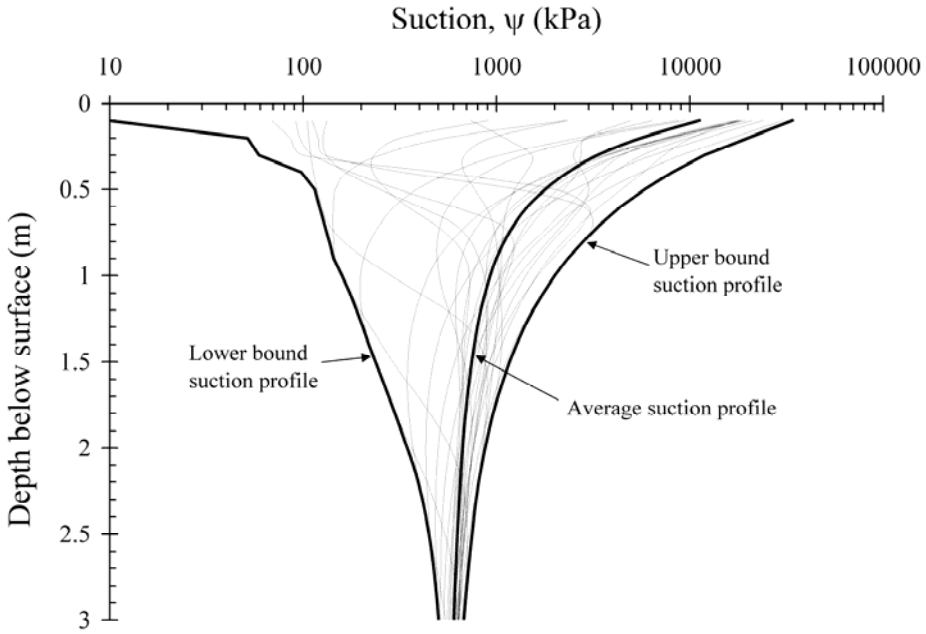

Figure A.10 Predicted variation of suction profile over the course of a year for Eagle Ford clay under Austin, TX weather conditions

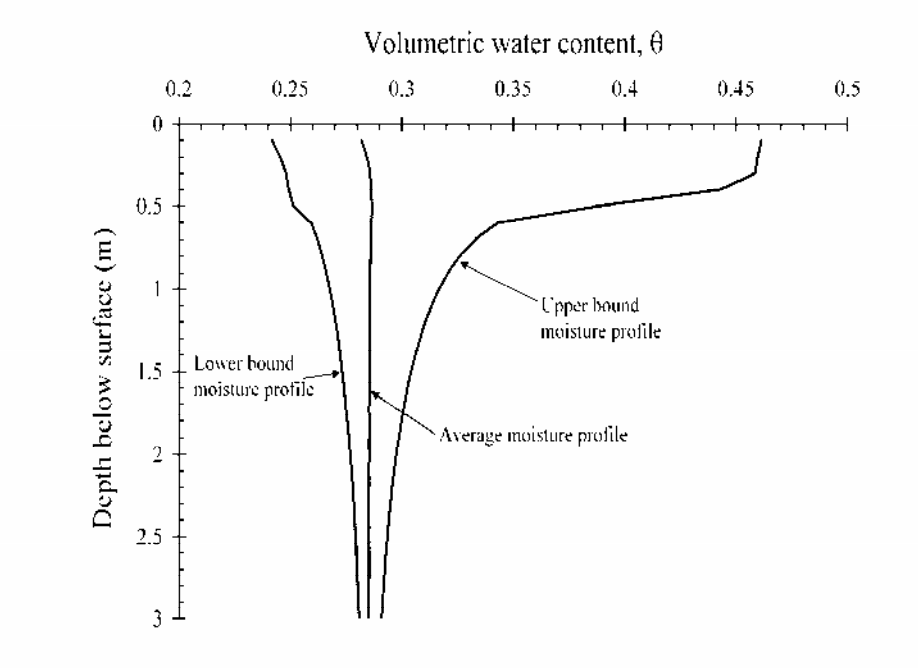

Figure A.11 Predicted variation of volumetric water content profile over the course of a year for Eagle Ford clay under Houston, TX weather conditions

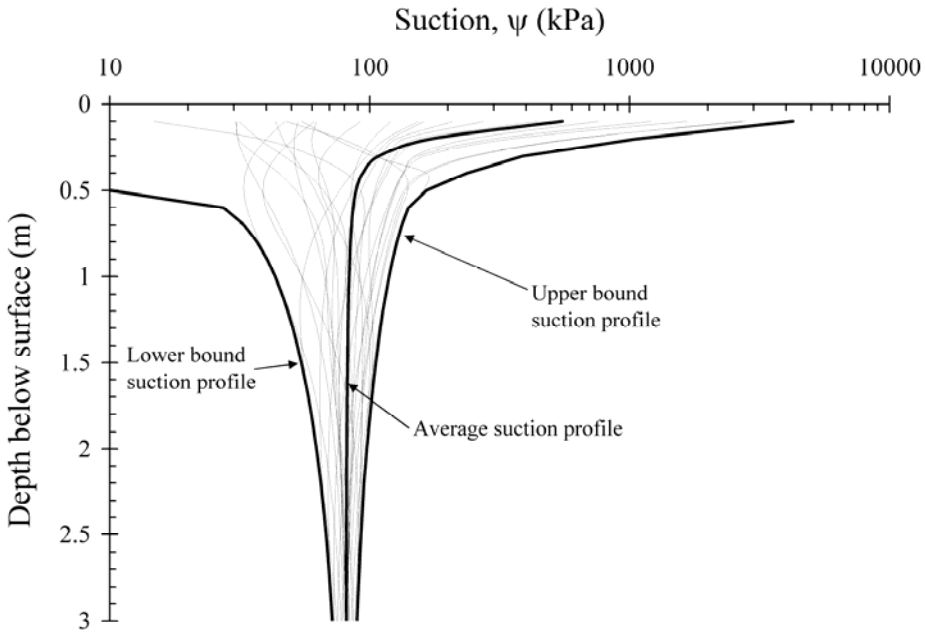

Figure A.12 Predicted variation of suction profile over the course of a year for Eagle Ford clay under Houston, TX weather conditions

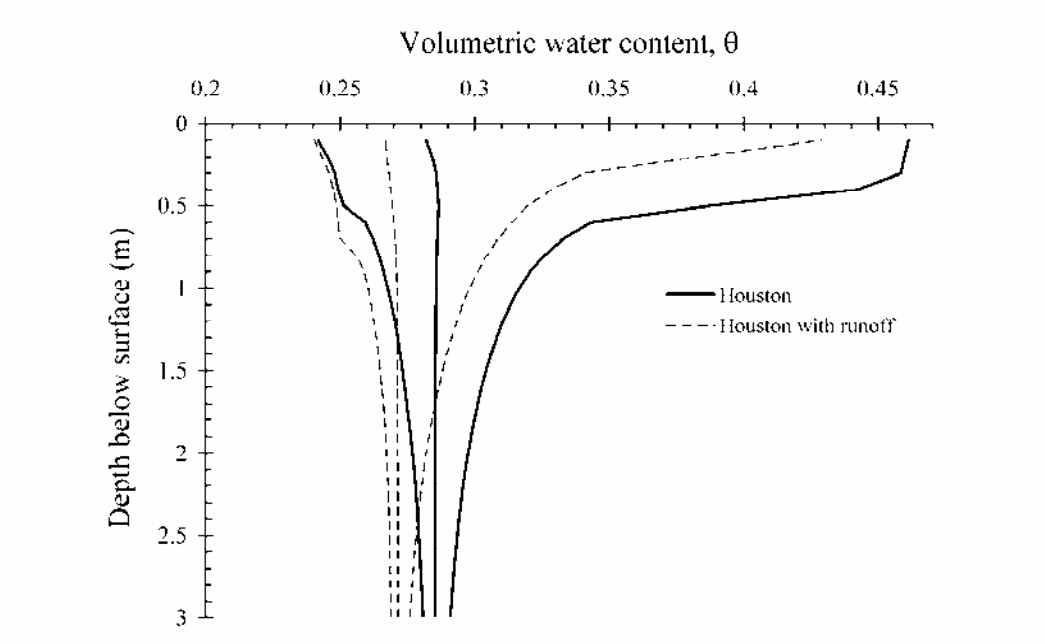

Figure A.13 Predicted variation of volumetric water content profile over the course of a year for Eagle Ford clay under Houston, TX weather conditions with and without accounting for runoff

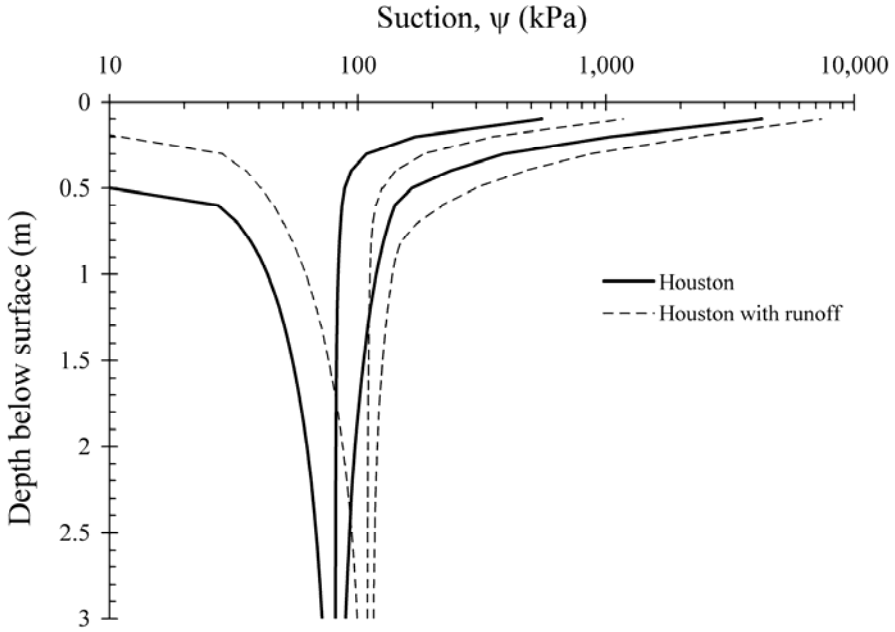

Figure A.14 Predicted variation of suction profile over the course of a year for Eagle Ford clay under Houston, TX weather conditions with and without accounting for runoff

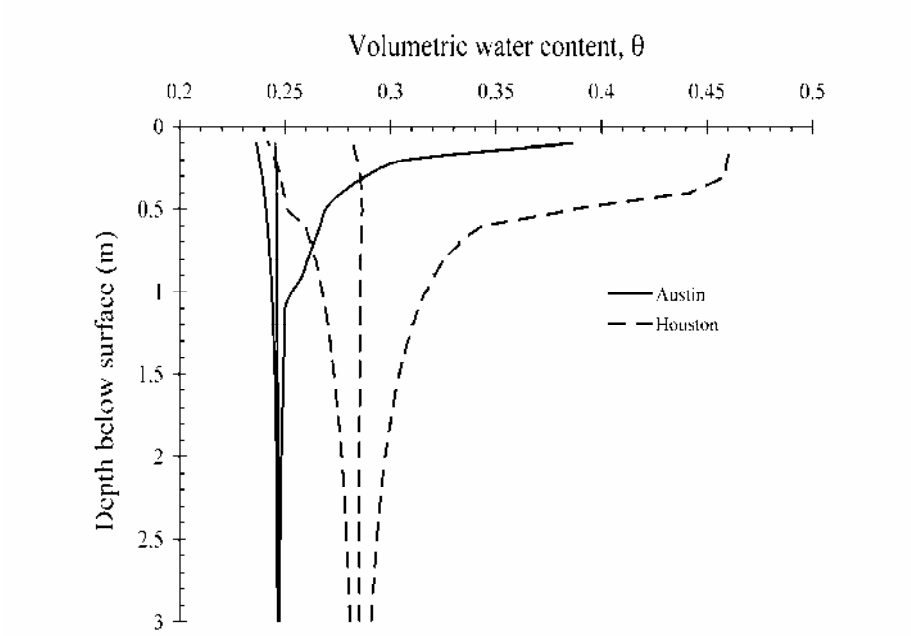

Figure A.15 Predicted range of volumetric water content profile over the course of a year for Eagle Ford clay under Austin and Houston, TX weather conditions

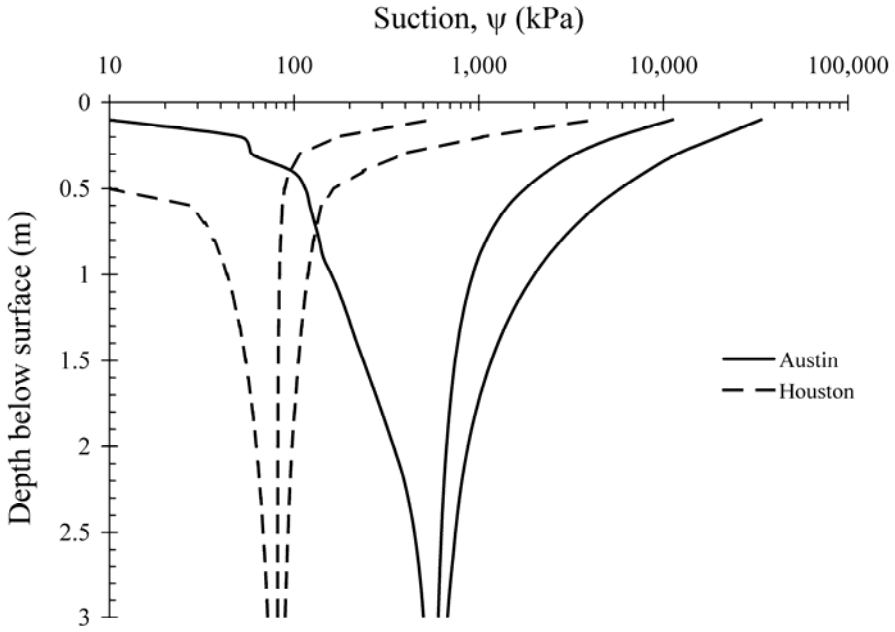

Figure A.16 Predicted range of suction profile over the course of a year for Eagle Ford clay under Austin and Houston, TX weather conditions

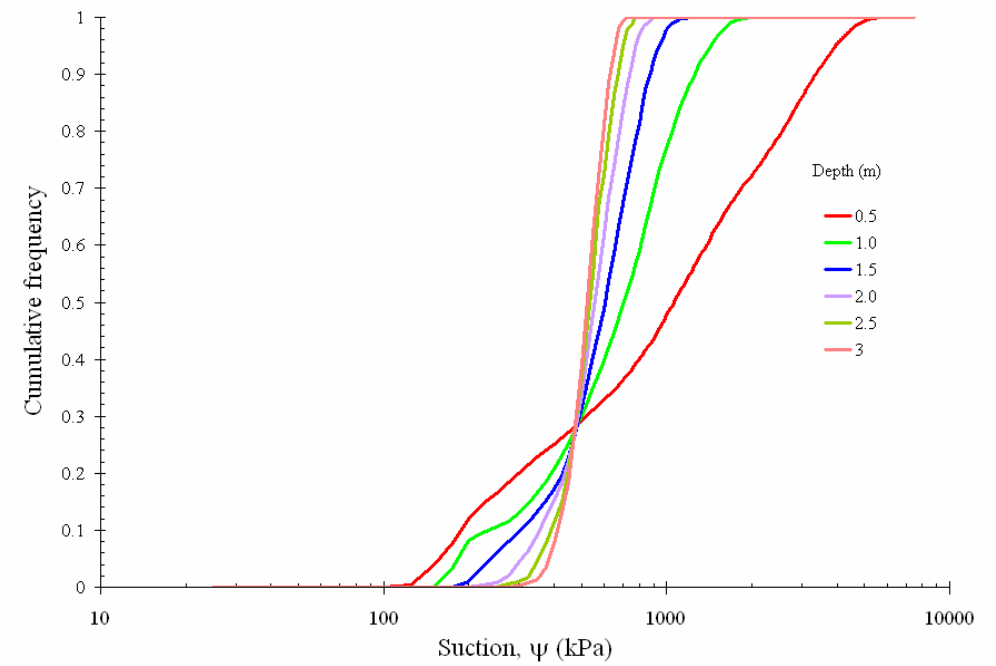

Figure A.17 Histogram and cumulative frequency for predicted values of suction over the course of a year for Eagle Ford clay under Austin, TX weather conditions

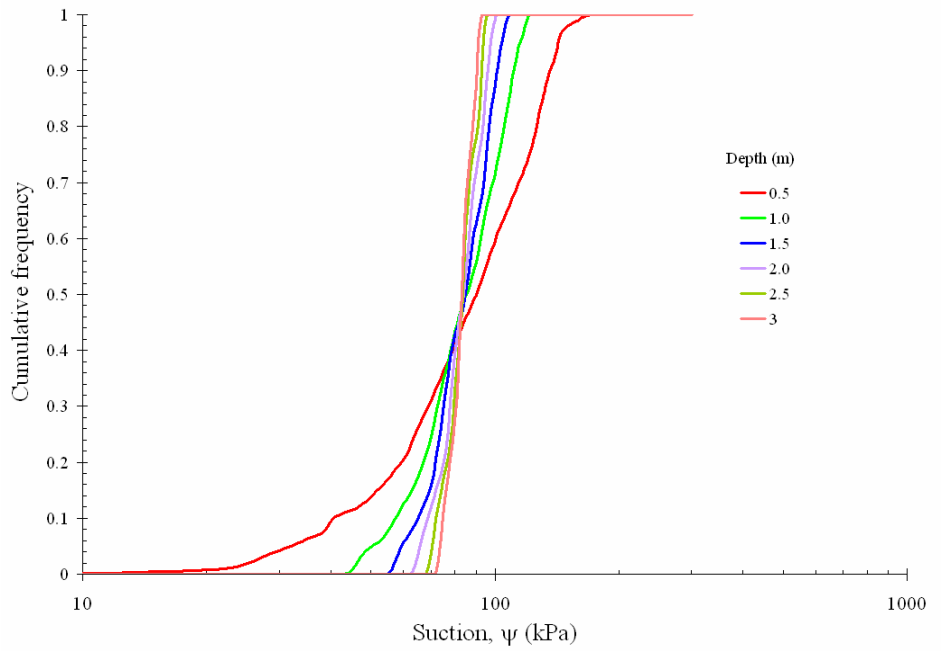

Figure A.18 Histogram and cumulative frequency for predicted values of suction over the course of a year for Eagle Ford clay under Houston, TX weather conditions

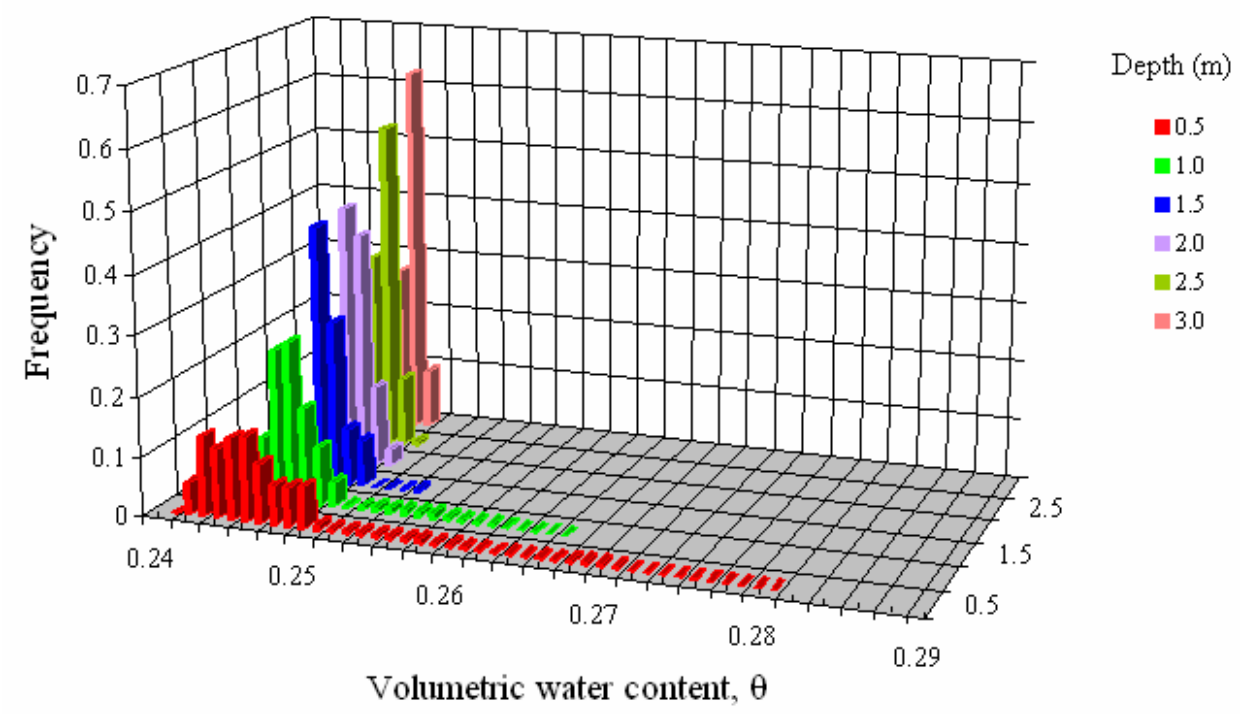

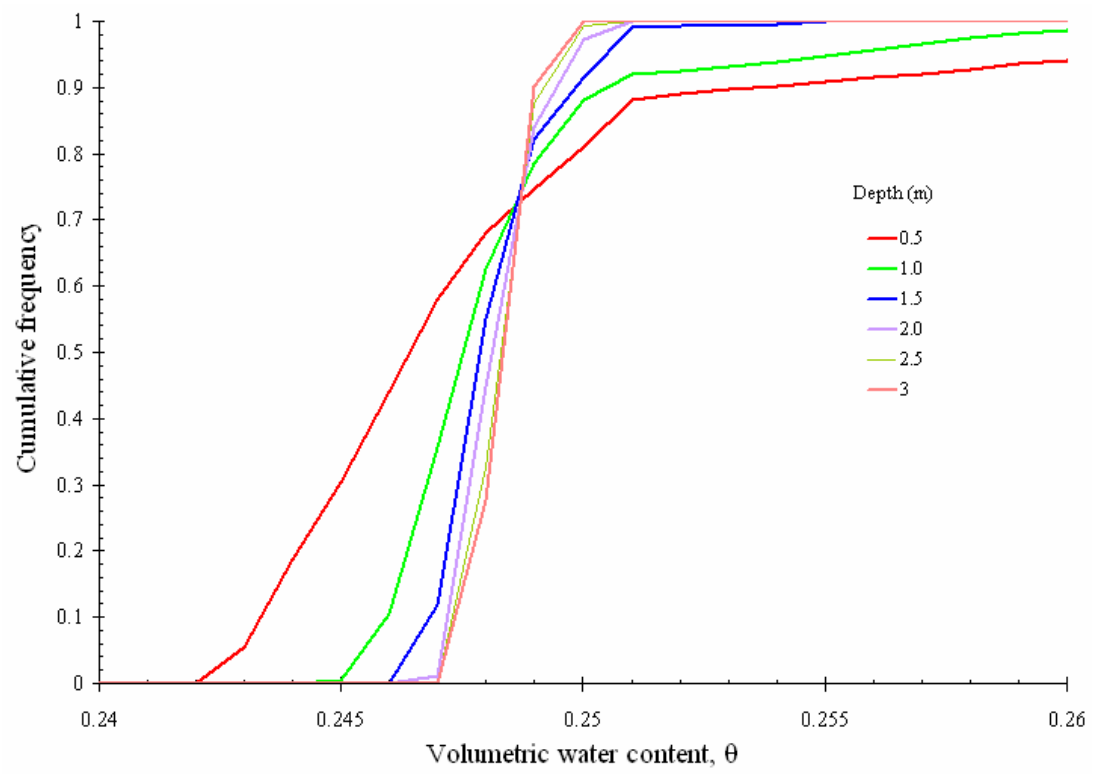

Figure A.19 Histogram and cumulative frequency for predicted changes in water content over the course of a year for Eagle Ford clay under Austin, TX weather conditions

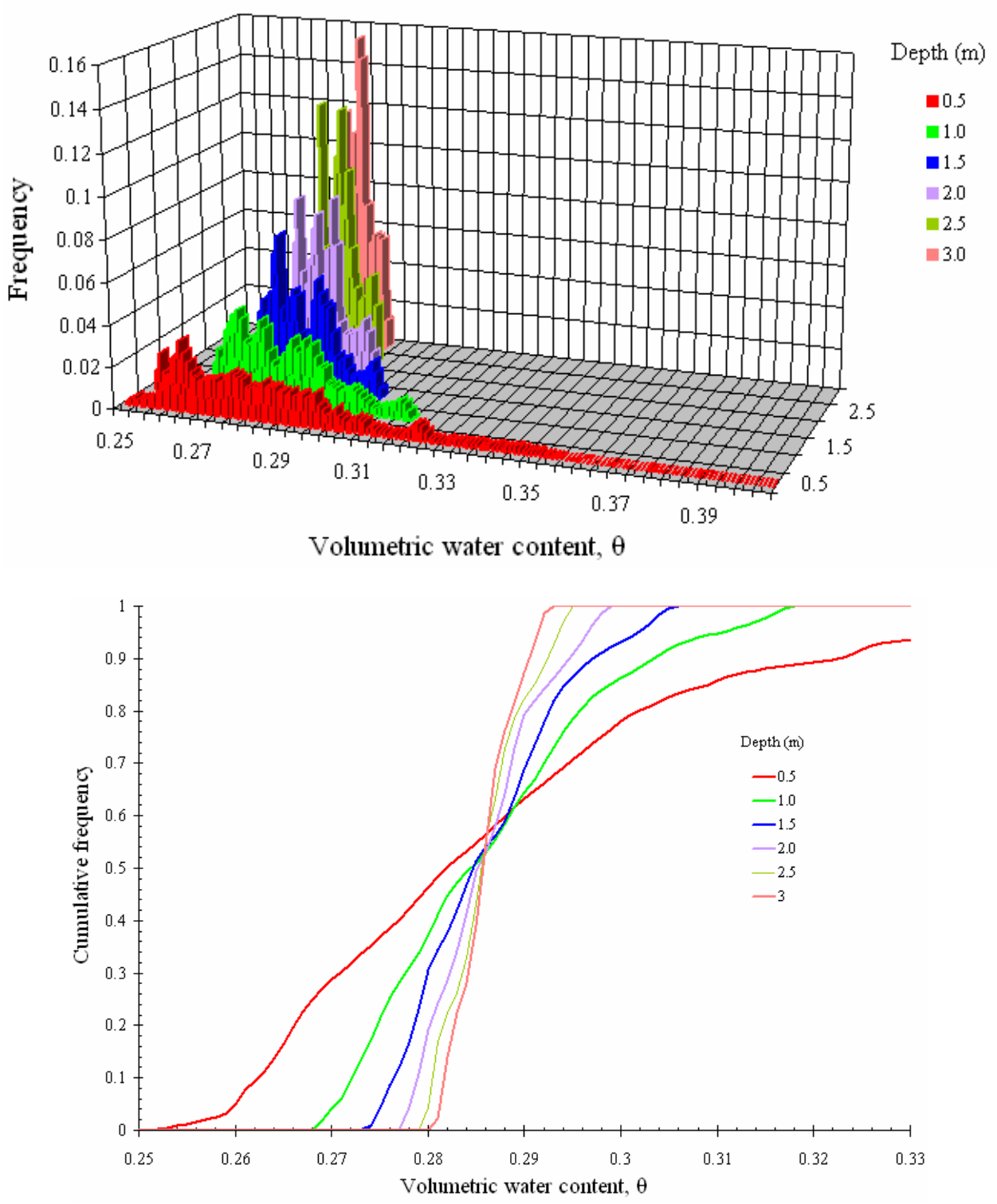

Figure A.20 Histogram and cumulative frequency for predicted changes in water content over the course of a year for Eagle Ford clay under Houston, TX weather conditions

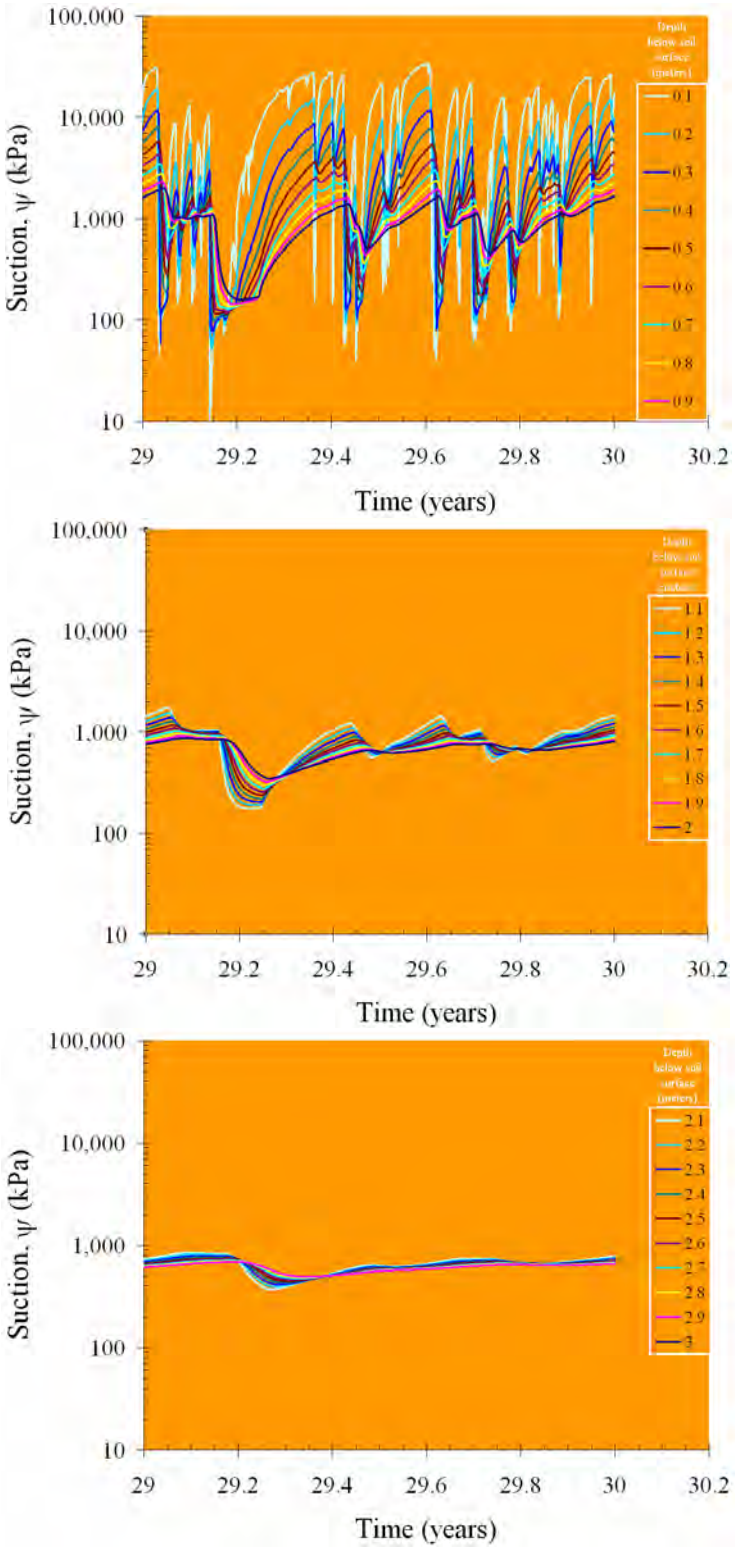

Figure A.21 Predicted changes in suction profile over the course of a year for Eagle Ford clay under Austin, TX weather conditions

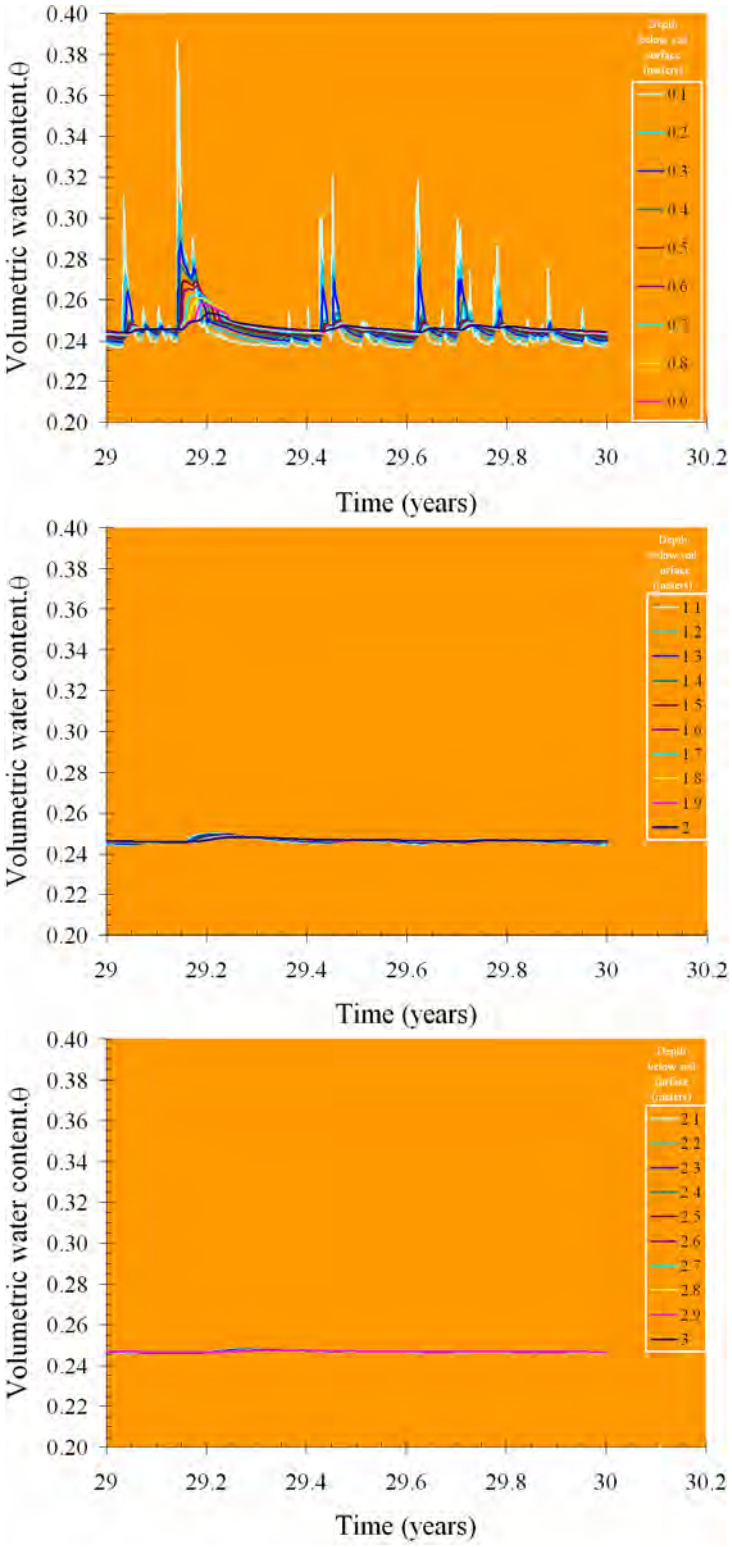

Figure A.22 Predicted changes in water content profile over the course of a year for Eagle Ford clay under Austin, TX weather conditions

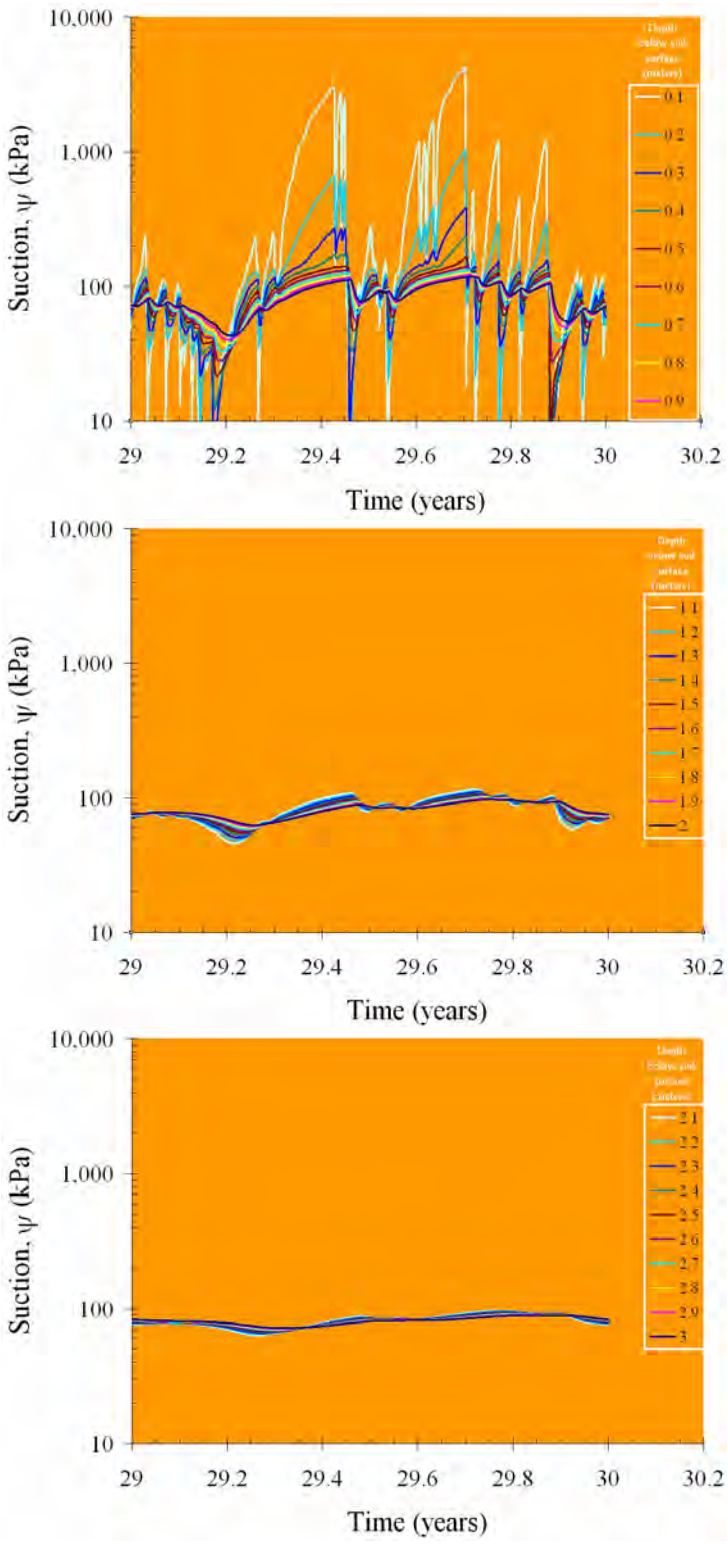

Figure A.23 Predicted changes in suction profile over the course of a year for Eagle Ford clay under Houston, TX weather conditions

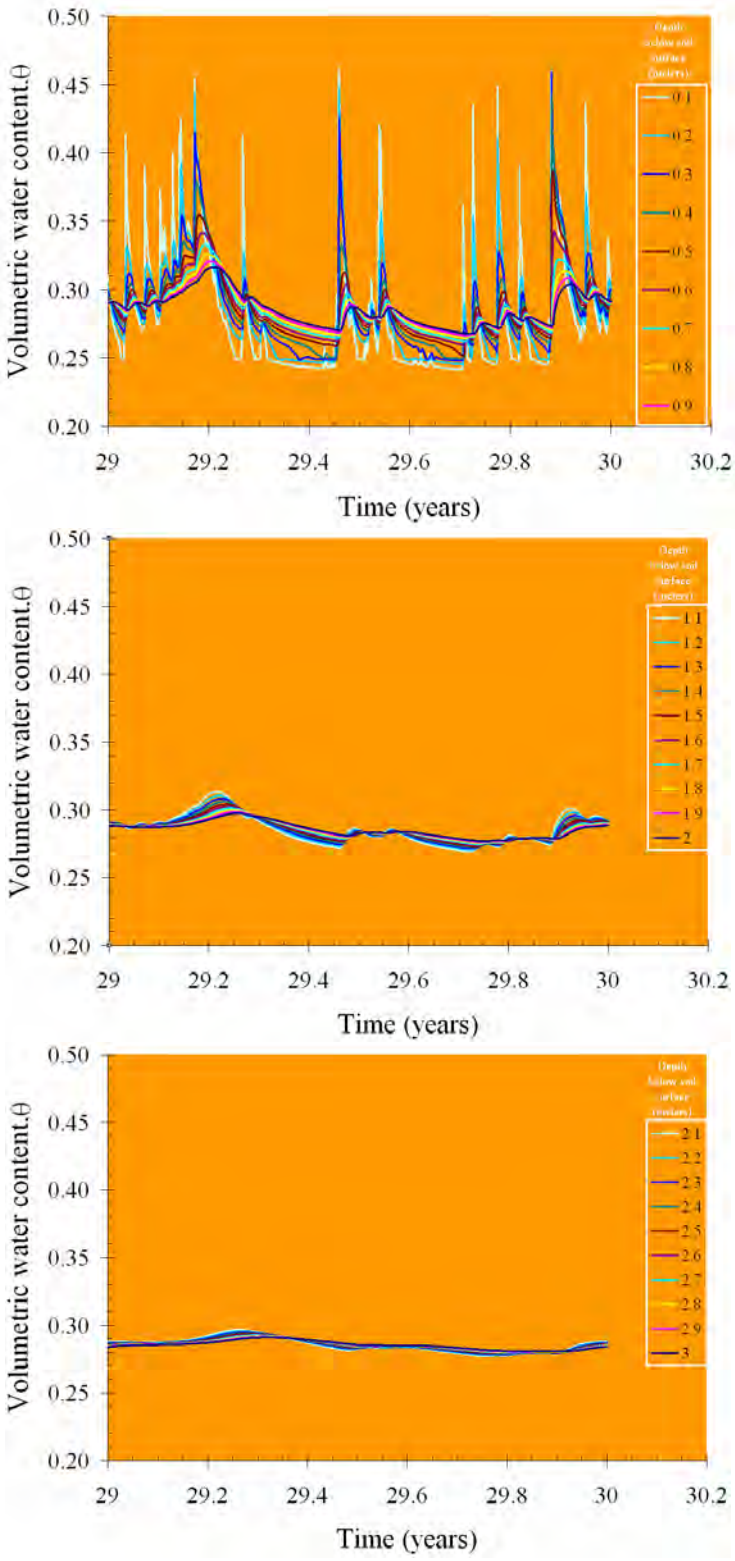

Figure A.24 Predicted changes in water content profile over the course of a year for Eagle Ford clay under Houston, TX weather conditions

Appendix B. Slope Stability Analysis for Weathered Highly Plastic Clay Slopes

B.1 Infinite Slope Analysis and Negative Pore Water Pressures

In order to gain further insight into the stability of a weathered, highly plastic clay slopes, a series of infinite slope analysis were conducted using shear strength parameters measured as part of this study. Infinite slope analyses were also conducted in a previous TxDOT research study investigating shallow slope failures in highly plastic clay slides (Aubeny and Lytton 2003). In Aubeny and Lytton's study, failures were attributed to a time-dependent loss in suction. Shear strength testing performed by the research team indicates that failure is due to discrete precipitation events. The research team has determined that positive pore water pressures must be present at the time of slope failure when the cotangent of the slope angle is greater than 2.5.

The conclusion of Aubeny and Lytton (2003) that failures occurred under conditions of negative pore water pressures was evaluated by using the shear strength properties of weathered highly plastic clay. Specifically, an infinite slope analysis was conducted for a slope inclination of 18 degrees, the maximum slope at the borrow site for the Eagle Ford clay used in the study (TxDOT Report 0-5202-3, Section 8). A series of linear shear strength envelope were fit to the shear strength data presented in Figure 6.6 of TxDOT Report 0-5202-3 over different ranges in effective normal stress. The reasonable range of the internal angle of friction for this linear fit is from 18 to 25 degrees.

The back-calculated pore water pressure at failure based on this linear fit is shown in Figure B.1. Based on a number of case histories of shallow slope failures reported by Wright and Kayyal (1991) where the average depth of failure is approximately 1.3 meters (4.25 feet) in Houston, TX. The average depth of the failure plane of 1.3 meters is in agreement with the 1.1 meter depth of moisture fluctuations determined in Appendix A. Assuming a failure depth of 1.1 meters, an infinite slope analysis using a linear envelope the pore water pressure at failure could have ranged from approximately 0 to 5 kPa. The pore water pressure at the failure depth for conditions of seepage parallel to the slope face is also plotted in Figure B.1. Since the pore water pressure for conditions of seepage parallel to the slope face exceeds the pore water pressure back-calculated from a limit equilibrium analysis regardless of the internal angle of friction, the slope is expected to fail if seepage were parallel to the slope face. The results of the slope stability analysis are, however, significantly different when the non-linearity of the shear strength envelope of highly plastic clay at low stresses is taken into account.

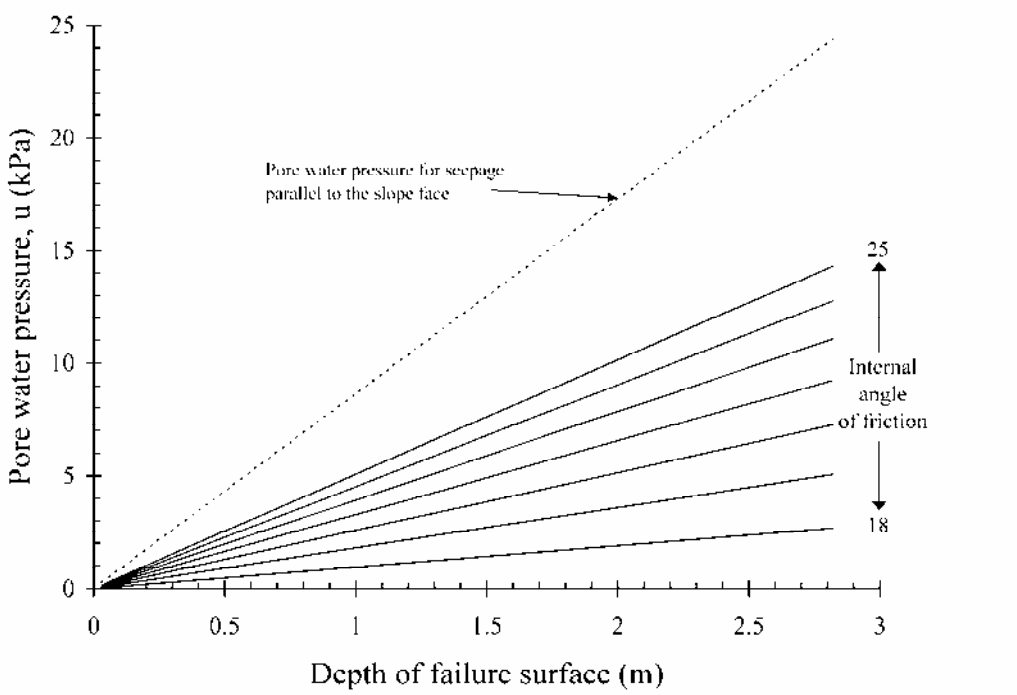

Figure B.1 Back calculated pore water pressure at failure for an 18 degree slope and a range in tangent friction angles for weathered Eagle Ford clay

B.2 Infinite Slope Analysis Considering a Curved Shear Strength Envelope

The results of the infinite slope analysis are significantly different if the shape of the failure envelope is represented by a non-linear relationship. If the failure envelope is examined for the Eagle Ford clay that has undergone cyclic wetting and drying, it is evident that the envelope is significantly curved at lower effective stresses. Accordingly, a linear approximation of the shear strength envelope tends to misrepresent the shear strength at lower effective stresses. This is of particular importance since the failures of interest are occurring at shallow depths under these lower effective stresses.

The factor of safety in a slope stability analysis is represented by the available shear strength divided by the shear stress. For a linear envelope the available shear strength is represented by a cohesion and friction angle. In this case the internal angle of friction of the Eagle Ford clay was measured with consolidated undrained triaxial compression tests with pore water pressure measurements. Rather than representing the shear strength envelope by a linear fit, the secant friction angle of the envelope can be related to the effective normal stress. In this case, the methodology originally proposed by Duncan was followed in which the secant friction angle is plotted versus the effective normal stress. The secant friction angle as a function of the effective normal stress is plotted in 0 for Eagle Ford (Wright and Aguettant 2006), Paris, and Beaumont Clays (Wright and Kayyal 1991).

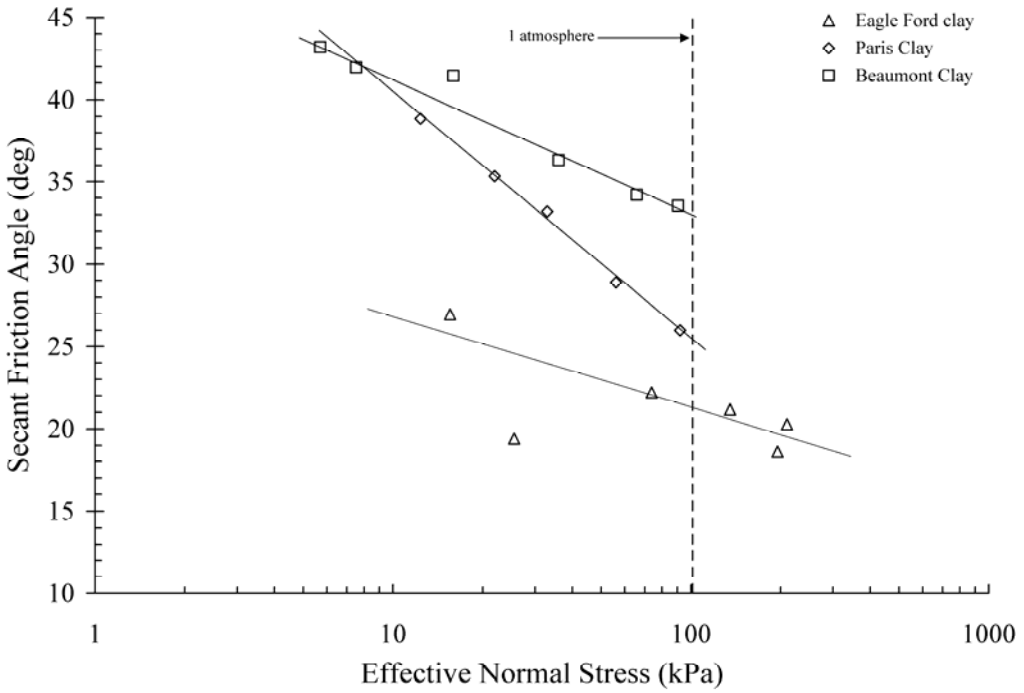

Figure B.2 Secant friction angle as a function of effective normal stress for fully-softened Eagle Ford, Paris, and Beaumont Clays subjected to cyclic wetting and drying

A log-linear trend for the secant friction angle with effective confining normal stress is evident for all three soils. The log-linear trend used for this analysis is plotted in 0. The secant friction angle and effective confining stress can be expressed as follows:

$$\phi'_{secant} = \phi'_0 - \Delta\phi \cdot \log_{10}\left(\frac{\sigma_f'}{P_{atmospheric}}\right)$$

Where, ϕ'_{secant} is the secant friction angle, ϕ'_o is the secant friction angle at 1 atmosphere of pressure, $\Delta\phi$ is the change in friction angle per log cycle in normal stress, σ_f' is the effective stress on the failure plane, and $P_{atmospheric}$ is atmospheric pressure in the same units used for normal stress. For the Eagle Ford, Paris, and Beaumont clays the secant friction angle at 1 atmosphere of pressure and the change in friction angle per log cycle in normal stress are presented in Table B.1 . A more general equation for the fully-softened shear strength of Eagle Ford Shale established by Wright is expressed in the companion report, TxDOT Report 0-5202-3.

Table B.1 Secant friction angle parameters for Eagle Ford, Paris, and Beaumont clays subjected to cyclic wetting and drying

	Effective secant friction angle at 1 atmosphere, ϕ'_o (degrees)	Change in secant friction angle per log cycle of effective normal stress, $\Delta\phi'$ (degrees)
Eagle Ford clay	21.2	5.6
Paris clay	25.4	15.1
Beaumont clay	32.9	8.3

The shear strength for a linear Mohr-Columb envelope is expressed as:

$$\tau = c' + (\gamma z \cos^2 \beta - u) \tan \phi'$$

Using the relationship determined for the secant friction angle the shear strength can instead be expressed in terms of the secant friction angle as follows,

$$\tau = \left\{ \left[\gamma z \cos^2 \beta - u \right] \cdot \tan \left[21.5^o - 7^o \cdot \log \left(\frac{\gamma z \cos^2 \beta - u}{P_{atmospheric}} \right) \right] \right\}$$

An infinite slope stability analysis may again be conducted using this alternate definition for the shear strength. The relationship for the factor of safety for an infinite slope failure can now be expressed as:

$$F = \frac{\left\{ \left[\gamma z \cos^2 \beta - u \right] \cdot \tan \left[21.5^o - 7^o \cdot \log \left(\frac{\gamma z \cos^2 \beta - u}{P_{atmospheric}} \right) \right] \right\}}{\gamma \cdot z \cdot \cos \beta \cdot sin \beta}$$

A limit equilibrium analysis was conducted for a series of slope angles over a range of failure depths from 1 to 6 meters. In this analysis, different trial values of pore water pressure were used until a factor of safety of 1 was achieved. The results of the analysis are plotted in Figures B.3 to B.5. The values of pore water pressure determined from the analysis reveal that the pore water pressure at failure are expected to be positive (in excess of atmospheric pressure) for slopes with a cotangent slope angle of greater than 2.5 for Eagle Ford clay, 2.0 for Paris clay, and 1.5 for Beaumont clay.

As an example for Eagle Ford clay, a for a slope of 18^0 and a depth of failure of 1.1 meters, a pore water pressure of 6.5 kPa is needed to produce a factor of safety of 1. The resulting pore water pressure is greater than the 0-5 kPa range presented in the analysis in B.1.

In order to compare this example calculation with the results of TxDOT report 0-5202-3, the pore water pressure can be expressed in terms of the pore water pressure ratio. The pore water pressure ratio, r_u, is the ratio of the pore water pressure to the total stress at the point of interest. In this case, the failure plane is the point of interest and the total stress is calculated by

multiplying the bulk unit weight of the soil by the depth of failure. Using the aforementioned example of a 18^0 slope with a depth of failure of 1.1 meters leads to a pore water pressure ratio of 0.34. The pore water pressure ratio reported by Wright and Aguettant in TxDOT report 0-5202-3 ranged from 0.5 to 0.6. The range in pore water pressure ratio suggested by Wright and Aguettant is plotted along with the pore water pressure ratio calculated for each of the soils in Figures B.6 through B.8 for a range in slope inclinations and failure depths.

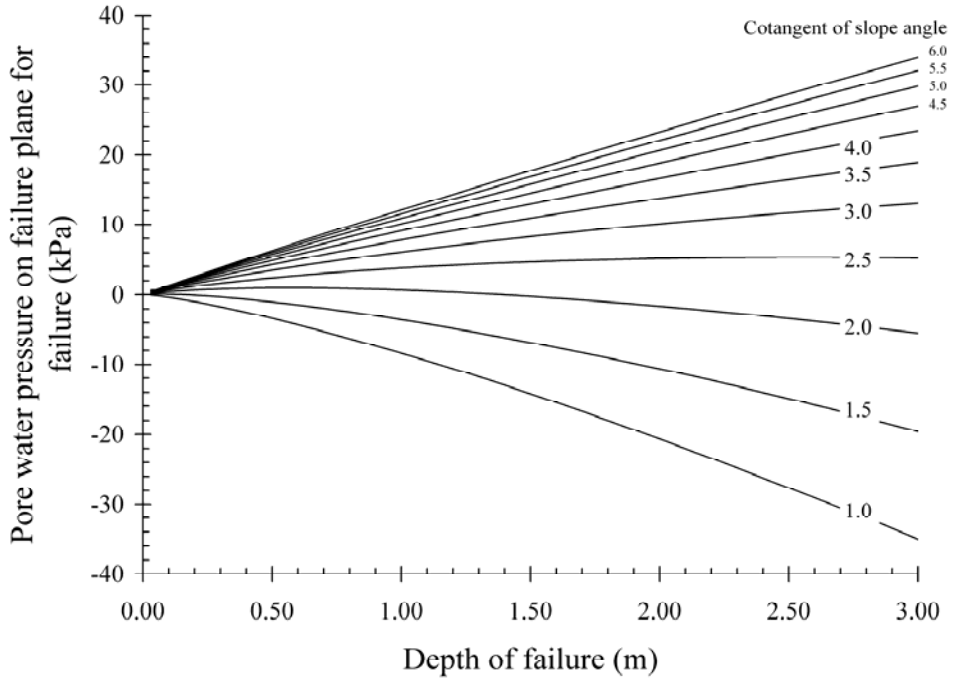

Figure B.3 Back calculated pore water pressure at failure using the secant friction angle for weathered Eagle Ford clay

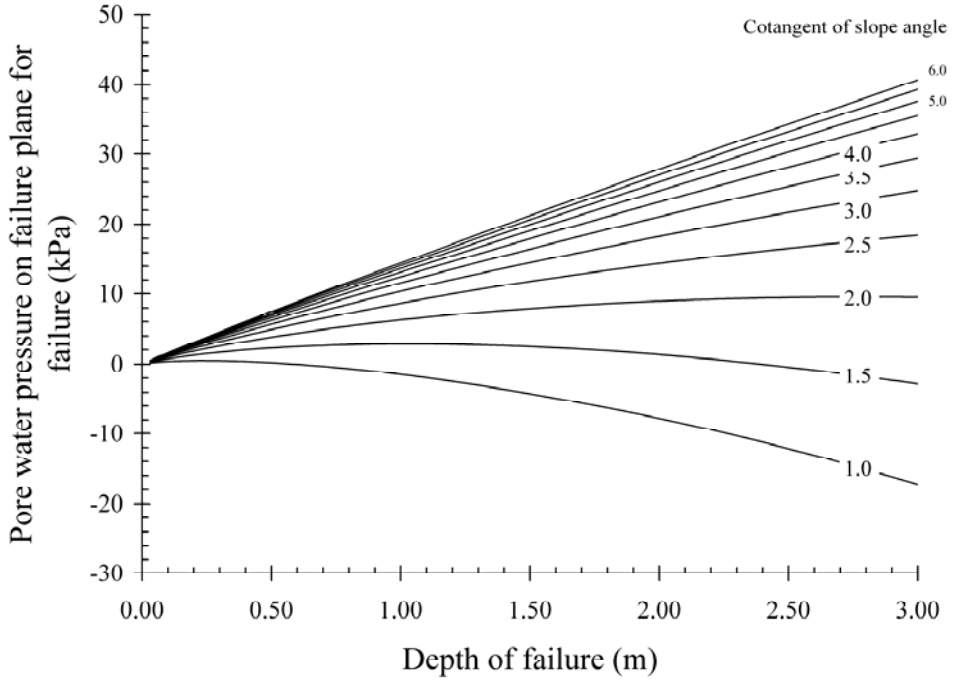

Figure B.4 Back calculated pore water pressure at failure using the secant friction angle for weathered Paris clay

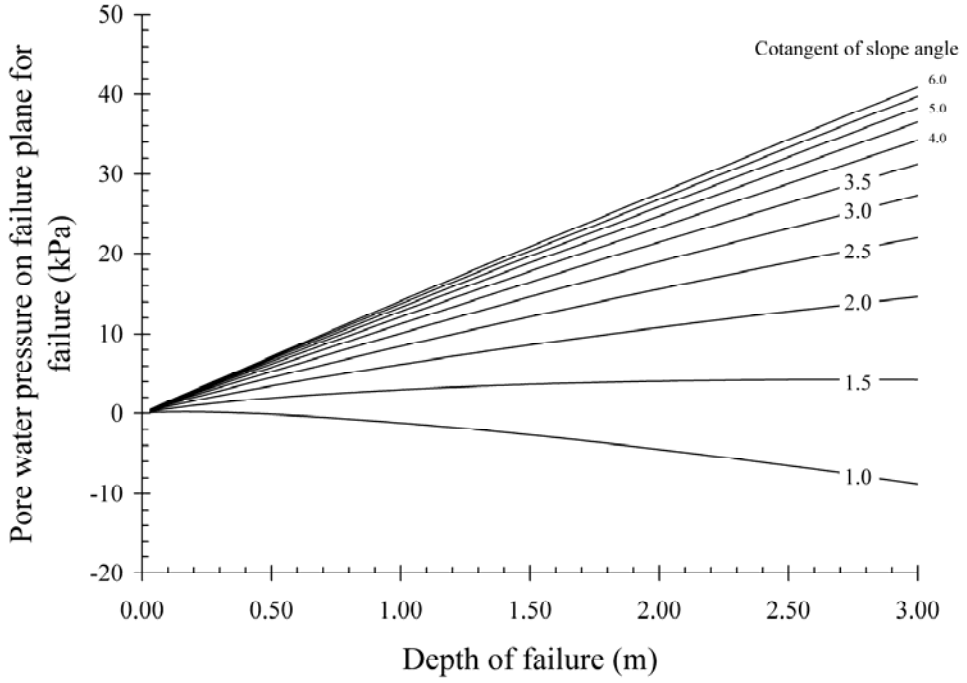

Figure B.5 Back calculated pore water pressure at failure using the secant friction angle for weathered Beaumont clay

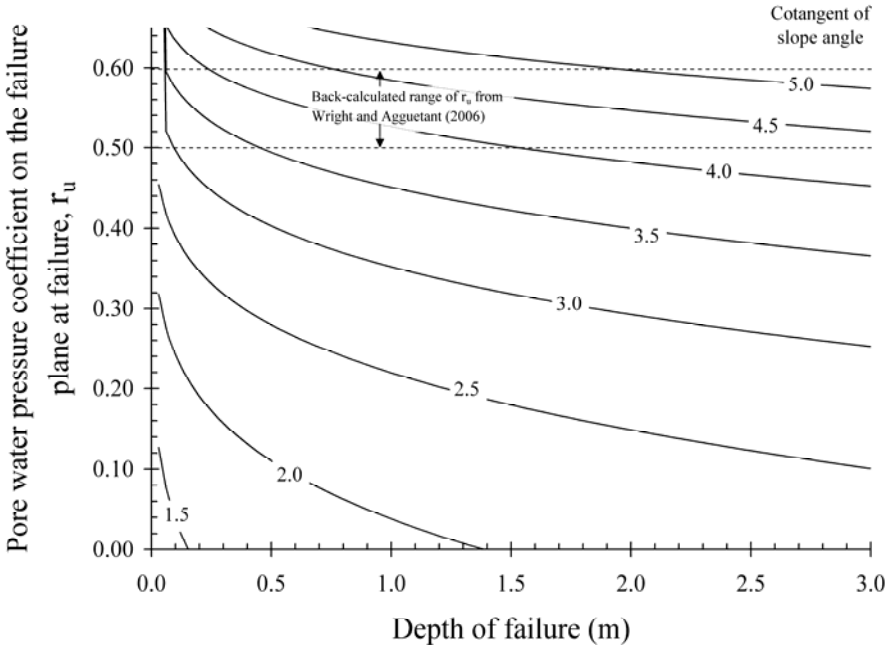

Figure B.6 Back calculated pore water pressure coefficients at failure using the secant friction angle for weathered Eagle Ford clay

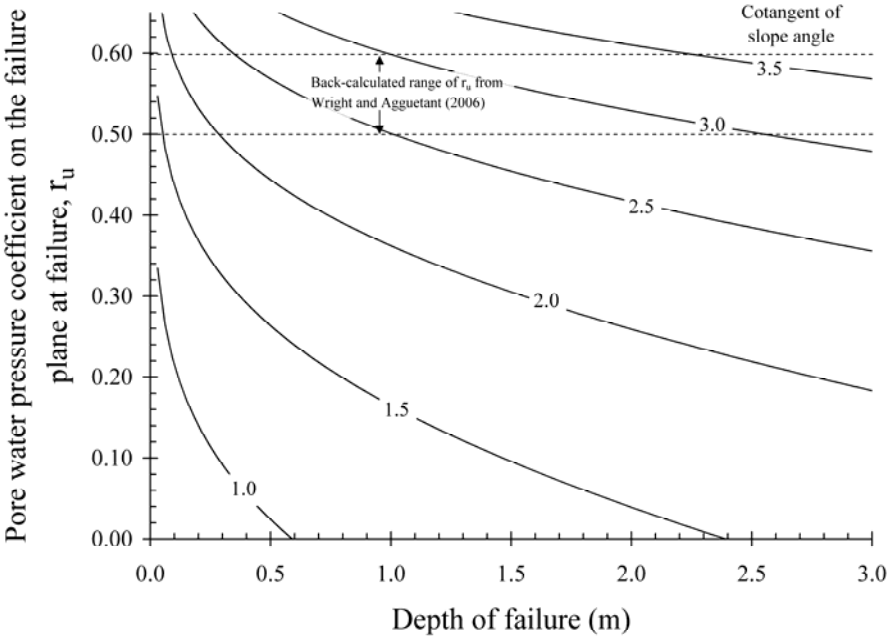

Figure B.7 Back calculated pore water pressure coefficients at failure using the secant friction angle for weathered Paris clay

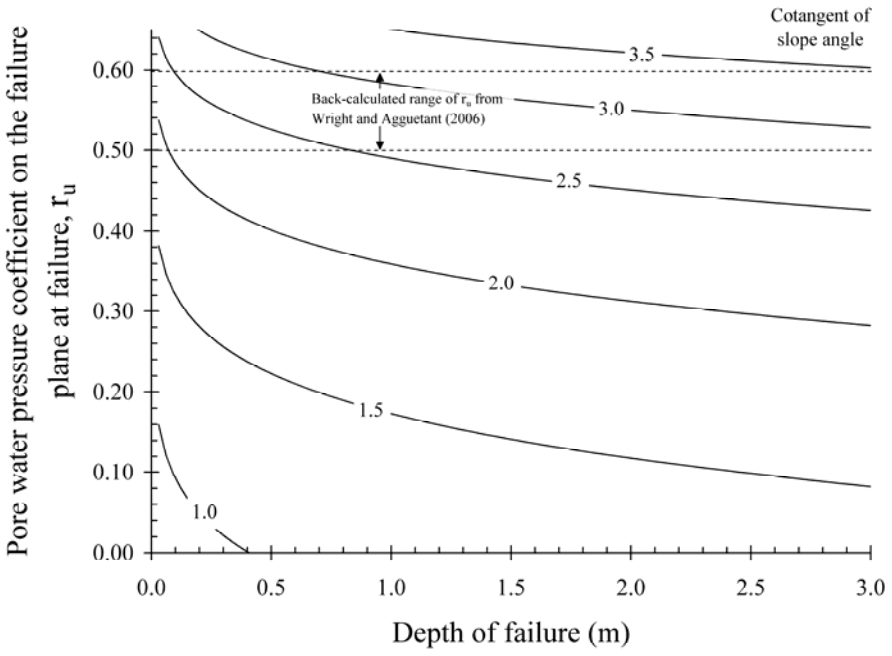

Figure B.8 Back calculated pore water pressure coefficients at failure using the secant friction angle for weathered Beaumont clay

In addition to calculating the pore water pressure on the failure plane for conditions of failure for a range of slope angles and failure depths, the maximum possible slope angle under conditions of seepage parallel to the slope face was calculated based on different failure depths. The resulting relationship between the maximum slope angle and the depth of the failure plane for conditions of seepage parallel to the slope face is plotted in 0. This relationship was achieved by solving a set of two non-linear equations representing the pore water pressure on the failure plane due to seepage and conditions of limit equilibrium. For the example case of a failure depth of 1.1 meters in Eagle Ford clay, a slope of 4.1:1 would provide a factor of safety of one for an infinite slope analysis assuming seepage parallel to the slope face. The pore water pressure on the failure plane at failure associated with a failure depth of 1.1 meters for each of the soils is presented in 0. These pore water pressures will be used in Appendix C. to evaluate the recurrence rate of failures for a depth of moisture fluctuations 1.1 meters.

By considering seepage parallel to the slope face, a design engineer can consider the worst case scenario for pore water pressures. Furthermore, when this seepage condition is combined with the shear strength parameters measured for weathered highly plastic clay, it should yield a slope inclination for design that will allow the slope to have a long service life. Overall, stability analyses presented in this appendix indicate that even for slopes in highly plastic clays, positive pore water pressures are required to induce failure of typical slopes (e.g., 4:1 slopes). Effective shear strength properties from wetted and dried specimens are recommended for these analyses.

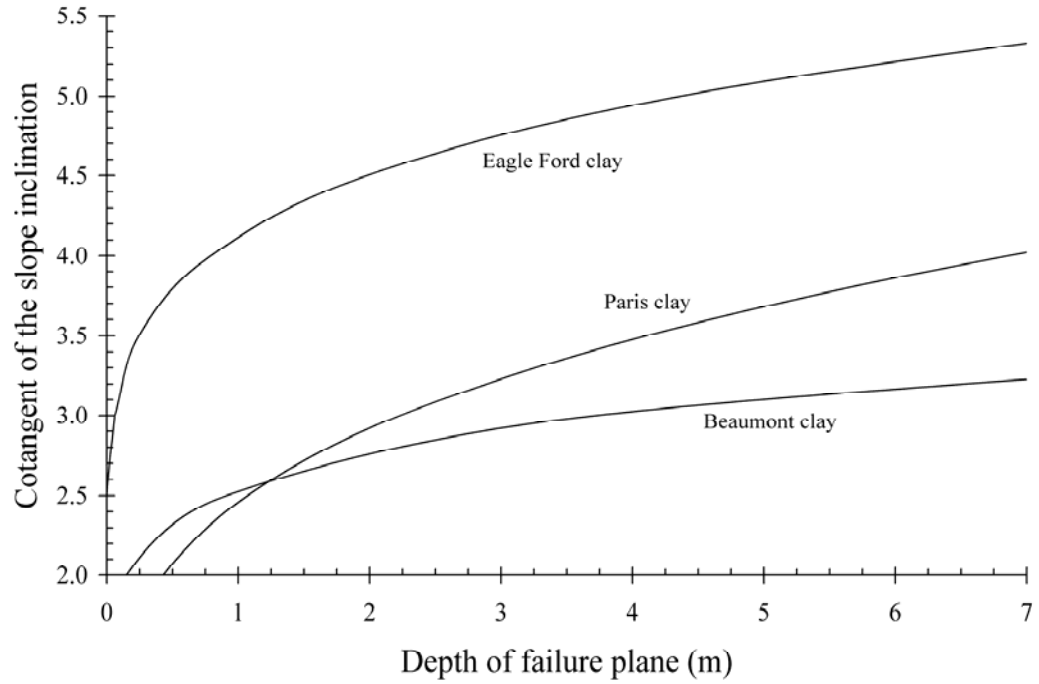

Figure B.9 Slope inclination for a given failure depth for conditions for limit equilibrium for infinite slope with flow parallel to the slope surface

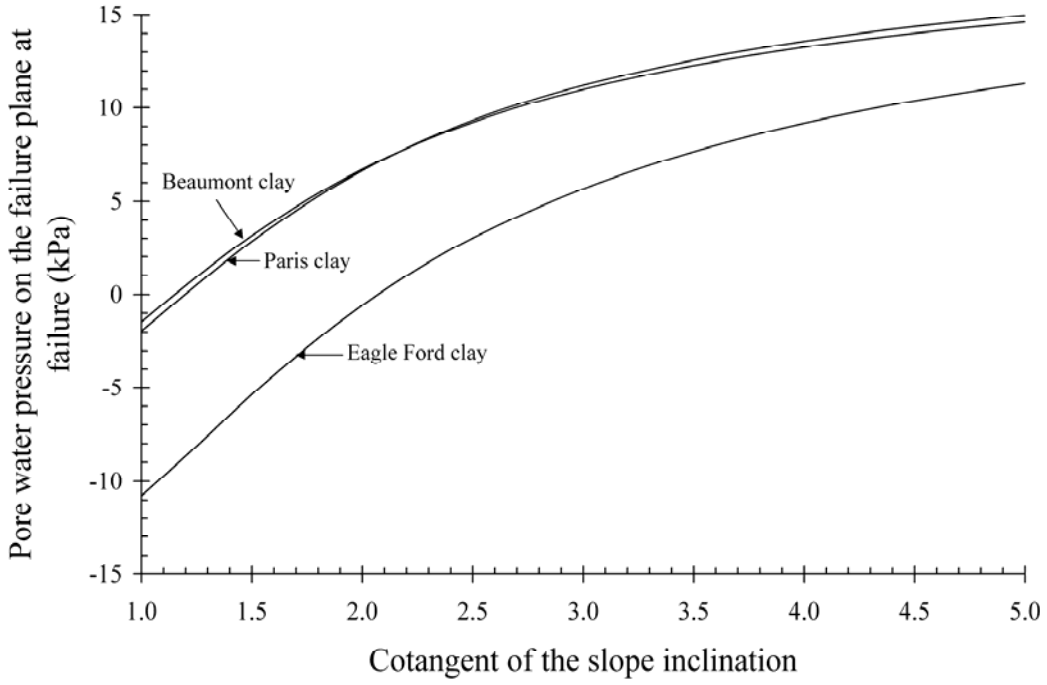

Figure B.10 Pore water pressure on the failure plane at failure for an assumed failure depth of 1.1 meters

Appendix C. Recurrence Rate of Slides in Compacted Highly Plastic Clay Slopes Considering Discrete Precipitation Events

In order to assess the stability of compacted highly plastic clays with time, it is necessary to have a clear understanding of the effect of time on the shear strength and hydraulic properties of compacted highly plastic clays. Chapters 1 of this report provides the hydraulic properties of cracked highly plastic clay, TxDOT report 0-5202-3 provides a shear strength characterization of compacted highly plastic clay that has undergone cyclic wetting and drying, Appendix A. provides an analysis of the depth of moisture fluctuations, and Appendix B. provides a slope stability analyses. This appendix presents an assessment of the recurrence of slope failure of compacted highly plastic clay.

C.1 Time Dependency of failures

A time-dependent drying process is expected after construction of a compacted embankment. This long term drying trend will, however, be affected by discrete rainfall events. These rainfall events will lead to swelling of the compacted material. Cracking will result due to the cycles of wetting and drying. As discussed in Chapter 5.4 and TxDOT report 0-5202-3, this cyclic wetting and drying process will result in changes in the shear strength and hydraulic properties of the soil. Specifically, cyclic moisture fluctuations will lead to a reduction in shear strength and cracking of the soil during moisture fluctuations will lead to preferential flow. While changes in shear strength and hydraulic properties were observed in the laboratory, a useful evaluation is to consider the shear strength and hydraulic properties determined in the laboratory for long-term conditions. These long-term values of shear strength and hydraulic properties can then be used to model the stability of the slope after the effect of wetting and drying in highly plastic clays.

C.2 Net Infiltration Required to Cause Failure

The proposed model for failure under discrete precipitation events is shown in Figure C.1. For this model, the depth of the moisture fluctuations is assumed as the depth where positive pore water pressures will develop due to contrasting hydraulic properties. Conditions within the embankment are split into an equilibrium condition before failure and a condition at failure. For equilibrium condition of the soil, a uniform moisture profile with depth is assumed as the mean moisture content determined in Appendix A. and presented in 0. In the case of Eagle Ford clay model under Austin weather conditions the equilibrium volumetric water content is approximately 0.25.

The second case is failure conditions. For failure conditions, the critical height of an elevated water table above the depth of moisture fluctuations is calculated by dividing the pore water pressure required for limit equilibrium conditions determined in the analysis presented in Appendix B.

The volume of water required to cause failure under a discrete event can be calculated by first determining the change in volumetric water content between equilibrium conditions and conditions of saturation. This change in volumetric water content is taken as the difference between the effective porosity of the soil and the equilibrium volumetric water content as follows:

$$\Delta\theta = n_e - \theta_i$$

Where, $\Delta\theta$ is the change in volumetric water content from the initial condition to a saturated condition and n_e is the void ratio of the soil. For Eagle Ford clay, the effective porosity was approximately 0.45, resulting in a change in volumetric moisture content of 0.20 between equilibrium conditions and conditions of saturation. From the change in volumetric water content, the infiltration required to cause failure can be determined by multiplying the change in volumetric water content by the head of water required for failure as follows:

$$Infiltration\ for\ \ failure = \Delta\theta \cdot H_{water}$$

Where, H_{water} is the head of water required to cause failure at a particular failure depth. The resulting net infiltration required to cause failure for different failure depths and initial saturations is then plotted in Figure C.2. Assuming a failure depth of 1.1 meters (3.6 feet), an initial saturation rate ranging from 20 to 80% will result in 35 to 50 cm of net infiltration to cause failure.

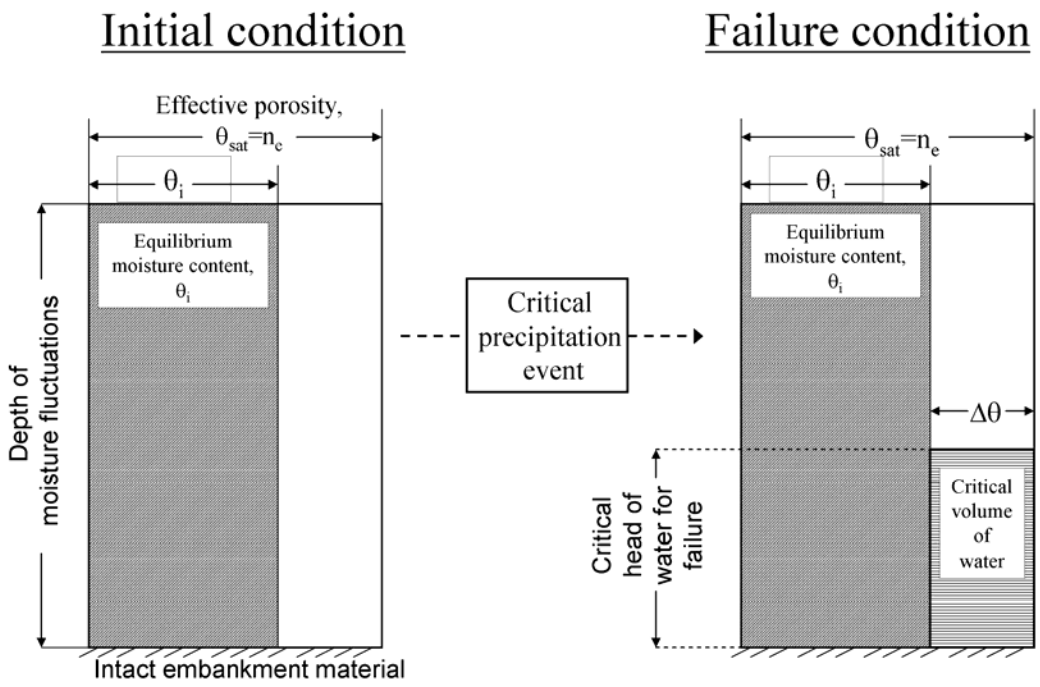

Figure C.1 Model for failure under discrete precipitation events

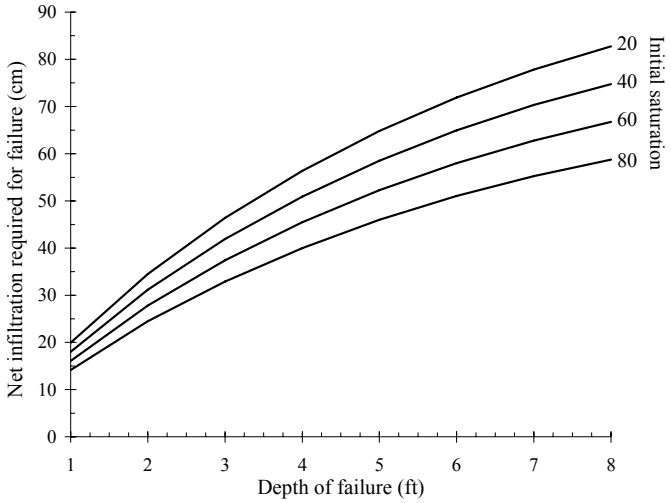

Figure C.2 Net infiltration required for failure for different depths of failures and initial saturations

C.3 Recurrence rate of failures

In order to determine the recurrence of failure for a given slope of highly plastic clay under a discrete rainfall event, the intensity, duration, and frequency of rainfall events must be considered. The rainfall intensity-duration-frequency (IDF) relationship for Austin, Texas reported by McKinney (2006) is shown in 0. The IDF relationship and slope failures in highly plastic clay can be related by making use of the shear strength parameters for Eagle Ford Clay (Appendix B.), the mean volumetric water content profile obtained in the depth of moisture fluctuation analysis (Appendix A.) and the pore water pressure required to cause failure for a given slope angle at a failure depth of 1.1 meters (Appendix B.). Given this information, a relationship between the cotangent of the slope angle and the combination of intensity and duration to cause failure was established and is shown in 0. For this analysis the rainfall intensity is assumed to be equal to the infiltration. This is considering the worst case scenario because any amount of runoff would reduce the amount of infiltration per a given precipitation event. However, runoff will be less significant at lower and more critical precipitation rates so should not change the relationship significantly.

This relationship can be plotted more clearly in terms of storm duration and storm intensity as shown in 0 and 0 respectively. Both charts were established for rainfall durations of less than 100 minutes. Assuming infiltration will most closely approximate precipitation for the longer duration (i.e., 100 minute events), the cumulative infiltration, is plotted in 0 assuming no runoff. Based on a rainfall duration of 100 minutes, it appears that failure under a discrete event for a slope of 3.0:1 should be expected to have a mean recurrence rate of approximately 30 years.

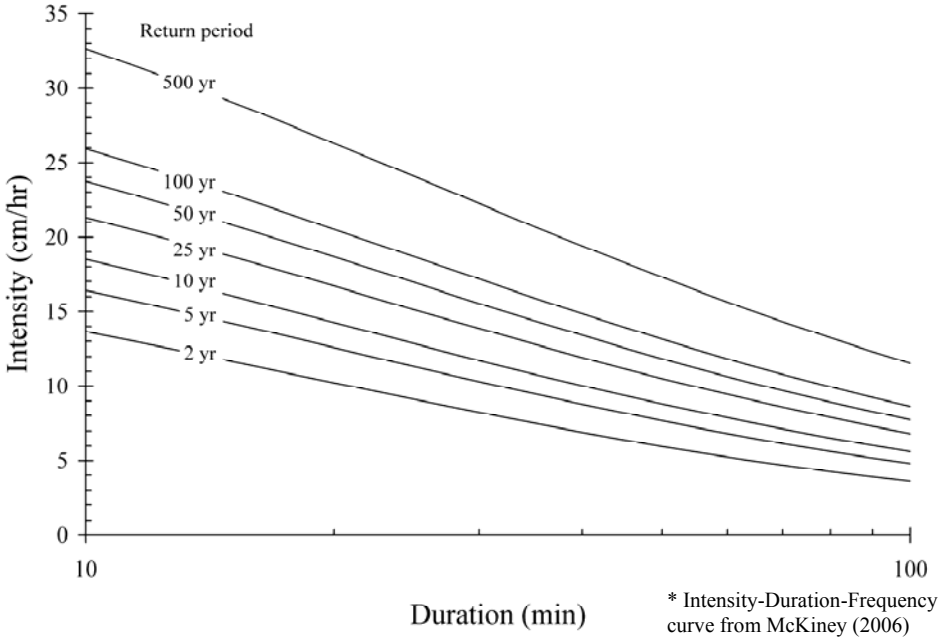

Figure C.3 Rainfall intensity-duration-frequency curve for Austin, TX

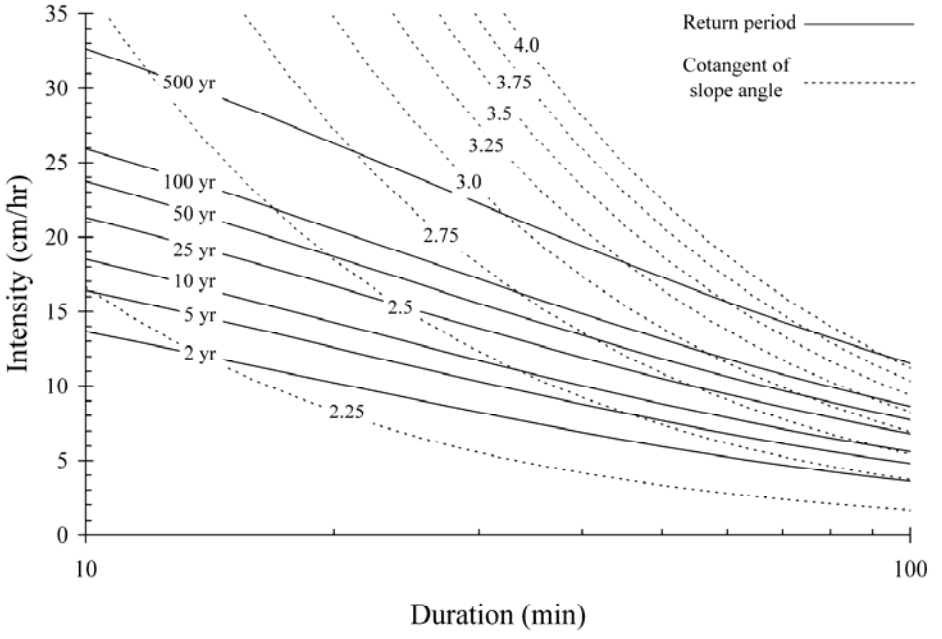

Figure C.4 Recurrence rate of failures for cracked Eagle Ford clay under Austin weather conditions given a failure depth of 1.1 meters

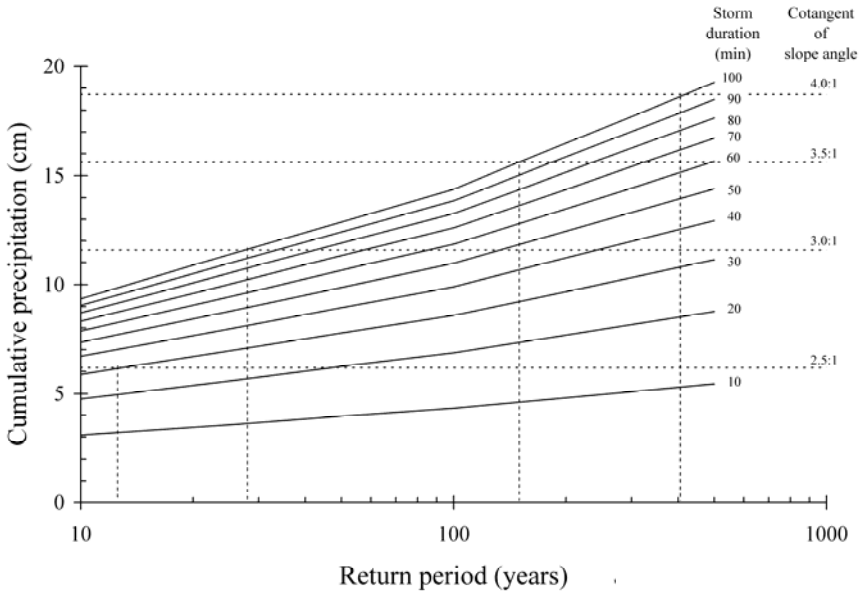

Figure C.5 Recurrence rate of failures for cracked Eagle Ford clay under Austin weather conditions given a failure depth of 1.1 meters in terms of storm duration

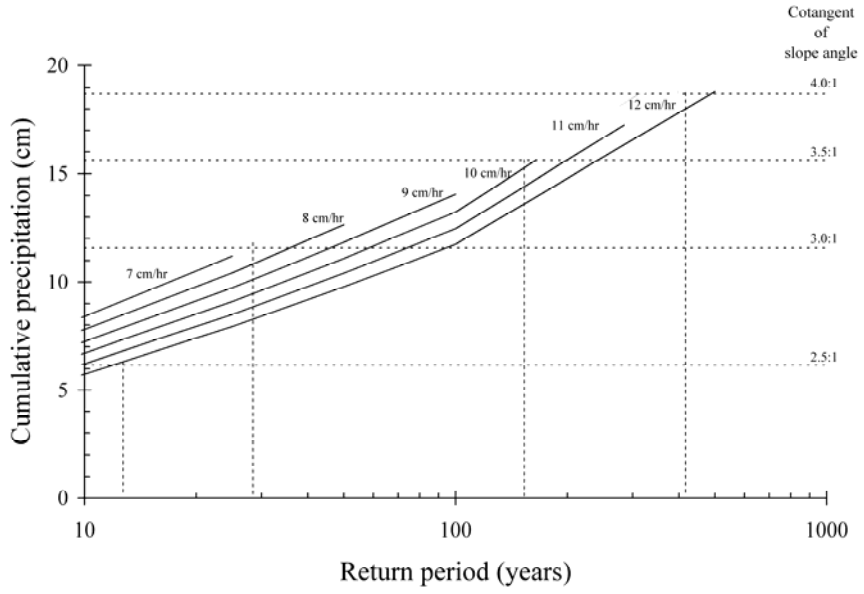

Figure C.6 Recurrence rate of failures for cracked Eagle Ford clay under Austin weather conditions given a failure depth of 1.1 meters in terms of storm duration considering events of less than 100-minute duration

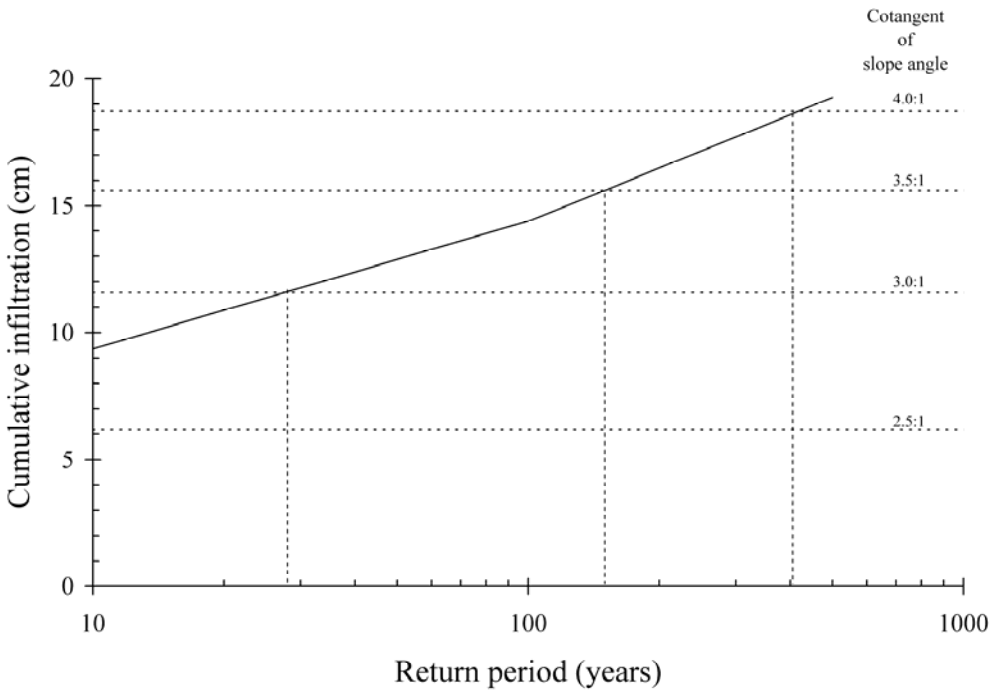

Figure C.7 Recurrence rate of failures for cracked Eagle Ford clay under Austin weather conditions given a failure depth of 1.1 meters for a storm duration of 100 minutes

C.4 Implications for design

Based on the analysis conducted to determine the recurrence rate of slopes failures in highly plastic clays, a slope of 3.5:1 was found to lead to a mean recurrence rate of failure exceeding 100 years. If a depth of moisture fluctuation of 1.1 meters is considered, and seepage parallel to the slope face is considered, then a slope of 4.2:1 will lead to a factor of safety of 1.0 for an infinite slope analysis. Given the difference between these two maximum slope angles, it is important to note that the recurrence analysis was conducted considering only discrete events and initial volumetric moisture content predicted by the mean moisture profile in the depth of moisture fluctuation analysis (Appendix A.). Furthermore, this analysis does not consider alternate moisture profiles or multiple events, and only considers the mean IDF curves. Therefore, it is prudent to design for conditions of seepage parallel to the slope face. The slides reported by Kayyal and Wright (1991) have an average depth of 1.3 meters, which is consistent with the results of the numerical simulations in Appendix A. According to the results of the slope stability analysis performed in Appendix B. , a failure depth of 3 meters will have a factor of safety of 1.0 for a slope of 4.8:1.

Appendix D. Site Visits Involving Failure in Highly Plastic Clay

In order to gain a better understanding of the mechanisms leading to slope failures in compacted embankments of highly plastic clay, the research team has performed a number of field visits to failed slopes. In addition to documenting the slope failures at these sites, the field visits have given the team the opportunity to interview TxDOT employees concerning there thoughts on the failures. The sites that have been visited to date are shown in Table D.1.

Table D1 Site visits

	Site	Cut or fill?	Remedial efforts	Date of visit	TxDOT contact
1	*Hester's Crossing, Williamson County, TX*	cut	*Plans for an MSE wall*	*10/15/2004*	*Marcus Galvan*
2	*183 & Boggy Creek, Travis County, TX*	cut	*Plans for a gabion tie-back wall*	*03/03/2005*	*Marcus Galvan*
3	*183 and MLK, Travis County, TX*	cut	*None so far*	*03/08/2005*	*Marcus Galvan*
4	*IH 30 in Fort Worth Tarrant County, TX*	cut/fill	*Tire Bales*	*04/07/2005*	*Richard Williammee*
5	*SH 6 and SH 105 Travis County, TX*	fill	*Fiber Reinforcement*	*05/25/2005*	*Darlene Goehl*
6	*SH & Little Brazos River, Brazos County, TX*	fill	*Backfill with granular material*	*02/16/2006*	*Darlene Goehl*

Details of each site visit are included with this appendix. Sites visited have included both cuts and fills into highly plastic clay. Remedial efforts that have been planned and or carried out are also presented in the table.

D.1 Hester's Crossing

Location: Round Rock, Texas, USA

The laboratory testing of this research project required a large quantity of highly plastic clay. TxDOT presented the opportunity to obtain a large quantity of highly plastic clay from a site that was currently under repair. This also presented the opportunity for a site investigation. The samples obtained for laboratory work were taken form the south-east embankment of the intersection of interstate highway 35 (IH-35) and Hester's Crossing in Round Rock, Texas. A schematic of the intersection of interstate 35 and Hester's crossing is shown in Figure D.1. The four embankments at this intersection have various histories but were all formed during the construction of IH-35 when the roadway was cut into the Eagle Ford formation. The following report presents a discussion of the four embankments and lessons taken from the slope failures.

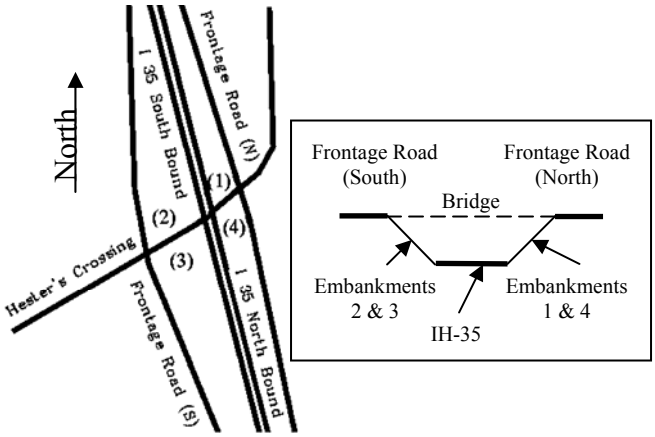

Figure D.1 Image of the Hester's Crossing – IH-35 overpass

The four embankments present at the intersection of IH-35 and Hester's Crossing are numbered from one to four in 0. Soil for the current research project was taken from Embankment 3. As of fall 2004, the slope on Embankment 3 had failed. This prompted TxDOT to regrade the slope and evaluate possible repair options. The presence of construction equipment at the site allowed for the excavation of Eagle Ford clay from 10 feet of depth into the embankment using a backhoe.

D.1.1. Site background

The embankments at the intersection of Hester's crossing and IH-35 are composed of Eagle Ford Shale. A TxDOT employee indicated that a stream crossed the site traveling west to East prior to the construction of the overpass. The plasticity index of the Eagle Ford clay removed from the site was measured as 60 (ASTM D4318). The frontage roads on both the northbound and southbound sides are elevated approximately 35 feet above IH-35 (with respect to the center of the intersection). Each of the four embankments has unique characteristics. Embankment 1 is an intact soil slope that is covered with trees. Embankment 2 is a shallow natural slope with little to no slope problems. Embankment 3 has recently failed and is currently under remediation. Embankment 4 has been stabilized with a mechanically stabilized embankment and has experienced two significant failures in the past.

D.1.2. Field observations

Observations of individual embankments are as follows:

[1] ***Embankment 1***. TxDOT has observed slope movement on this embankment. The presence of downward slanting trees, as pictured in Figure D.2, is evidence of this movement. The slope of Embankment 3 was measured at 6:1. TxDOT emphasized that there was no immediate concern over the stability of this embankment.

[2] ***Embankment 2***. TxDOT has not reported slope stability concerns regarding Embankment 2, nor was there any evidence of failure after visual inspection. The slope was measured at 6:1, the same as Embankment 1. The growth of Typha latifolia (i.e., cat of nine tails), which are typically found in marshy areas, at the toe of the embankment in a marshy area indicates that the location

remains reasonably wet throughout the year. Embankment 3 drains to the toe of Embankment 2 and may be responsible for a portion of the water ponded at the toe of Embankment 2. According to a member of the maintenance crew, a creek ran its course under IH-35 prior to the construction of the overpass. The presence of water at the toe of Embankment 2 as a result of water draining from Embankment 3 was further supported by TxDOT workers who indicated that Embankment 3 remains wet throughout the year. To date there have been no signs of instability of Embankment 2.

[3] ***Embankment 3***. Currently, Embankment 3 is under remediation for a recent slope failure. This is the third documented slope failure for this embankment. TxDOT employees indicated that the as-constructed slope of Embankment 3 was 2:1. The first slope failure that occurred is shown in Figures D.3 and D.4. A progressive failure is evidenced by the bulging appearance of the slope face. This failure led the TxDOT to re-grade to a 6:1 slope. Although 6:1 is generally considered the lower limit for slopes that may experience failures in the Austin area, it did not seem to apply in this particular case. The second slope failure occurred in the 6:1 slope.

One of the difficulties with Embankment 3, as indicated by the marshy region in Embankment 2, is the continual seepage of water through the hillside as discussed in the previous section of this report. Samples collected from 10 to 15 ft of depth displayed flow markings indicative of seepage. Samples collected at depths between 2 and 10 ft displayed slickensides, indicative of shearing across clay particles. A preliminary discussion of remedial efforts indicated that grave drains would be installed to provide relief from seepage. TxDOT personnel indicate the presence of a perched water table at the head of the slope. Slope failures within Embankment 3 occurred within close proximity to large rainfall events. One possible failure mechanism for this slope is positive pore water pressure generation. A large rainfall event combined with the presence or generation of a perched water table could have resulted in the generation of positive pore water pressure and consequently surficial slope failure.

[4] ***Embankment 4.***

Soldier pile failure - A series of slope failures on Embankment 4 prompted TxDOT to seek more permanent solutions. Initial remediation efforts involved the installation of soldier pile walls. Specifications called for the removal of all failed material and installation of the soldier piles to a depth greater than the failure surface. The contractor installing the soldier pile walls neither removed all of the failed material nor installed the soldier piles to sufficient depth. As shown in Figures D.5 and D.6, improper installation resulted in failure. The failure surface started at the bottom of the soldier pile wall and ended in the middle of the frontage road (Figure D.6).

Temporary Stepped Slope failure - Following failure of the soldier pile wall, TxDOT called for the installation of a mechanically stabilized embankment. The slope was restored with compacted high plasticity clay and excavation began for the installation of the mechanically stabilized embankment. Again, the contractor did not remove all of the failed material. In an effort to streamline construction, the contractors decided to stair-step the clay rather then deal with shoring regulations. A permit was obtained for the excavation procedure and construction proceeded without consultation of the TxDOT bridge division. Significant cracking that occurred within the clay stair steps within two days time is shown in Figure D.7. A large precipitation event followed and resulted in the deep slide. The scarp of the failure is shown in Figure D.8.

The severity of cracking is shown in Figure D.9 by the breaking-off of a large block of clay. The extent of cracking and the ponding of water at the toe of the slope are evident in Figure D.10.

Post-failure Drilling - After failure of the stair-stepped slope, TxDOT contracted for a post-mortem inspection of the slope. Six bore holes were drilled in the embankment. The typical strata consisted of 2-5 ft of hard clay, 4-8 ft of gravely-clayey-sand, 18-20 ft of stiff clay, and a limestone substrata. The water table was encountered in three of the bore holes. Within 24 hours water levels in the three bore holes fell between 1 and 2 ft relative to their initial levels. This indicated the presence of a perched water table.

D.1.3 Lessons learned

The interchange at Hester's crossing offers a good look at several types of construction on high plasticity embankments. Although the construction methods have varied, the failure mechanisms appear to be similar. The following are lessons that can be learned from the series of failures that have occurred and the present state of the embankments at Hester's crossing.

[1] Full removal of the failed material is important for future stability
[2] All of the failures at Hester's crossing were within days of large precipitation events
[3] Boring logs and visual inspection after failure indicated the presence of a perched water table.

Figure D.2 Embankment 1 looking from Embankment 3

Figure D.3 Quadrant 3 looking south

Figure D.4 Quadrant 3 from Quadrant 4

Figure D.5 Quadrant 4 looking North

Figure D.6 Quadrant 4 looking South

Figure D.7 Quadrant 4 from Quadrant 3

Figure D.8 Quadrant 4 looking South

Figure D.9 Quadrant 4 looking Southeast

Figure D.10 Quadrant 4 looking Northwest

D.2 Boggy Creek

Location: Travis County, Texas, USA

The Route 183 bridge crossing Boggy Creek in Austin, Texas was in need of remedial work in 2005. The Northern bank of Boggy Creek had eroded considerably, leaving the bridge's foundation exposed. Since the construction of the bridge in the early 1960s, TxDOT has made efforts to suppress erosion occurring on the creek bank. The effectiveness of these efforts provides a good case history for erosion suppression. This section of this report documents observations from a site visit performed on March 3 of 2005 and a comparison between images taken by the Texas Transportation Institute in 1999. While it is unclear if the erosion occurred gradually from 1999 to 2005 or as the result of several distinct events, it is clear that impressive changes in both banks of the river have taken place in this time period. As of the spring of 2005, TxDOT is planning a $2 million remediation effort. Bidding for remediation goes out in August of the same year.

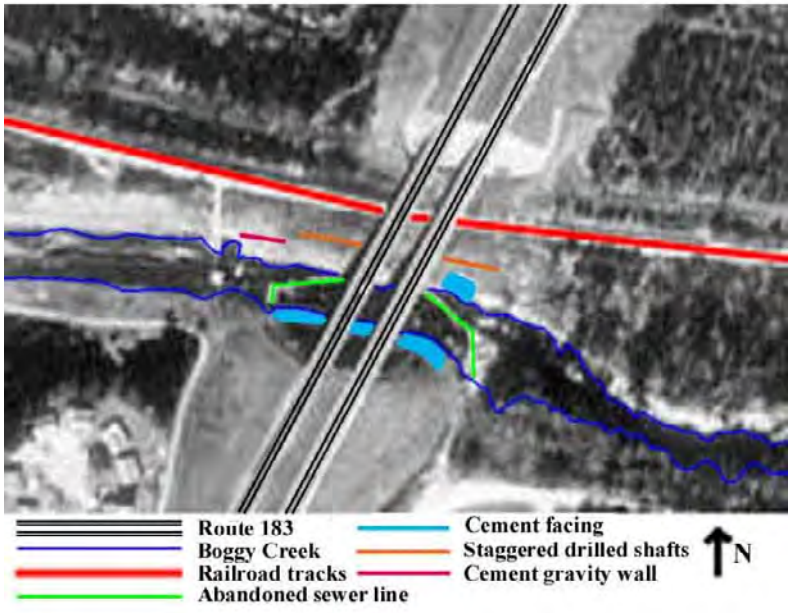

Figure D.11 Aerial image of the 183 – Boggy Creek overpass (modified USGS image)

D.2.1. Project background

Initial plans for remediation involved a joint effort between the City of Austin and the US Army Corps of Engineers (Corps). The Corps has a program that is intended to help with design and construction that is crucial to roadways. Under the program, the City of Austin would put forward $500,000 for the construction effort and the Corps would provide the remainder. Unfortunately, in February of 2005, TxDOT received the news that the project was not approved for the Corp's annual budget. The City of Austin had to choose whether to remedy the problem

without assistance from the Corps, or await the next fiscal year to see if the project is approved. Without guarantee of approval in the following year, the City of Austin decided to implement the remediation effort independent of the Corps. The City allocated $2 million for the remediation. As of spring 2005, TxDOT has proposed using 3 ft by 3 ft gabions at the toe of the slope. These gabions will be used in combination with pre-stressed ground anchors in an effort to intercept active failure surfaces. In addition to slope stabilization efforts, remediation will include adding newer, 125-ft spans to widen the bridge. A detailed map of the site is available in 0. The relative and specific location of the site is illustrated in 0 and 0.

D.2.2 Site background

The Boggy Creek stream bed consists of Quaternary alluvium. It flows east under the Route 183 bridge where it flows into the Colorado River. At the Route 183 crossing, the southern bank of the river consists of alluvium. The northern bank (0) of the river consists of the Taylor Group montmorillonitic clays (Bureau of Economic Geology). Conditions at the site are complicated by the presence of an abandoned sewer pipe (0). It is unclear whether or not the sewer pipe was originally exposed upon construction. It is apparent that the sewer pipe has caused sedimentation issues and meandering of the river due to its influence on the creek's flow.

D.2.3 Field observations

The site has a history of remedial efforts made in an attempt to keep the slope faces intact. These efforts involve the following:

[1] ***Concrete facing***. The southern bank the stream was covered with concrete facing at the time of construction. As of 2005, the concrete facing on the Southern bank has a slope of 25°. Failure of the concrete extends from 25 to 30 ft up the slope when measured from the original extent of the facing. It appears that erosion at the base of the facing has been so severe that much of the supporting soil at the toe has been removed and the structure has gradually collapsed. A 2005 image of the facing (0) reveals areas where soil has been removed to such an extent that concrete is solely held in place by the upper portion of the slope. When images from 2005 and 1999 (0, 0, 0, and 0) are compared, it is evident that failure of the concrete facing was well underway by 1999. Additionally, 0 and 0 illustrate the considerable amount of erosion that has taken place over this time period on the Northeast bank adjacent to the bridge. It appears that the extent to which concrete cover was intact in 1999, although already partly failed, was still somewhat effectively preserving the slope face.

[2] ***Drilled shafts***. A number of drilled shafts appear on the northern face of the bank approximately half way up the slope face. They are laid out perpendicular to the bridge in two staggered rows and span out on both sides of the bridge. The drilled shafts appear to be effective at intercepting deeper slide surfaces but have failed to prevent the lower portion of the bank from eroding to a considerably steep slope. When images of the Northwest slope from 2005 and 1999 are compared (0 and 0), it is apparent that a considerable portion of the erosion of the lower portion of the bank took place over this time period.

[3] ***Rip rap***. Rip rap has been placed beneath a portion of the failing concrete cover in what appears to be an effort to reinforce the toe of the slope. When images of the south foundation from 2005 and 1999 are compared (0 and 0), it is evident that the foundations are partially

exposed in 1999. The image from 1999 also reveals that the soil beneath the portion of the concrete facing has already been washed away. The success of the rip-rap is unclear, but the intact nature of the concrete cover above the rip-rap would suggest that its placement has to some effect prevented further degradation of the concrete facing within the immediate area.

[4] ***Stepped concrete gravity wall***. A stepped concrete gravity wall is exposed for a small section downstream of the damn but its extent is unclear (0). One can observe that the bank in front of the wall has undergone failure, and that the portion of the bank in back of the wall is still held back. Field observation revealed that soil in back of the wall appears to be creeping downhill.

D.2.4 Additional comments

Exposed drilled shafts

A 2005 image of the drilled shafts on the Northeast slope reveals that the upper 2 to 3 ft of the shafts is exposed. This would signify that since their installation the ground surface at the shafts has fallen, the ground surface was cleared away during construction, or the ground surface has eroded.

Exposed North foundation

Images from 2005 and 1999 (0 and 0) reveal that the Northern foundation has been exposed over that time period.

Alluvial deposits

Downstream and upstream images of Boggy Creek (0 and 0) reveal a downstream deposition.

Concrete facing on the Northern upper-tier

While the concrete facing on the lower portion of the Northern bank is in a state of collapse, the concrete facing on the upper tier of the bank (0) remains intact. The concrete facing on the upper-tier has a slope of 24°. The slope face adjacent to the upper tier has a slope of 21°. The material used in constructing the upper portion of the bank was said to be of a local origin. The toe of the upper tier is intact and aside from minor tension cracks, the concrete facing has undergone little or no damage. The lower tier however has as of the spring of 2005 almost completely deteriorated. However, it is apparent when images from 2005 and 1995 (0 and 0) are compared that one solitary portion of concrete slab on the northeast slope has remained intact. While this is an interesting fact to point out, only conjectures can be made as to the reason for this intact piece and the stability of the concrete on the upper tier. Possible causes include the removal of toe support, positive pore water pressures due to infiltration from the above ground surface, and the role of the concrete facing as a moisture barrier amongst others.

D.2.5 Lessons learned

[1] Concrete facing alone is not necessarily an effective retaining structure.
[2] The staggered drilled shafts may have prevented the formation of deep failure surfaces in the slope of highly plastic clay.
[3] Rip rap placed at the toe of the concrete facing has minimized further deterioration of the concrete facing.
[4] The stepped concrete gravity wall has stabilized the retained soil, but the soil in front of this structure has failed.

Figure D.12 Relative Location

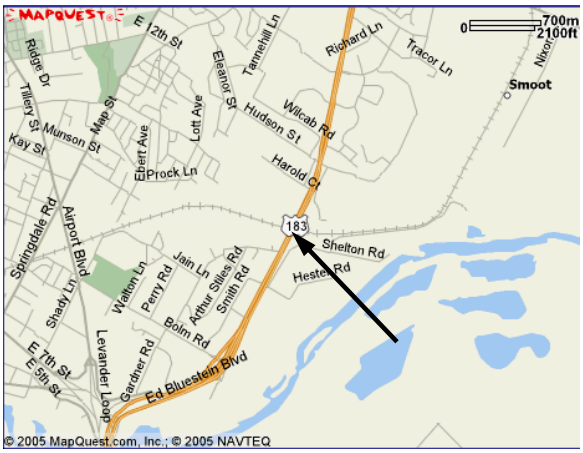

Figure D.13 Specific Location

Figure D.14 Taylor group strata (Northeast 2005)

Figure D.15 Abandoned sewer pipe (Upstream view - westward 2005)

Figure D.16 Concrete facing (Southwest bank 2005)

Figure D.17 Concrete facing (Southwest bank 1999)*

Figure D.18 Failed concrete cover (Northeast bank 2005)

Figure D.19 Failing concrete cover (Northeast bank 1999)*

Figure D.20 Drilled shafts (Northwest bank 2005)

Figure D.21 Drilled shafts (Northwest bank 1999)*

*Images from a 1999 Texas Transportation Institute study

Figure D.22 Exposed foundation with rip-rap (South foundation 2005)

Figure D.23 Partially exposed foundation (South foundation 1999)*

Figure D.24 Gravity retaining structure (Northwest - eastward 2005)

Figure D.25 Exposed drilled shafts (Northeast - southward 2005)

*Images from a 1999 Texas Transportation Institute study

Figure D.26 Exposed foundation (North foundation 2005)

Figure D.27 Enclosed foundation (North foundation 1999)*

Figure D.28 Alluvial deposits (Downstream view – eastward 2005)

Figure D.29 Failing slope faces (Upstream view - westward 2005)

*Images from a 1999 Texas Transportation Institute study

D.3 Martin Luther King Boulevard

Location: Travis County, Texas, USA

The shallow slope failure at the intersection of Martin Luther King Boulevard and route 183 was investigated by TxDOT personnel and the research group in March of 2005. The geometry of the failure obtained from inclination measurements on the face of the failure mass is shown in 0. From the observed ground displacements it is evident that the failure was rotational. The extent of the separation observed close to the scarp of the slope is shown in 0. The lateral extent of the failure was approximately 100 feet and is shown in 0.

The exposed clay throughout the failure mass appeared weather and consisted of clumps of soil (0). The geometric cracking pattern typical for highly plastic clays was observed along the face of the failed soil mass and is shown in 0. A continuous 1.5-ft deep lateral crack appears in the failed mass approximately one third of the way up the slope. The lateral crack is pictured in 0 and 0. The location of the crack is also noted in 0.

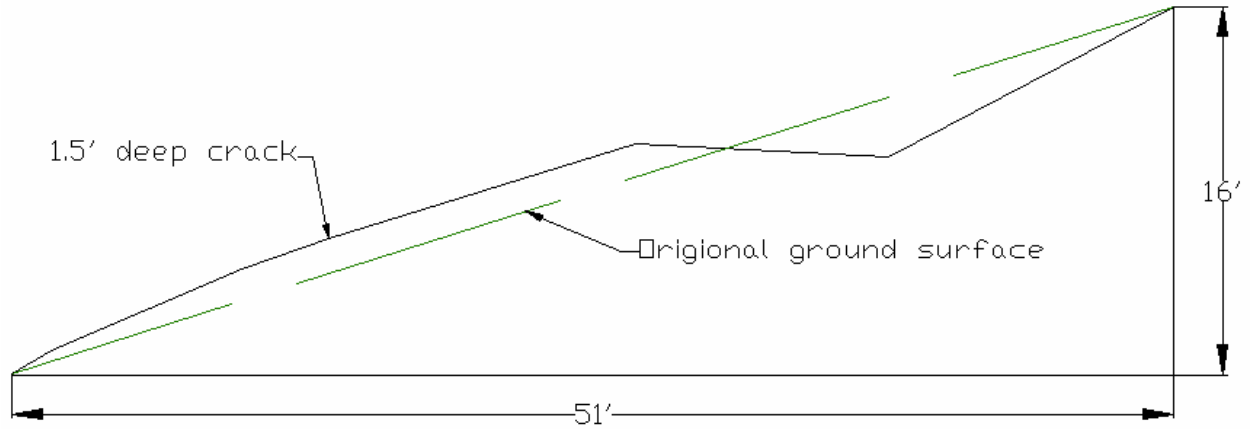

Figure D.30 Geometry of failure

Figure D.31 Vertical extent of separation at the scarp

Figure D.32 Lateral extent of slope failure

Figure D.33 Weathered clay material in failure mass

Figure D.34 Pattern of cracking within on the top of the failed mass

Figure D.35 Lateral crack cutting through the center of the failed mass

Figure D.36 Close-up of lateral crack cutting through the center of the failed mass

D.4 Highway 30 Tire Bale Slope Stabilization

Location: Forth Worth, Texas, USA
Additional author: LaRocque, Christopher

Between February 2002 and August 2002 a total of 360 tire bales, composed of approximately 36,000 scrap tire bales, were used in the repair of a slope failure on Interstate 30, east of Ft. Worth. The project was led by Richard Williammee (TxDOT), Fort Worth District's Construction and Maintenance Recycling Coordinator, in accordance with the Texas Legislature's mandate to increase the use of scrap vehicle tires in highway applications. The soil at the site consisted of a highly plastic clay. A series of shallow slopes failures made the site a good candidate for remedial efforts.

Tire bales were installed within the slope by first removing the failed material and cutting past the greatest extent of the failure plane. Then, tire bales were placed in layers with soil layers in between them. The soil layer was intended to separate the tire bale layers in the event of combustion. The upper most tire bale layer was covered with soil and seeded. The geometry that existed prior to remediation was restored. As of mid-October 2002, the Fort Worth area had received almost 50 in. of rain since placement of the first tire bales in mid-February. A site visit at that time revealed some small cracks developing along the top ridge of the slope. These cracks, along with some noticeable subsidence were confirmed during the most recent site visit on April 7, 2005. A geotechnical engineer under contract to the Fort Worth office was hired by TXDOT to perform a preliminary slope stability analysis of the final product. Initial analysis revealed that the use of tire bales instead of the original soil slope had improved the Factor of Safety by 2-3 times. A slope stability analysis is currently being repeated, using the tire bale properties determined in Project 5-9023-01. The District is stockpiling additional bales for use in a future failure and has been awarded an Implementation Project by the ROC (Research Oversight Committee) to repair and instrument the next site for a more detailed evaluation of the tire bales and their benefit to slope retention. A site visit in April 2005 confirmed a slope failure in the adjacent area.

Figure D.37 Original slope after remediation with tire bales. (TXDOT)

D.4.1 Project background

Initial plans for using tire bales as building blocks for a slope remediation project were made in the spring of 2001. A failed slope along IH-30 approximately 3 miles east of Fort Worth was identified for the project (0). The slope had initially failed due to excessive rainfall in the area (0). TXDOT required all bales to be donated, as the maintenance division did not have funds appropriated for such a project. In January of 2002, a total of 240 bales were available for the project. A representative from Encore Systems in Minnesota constructed these bales using a vertical baler and scrap tires from Texas (0). After placement of the first two layers of tire bales, there were no remaining bales to use for the third layer. A 5-month delay was encountered as 120 additional bales were acquired. During this period, there was no monitored movement of the placed bales. More than 25 in. of rainfall was experienced during the delay. The water was observed to drain freely through the second layer of bales. Because water was suspected as the cause of the failed slope, the observation of easy drainage was determined to be a success. No drainage layer was provided however, which eventually proved to be detrimental. A geotechnical engineer was hired by TXDOT to perform a slope stability analysis, which revealed the Factor of Safety improved 2-3 times by using tire bales instead of the original slope soil. The project was concluded to be a success.

D.4.2 Site background

The failed slope was first excavated and the foundation was prepared for tire bale placement (0). As previously mentioned, no drainage layer was provided during the preparation of the slope foundation. Initial design required 6 in.-8 in. gap between each bale in order to encapsulate them with soil and prevent potential combustion. During construction, this requirement was not met and tire bales were placed tightly against each other. This required more bales per layer, which meant that additional bales would be needed.

The first layer of bales was placed tightly together with a front-end loader (0). A soil layer was then placed over the bale layer to provide additional protection from potential combustion (0). After placement of the soil layer, the layer was compacted and leveled to serve as a foundation for the next layer of tire bales (0). This process was repeated for a total of three layers of tire bales. The topmost soil layer was returned to the original shape of the slope and seeded with vegetation to provide protection from erosion (Figure D.44).

D.4.3 Field observations

Slope failures are typically repaired in the following manners:

[1] The failed material was simply moved back to its original location by maintenance crews. This has not prevented recurrence of slope failures.

[2] Steel I-beams are placed with metal beam guard-fence sections since these are materials that the maintenance division already has in-house. These materials are placed in the middle of the slope and extend below the potential failure plane. This wall is then buried within the slope repair.

[3] This slope remediation was initiated with the second type of repair, and stopped in order to implement the donated tire bales. No monitoring equipment was installed to quantify the long-term bale performance.

[4] A visit in April 2005 revealed that vegetation was plentiful and that the original shape of the slope was largely maintained (Figure D.45). While the repaired slope appears to remain stable, the area immediately adjacent to the slope was failed (Figure D.46). The toe of the failed slope was observed to be saturated. In addition, water was collected in puddles even though there was no recent rainfall in the previous few days. Drainage through the second layer of tire bales that was originally observed during the 5-month layoff in 2002 before construction was completed is shown in Figure D.47. Free drainage throughout the tire bale zone combined with no provided drainage layer is suspected to be the cause of the adjacent slope failure. The rainfall was likely redirected to the adjacent slope where it caused the failure.

[5] A slope indicator was used to take measurements of the slope at 50-ft intervals along its length in order to gauge slope performance. The results are shown in Figure D.48. Subsidence can be seen in the measured soil profiles, but this appears to be confined to the surface soil cover layer. The scarp from the adjacent failure is also plotted in Figure D.48 for comparison.

D.4.4 Lessons learned

[1] A drainage layer is necessary underneath tire bales. In addition, a French drain at the toe of the completed slope would allow easier drainage of groundwater and possibly prevent surficial failures in the soil cover layer.
[2] The soil cover layer experiences surficial failures and minor subsidence. This can be addressed with the use of reinforcement and French drains at the toe of the slope.
[3] The area of the slope that was repaired with tire bales seems to be stable except for some surficial subsidence.

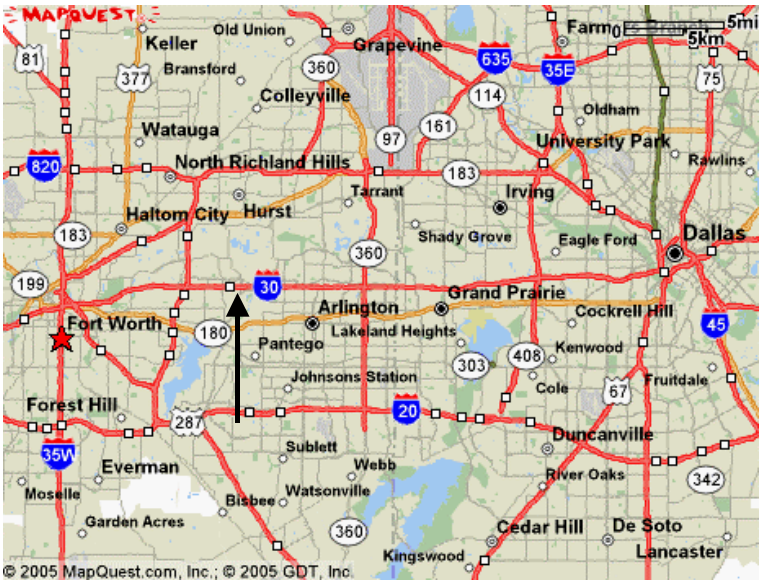

Figure D.38 Relative Location

Figure D.39 Failed Slope 2001

Figure D.40 Construction of tire bale 2001

Figure D.41 Foundation preparation 2001

Figure D.42 Placement of first layer of tire bales 2001

Figure D.43 Placement of soil layer 2001

Figure D.44 Compacted soil layer 2001

Figure D.45 Repaired slope 2001

Figure D.46 Repaired slope 2005

Figure D.47 Adjacent slope failure 2005

Figure D.48 Groundwater drainage through bales 2001

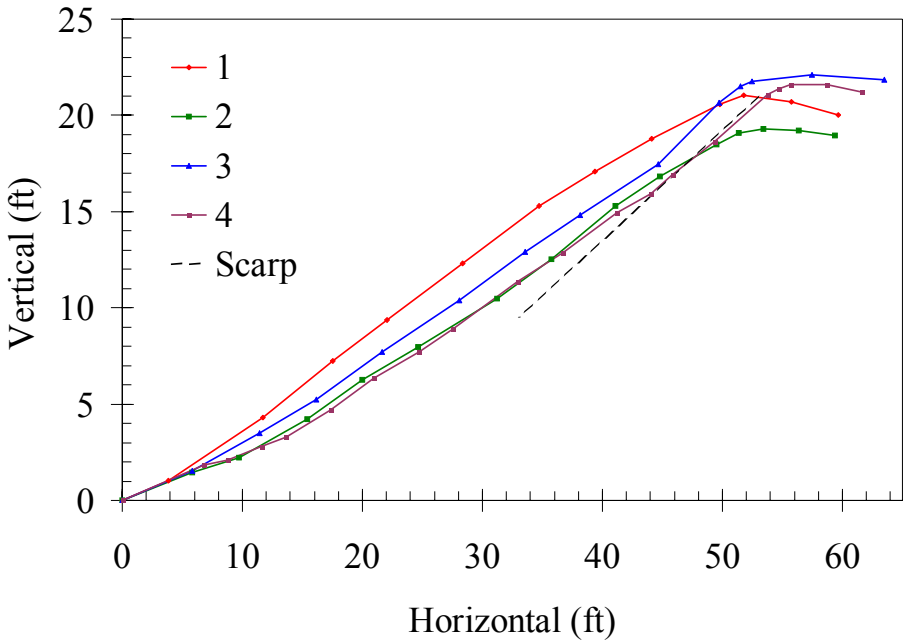

Figure D.49 Repaired slope profile measurements 2005

Figure D.50 Adjacent slope failure 2005

D.5 SH 6 – SH 105 Fiber Reinforced Slope

Location: Grimes County, Texas, USA
Additional author: Freilich, Bryan

During the summer of 1998, two embankments located at the south side of the SH 6 and SH 105 intersection in Bryan, Texas (shown by the arrows in Figure D.50) failed shortly after a heavy rainfall event. The embankments consisted of highly plastic clay and it is thought that the additional weight of water from infiltration loaded the slope and caused a progressive failure. Both slopes failed along the top edge of the highway and slid down into the concrete ditch located at the bottom. After failure, two methods were used to repair the slope. These included adding fibrillated polypropylene fiber reinforcements (Goofier, produced by Synthetic Industries) and adding flume drains to the surface of the slope. This document discusses a site visit to both embankments to examine the performance of the fiber reinforcement.

Figure D.51 Map of Area Surrounding Intersection of SH 6 and SH 105

D.5.1 Project Background and Specifications

The $320,000 embankment remediation began with a site cleanup and preparation. Each of the drainage ditches surrounding the embankments were cleared of excess soil and debris deposited during failure. The failed slope areas were then excavated to a maximum depth of 5 ft and stockpiled adjacent to the site. The excavated soil was then placed back on the embankments

using a horizontal benching method so that horizontal layers of soil could be evenly compacted. Each compacted lift was no more then eight inches thick before compaction. Fibers were added to the soil prior to compaction by spreading them along the surface of the un-compacted layer and mixing them into the soil with a rotary tiller or a rotary pulverizer mixer. Either mixing method required at minimum of three passes over the compaction layer to achieve "uniform" mixing. Ideally, the fibers should be uniformly distributed within the soil after this process and if properly mixed, should be interlocked with the soil upon compaction. After compaction of the top soil layers, a series of concrete flumes were placed along the length of the embankment to provide a pathway for run-off. The flumes also help to catch water from the roadway and reduce the potential for ponding of water on the soil surface.

D.5.2 Site Background and Classification

The soil at the site was classified using visual manual classification techniques as described in ASTM D 2488-00 Standard Practice for Description and Identification of Soils. The top few feet of the embankment were found to consist of a silty or clayey sand with random large clumps of dark, slightly organic, clay (shown in Figure D.56). Testing on the original embankment material gave a plasticity index of around 20 with a moisture content of 16%. TxDOT personnel signified that prior to failure, large desiccation cracks had been observe along the surface of the slope. Desiccation cracks were observed during this investigation on the portions of the embankment that had not yet failed. This is a cause for concern of possible future failures.

In many of the TxDOT reports, moisture infiltration and loading of the embankment due to heavy rain was considered the main factor causing the slope failures. The portion of the slope that had been repaired with fiber reinforcement contained no significant desiccation cracking. Vegetation on the repaired portion of the embankment was significantly taller than the vegetation on surrounding slopes (shown in Figure D.59 and Figure D.60), another possible reason for the reduction in desiccation cracking.

D.5.3 Field observations

Inspection of the repaired site provided insight into the effectiveness of the construction techniques used to place the fiber reinforcement in the embankment and also the effectiveness of the fiber reinforcement on the embankment:

[1] ***Construction Methodology***. The original construction plans, recommended by Mark McClelland, P.E., called for the fibers to be uniformly mixed within the embankment. Visual inspection of the site proved that fibers were in fact not uniformly distributed within the soil and that a large percentage of the fibers were contained in the top few inches of the embankment (shown in Figure D.51 through Figure D.57). The target gravimetric fiber content of the embankment was specified in the design as 0.4%, but in many cases no fiber was found within the soil, or an excessive amount of fiber was found in the soil. Fiber contents in samples taken from the site ranged from 0% to 1%. This non-uniform distribution of fiber might indicate that either the mixing technique or equipment used to place the fibers was ineffective. One possible solution to this problem would be mixing fibers in with the soil while it is stockpiled on the site, and allowing visual inspection of the soil-fiber mixture as it is being placed and compacted. Additional problems may, however, be encountered with stockpiling.

[2] ***Effects of Fiber Reinforcement***. As previously noted, desiccation cracks had been observed on the original embankment surface and on the un-repaired portion of the embankment. The addition of fibers to the top few feet of the embankment appears to have decreased the amount of desiccation cracking that occurred on the repaired slope. A reduction in cracking reduces the potential pathways for infiltration into the embankment and may help explain why the slope has not failed to date. Research has determined that the addition of fibers also increases the shear strength of the soil, but it is not certain by how much the strength was increased in this case, or even if the increase in strength is what has prevented failure so far. Another possibility is that the process of removing the soil from the embankment and recompacting it on the embankment may have helped to establish a dense soil structure that might have been lost since the original embankment construction due to progressive swelling of the soil.

[3] ***Effects of Flume Drains***. The addition of surface drains along the length of the embankment has provided a pathway for water to flow off of the surface of the embankment during rain storms. This may aid in increasing the quantity of runoff and may result in a decrease in infiltration into the embankment. The effect of directly moving water from the roadway at the top of the embankment to the base of the embankment while bypassing the slope, combined with the lower potential for ponding, would seem advantageous. In a recent meeting with Darlene Goehl, P.E. of the Bryan District Laboratory of TxDOT, she was inclined to say that the flume drains were probably the main reason that the embankments had not failed, both by reducing the ponding of water on the slope and increasing the flow of water off of the slope.

[4] ***Combined Effects of Fiber Reinforcement and Flume Drains***. As mentioned previously, moisture infiltration was considered the main reason for the embankment failures. Then by preventing moisture from entering the slope, we prevent the embankment from failure. By using fibers to prevent desiccation cracks in the surface of the soil, we reduce the infiltration into the embankment. Adding flume drains to the surface increases the flow of water off of the embankment sides and reduces the amount of ponding.

D.5.4 Conclusions

(1) Fibers added to the embankment surface decreased the desiccation cracking on the slope and also decreased the size of any cracks that were present.

(2) Flume drains along the embankment provide an increase in flow off of the embankment and decrease the amount of ponding that occurs during rain events.

(3) Mixing fibers in with the stockpiled soil before compaction led to a more uniformly distributed and homogeneous material. This may reduce the clumps of fibers that were seen in the top few inches of the embankment. The fiber-soil mixture can also be examined as it is compacted to ensure that fibers are uniformly mixed in with the soil. The downside is that this increases the cost of the embankment construction.

(4) The addition of flume drains to the slope face has allowed much of the water running off of the road surface to bypass the slope face.

Figure D.52 Fibrillated Polypropylene Fibers Located at Embankment Surface.

Figure D.53 Randomly Distributed Fibers in the Top Few Inches of the Embankment

Figure D.54 Clumps of Fiber Reinforcement Located at Surface of Embankment

Figure D.55 Clumps of Fiber Reinforcements Located at Depth of About 1 Ft.

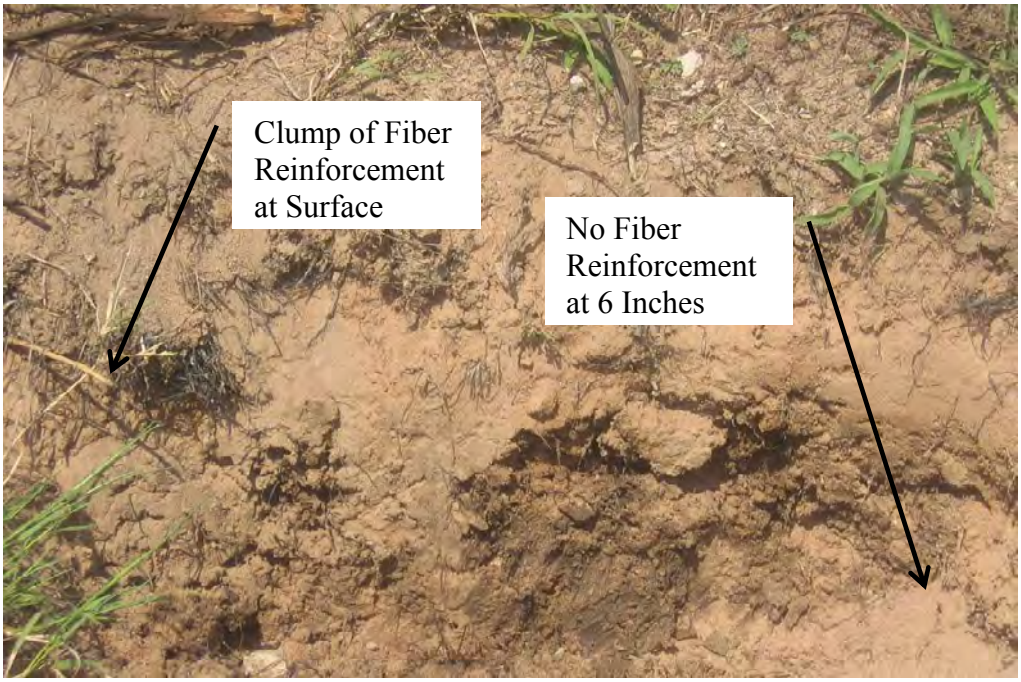

Figure D.56 Clumps of Fiber Reinforcement at Surface and at Depth of About 6 Inches.

Figure D.57 Large Clump of Dark Clay Material with Fiber Reinforcement Excavated from About 1 Ft.

Figure D.58 Plan View of Embankment Surface; Notice that there are not any Visible Desiccation Cracks.

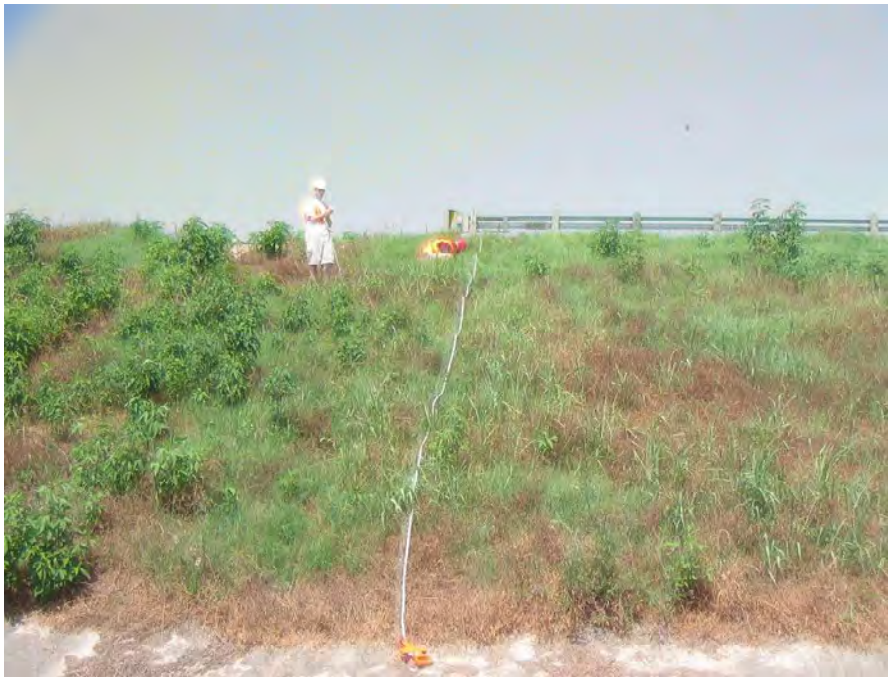

Figure D.59 Side View of Embankment on Southeast Side of Intersection.

Figure D.60 Uphill View of Vegetation on Southeast Embankment.

Figure D.61 Side View of the Southwest Embankment at the Intersection

D.6 Little Brazos River Embankment Failure

Location: Grimes County, Texas, USA

In the fall of 2005, a compacted embankment near the Little Brazos River failed. The embankment had been constructed approximately 20 years earlier when the highway was expanded to four lanes. The failure consisted of the rotation of a rotation with building at the toe of the slope (Figure D.61 and Figure D.62) and a split at the crest of the road immediately off to the side of the paved road. The entirety of the failure mass is pictured in Figure D.63.

The failure plane was determined to be shallow by pushing a cone penetrometer into the failure. The remedial effort taken in this case was to fill the gap at the crest of the slope created by the rotation of the slope with a granular material (Figure D.64). The slope is currently being monitored by TxDOT for indications of additional failure.

Figure D.62 View of toe bulge facing westward

Figure D.63 View of toe bulge facing the slope

Figure D.64 View of failure facing eastward

Figure D.65 View of remedial efforts at scarp of slide

References

Abu-Hejleh, A.N., and Znidarčić, D., 1995, "Desiccation Theory for Soft Cohesive Soils." *Journal of Geotechnical Engineering*, Vol. 121, No. 6, pp. 493-502.

Albrecht, Brian A. and Benson, Craig H., 1996, "Effect of Desiccation on Compacted Natural Clays," *Journal of Geotechnical and Geoenvironmental Engineering,* Vol. 127, No. 1, pp. 67-76.

Alonso, E.E., and Gens, A., 1999, "Modeling the mechanical behavior of expansive clays" *Engineering Geology*, Vol. 54, pp. 173-183.

Andraski, B. J., and Scanlon, B. R., 2002, "Thermocouple psychrometry," in Dane, J. H., and Topp, G. C., eds., *Methods of soil analysis, part 4, physical methods: Soil Science Society of America, Inc.*, No. 5, pp. 609–642.

Arbingast, S., Kennamer, L, Ryan, R., Buchanan, J., Hezlep, W, Ellis, L., Jordan, T., Granger, C., and Zlatkovich, C. 1976. "Mean Annual Relative Humidity." *Atlas of Texas*, p. 19.

Aubeny, C., and Lytton, R., 2003, "Long-term Strength of Compacted High-PI clays," Federal Highway Administration Report # TX-03/2100-1, Project No. 0-2100.

Aubeny, C., and Lytton, R., 2004 "Shallow slides in compacted high plasticity clay slopes" *Journal of Geotechnical and Geoenvironmental Engineering*, Vol. 130, No. 7, July, pp. 717-727.

Aubeny, C., and Lytton, R., 2003, "Long-term Strength of Compacted High-PI clays," Federal Highway Administration Report # TX-03/2100-1, Project No. 0-2100.

Augier, F., Coumans, W.J., Hugget, A., and Kaasschieter, E.F., 2002, "On the Risk of Cracking in Clay Drying." *Chemical Engineering Journal*, Vol. 86, pp. 133-138.

Bedient PB, WC Huber. 1989. *Hydrology and Floodplain Analysis*. Addison Wesley, New York, NY, USA. Bendix J. 1994.

Benson, C., and Daniel, D., 1990, "Influence of clods on the hydraulic conductivity of compacted clay." *Journal of Geotechnical Engineering*, Vol. 116, No. 8, pp. 1231-1248.

Bishop, A. W. and N. Morgenstern. 1960. "Stability Coefficients for Earth Slopes." *Géotechnique* 10, no. 4: 129-150.

Boynton, S, and Daniel, D, 1985, "Hydraulic conductivity tests on compacted clays." *Journal of Geotechnical and Geoenvironmental Engineering,* Vol. 111, No. 4, pp. 465-478.

Brooks, R., and Corey, A., 1966, "Properties of porous media affecting fluid flow." *Journal of Irrigation and Drainage*, Vol. 92, No. 2, pp. 61-88.

Bureau of Economic Geology 1992, "Geologic Map of the Austin Area, Texas"

Cabral, A.R., Burnotte, F., and Lefebvre, G., 1999, "Application of TDR Technology to Water Content Monitoring of Capillary Barriers Made of Pulp and Paper Residues." *Geotechnical Testing Journal*, Vol. 22, No. 1, pp. 39-43.

Daniel, D., 1983, "Permeability test for unsaturated soil." *Geotechnical Testing Journal*, Vol. 6, No. 2, 81-86.

Daniel, D., and Wu, Y.-K., 1993, "Compacted clay liners and covers for arid sites." *Journal of Geotechnical Engineering*, ASCE, Vo. 119, No. 2, pp. 223-237.

Day, Robert .W., 1997 "Discussion of 'Unsaturated Hydraulic Conductivity of Two Compacted Barrier Soils.'" *Journal of Geotechnical Engineering*, Vol., No., p. 1186.

Flint, A.L., Campbell, G.S., Ellett, K.M. and Calissendorff, C., 2002, "Calibration and Temperature Correction of Heat Dissipation Matric Potential Sensors." *Soil Science Society of American Journal*, Vol. 66, pp. 1439-1445.

Freilich, B., 2006, "Behavior of Fiber-Reinforced Highly Plastic Clay" MS thesis, The University of Texas, Texas.

Greenspan, 1976, "Humidity Fixed Points of Binary Saturated Aqueous Solutions" National Bureau of Standards

Kayyal, M.K., 1995, "Effect of the moisture evaporative stages on the development of shrinkage cracks in soils." *Unsaturated Soils*, Vol. 1, pp. 373-379.

Kayyal, M. K. and Wright S. G. 1991. "Investigation of Long-Term Strength Properties of Paris and Beaumont Clays in Earth Embankments," Research Report 1195-2F, Center for Transportation Research, The University of Texas at Austin, (November 1991):125 pgs.

Kleppe, J., and Olson, R., 1985, "Desiccation cracking of soil barriers", *Hydraulic barriers in soil and rock*, ASTM STP 874, pp. 263-275.

Konrad, J.M., and Ayad, R., 1997, "An Idealized Framework for the Analysis of Cohesive Soils undergoing desiccation." *Canadian Geotechnical Journal*, Vo. 34, pp. 477-488.

Kuhn, J., 2005, "Effect of Cracking on the Hydraulic Properties of Unsaturated Highly Plastic Clays." MS thesis, The University of Texas, Texas.

Lu, Ning, and Likos, William J, 2005, *Unsaturated Soil Mechanics*, Wiley, New York.

McKinney, Daene C. 2006. Course notes for Hydrology, Austin, TX.

Meerdink, J., Benson, C., and Khire, M., 1996, "Unsaturated hydraulic conductivity of two compacted barrier soils." *Journal of Geotechnical Engineering*, Vol. 122, No. 7, pp. 565-576.

Meerdink, J., Benson, C., and Khire, M., 1997, "Discussion of 'Unsaturated Hydraulic Conductivity of Two Compacted Barrier Soils.'" *Journal of Geotechnical Engineering*, Vol. 122, No. 7, p. 1186 – 1187.

Miller, C.J., Yesiller, N., Yaldo, K., and Merayyan, S., 2002, "Impact of Soil Type and Compaction Conditions on Soil Water Characteristic Curve." *Journal of Geotechnical and Geoenvironmental Engineering*, Vol. 128, No. 9, pp. 733-742.

Mitchell, J.K., Hooper, D.R., and Campanella, R.G., 1956, "Permeability of compacted clay." *Journal of the Soil Mechanics and Foundations Division*, Vol. 91, No. 4, pp. 41-65.

Mortimer, C.E., 1967, *Chemistry: A Conceptual Approach*, Reinhold, New York.

Mualem, Y., 1978, "Hydraulic conductivity of unsaturated porous media: generalized macroscopic approach." *Water Resources Research*, Vol. 91, No. 2, pp. 325-334.

Olive, W.W., Chleborad, A.F., Frahme, C.W., and Schlocker, J, 1989, "Swelling Clays Map of the Conterminous United States." *United States Geological Survey*, Report No. 1940.

Olsen, H.W., 1962, "Hydraulic flow through saturated clays." Proceedings of the 9th National Conference on Clays and Clay Minerals, pp. 131-160.

Olson, R.E, and Daniel, D., 1979, "Field and Laboratory Measurement of the Permeability of Saturated and Partially Saturated Fine-grained Soils." ASTM Symposium on Permeability and Groundwater Contaminant Transport.

Patterson, D.E., and Smith, M.W., 1985, "Unfrozen Water Content in Saline Soils: Results Using Time-domain Reflectometry," *Canadian Geotechnical Journal*, Vol. 22, pp. 95-101.

Phene, C.J., Clark, D.A., Cardon, G.E., and Mead, R.M., 1992, "Soil matric potential sensor research and application", in G.C. Topp et al., eds., "Advances in measurement of soil physical properties: Brining theory into practice", Soil Science Society of America Special Publication, No. 30, pp. 263-280.

Reedy, R., 2004, Personal Communication. Bureau of Economic Geology, Austin, TX.

Roth, K., Schulin, R., Fluhler, H., and Attinger, W., 1990, "Calibration of Time Domain Reflectometry for Water Content Measurement Using a Composite Dielectric Approach," *Water Resources Research,* Vol. 26, pp. 2267-2273.

Scanlon, B. R., Andraski, B. J., and Bilskie, J., 2002, "Miscellaneous methods for measuring matric or water potential", in Dane, J. H., and Topp, G. C., eds., "Methods of soil analysis, part 4, physical methods": Soil Science Society of America, Inc., No. 5, pp. 643–670.

Siddiqui, S.I., Drnevich, V.P., and Deschamps, R.J., 2000, "Time Domain Reflectometry Development for Use in Geotechnical Engineering," *Geotechnical Testing Journal,* Vol. 23, pp. 9-20.

Sims, J., Elsworth, D., and Cherry, J., 1996, "Stress-dependent flow through fractured clay till: A laboratory study." *Canadian Geotechnical Journal*, Vol. 33, pp. 449-457.

Texas Department of Transportation, Images
http://www.dot.state.tx.us/GSD/recycle/tirebales.htm

Texas Evapotranspiration network, Evapotranspiration data for SVflux analysis
http://texaset.tamu.edu/

Texas Transportation Institute – Digital images, 1999.
http://tti.tamu.edu/enviro_mgmt/projects/1836/north_travis.stm

Tindall, J.A., and Kunkel, J.R., 1999, *Unsaturated Zone Hydrology for Scientists and Engineers*, Prentice Hall, New Jersey.

Tinjum, James M., Benson, Craig, H., and Blotz, L., 1997, "Soil-Water Characteristic Curves for Compacted Clays." *Journal of Geotechnical and Geoenvironmental*, Vol. 123, No. 11, pp. 1060-1069.

Topp, G.C., Davis, J.L, and Annan, A.P., 1980, "Electromagnetic determination of soil water content: measurements in coaxial transmission lines." *Water Resources Research*, Vol. 16, pp. 574-582.

USGS Terraserver Image
http://terraserver.microsoft.com/

van Genuchten, M., 1980, "A closed-form equation for predicting the hydraulic conductivity of unsaturated soils." *Soil Science Society of America Journal*, Vol. 44, pp. 892-898.

Wendroth, O., Ehlers, W., Hopmans, J., Kage, H., Halbertsma, J., and Wösten, J.H., 1993 "Reevaluation of the Evaporation Method for Determining Hydraulic Functions in Unsaturated Soils." *Soil Science Society of America Journal*, Vol. 57, 1436-1443.

Zornberg, J., LaFountain, L., and Caldwell, J., 2003, "Analysis and Design of Evapotranspirative Cover for Hazardous Waste Landfill." *Journal of Geotechnical and Geoenvironmental Engineering*, Vol. 129, pp. 427-483.